Unraveling the cellular context of cyclic nucleotide signaling proteins by chemical proteomics

Eleonora Corradini

Ad Augusta e Luigi

ISBN 978-94-6295-198-3

The research in this thesis was performed in the Biomolecular Mass Spectrometry & Proteomics Group, Utrecht University, Utrecht, The Netherlands.

Printed by proefschriftmaken.nl || Uitgeverij BOXPress

Unraveling the cellular context of cyclic nucleotide signaling proteins by chemical proteomics

Ontwikkeling en applicatie van chemische proteomics benaderingen die bijdragen aan het begrijpen van cyclische nucleotide gereguleerde signaaltransductie.

(met een samenvatting in het Nederlands)

Proefschrift

ter verkrijging van de graad van doctor aan de Universiteit Utrecht op gezag van de rector magnificus, prof. dr. G.J. van der Zwaan, ingevolge het besluit van het college voor promoties in het openbaar te verdedigen op maandag 6 juli 2015 des ochtends te 10.30 uur

door
Eleonora Corradini
geboren op 8 september 1984, te Rome, Italië

Promotor	Prof. dr. A.J.R. Heck
Copromotor	Dr. A. Scholten

Part of the research was financially supported by the Netherlands Proteomics Center (NPC) and by the European Community's Seventh Framework Programme (FP7/2007-2013) through the PRIME-XS project grant agreement number 262067.

TABLE OF CONTENTS

Chapter 1

Introduction

1 PROTEIN PHOSPHORYLATION: SECOND MESSENGERS, PROTEIN KINASES, PROTEIN PHOSPHATASES AND PHOSPHODIESTERASES

Reversible phosphorylation of proteins regulates nearly every aspect of cellular life. Phosphorylation and dephosphorylation catalyzed by protein kinases and protein phosphatases can modify the function of a protein in almost every conceivable way. For example by increasing or decreasing its biological activity, stabilizing it, facilitating movements between subcellular compartments and by initiating or disrupting protein-protein interactions. Ever since the discovery of reversible phosphorylation of glycogen phosphorylase in the late '30s of the previous century[1] and the first observation of protein kinase activity by radioactivity measurement in 1954[2], a large variety of different kinases have been discovered. At the same time the functional importance of these enzymes was recognized. In 1973 the isolation of the first serine/threonine protein phosphatase, the enzyme that removes the phosphate groups from the kinase substrates, shed more light on the mechanism of reversible phosphorylation [3]. In 2002 the completion of the human genome sequence allowed the first glimpse at the extent of the human kinome.[4] Manning et al. catalogued 518 kinases that were assigned to seven major groups on the basis of characteristic sequence features. The involvement of kinases in diseases such as cancer, partly initiated the development of more advanced proteomics techniques to map in more detail their substrates, mechanisms and interactions with signaling modules in the cell.

This thesis focuses on the use of chemical- and shotgun proteomics approaches to study the proteins involved in the different cyclic nucleotide signaling pathways. This introductory chapter will describe the discovery of signaling proteins, their functions and the fundamentals of the most frequently used mass spectrometry-based proteomic approaches to study signaling pathways.

1.1 cAMP signaling and PKA

Cellular metabolism and regulation of gene expression are often the result of extracellular signals. These signals are composed of different chemical origins such as polypeptides, steroids and amino acids, which interact with their cognate receptors. These signals are translated across the cell membrane through the synthesis of so-called second messengers, such as the 3',5'-cyclic adenosine monophosphate (cAMP). The cAMP molecule was discovered by Sutherland in 1958, when he showed that epinephrine induced the formation of cAMP which in turn promoted the phosphorylation and activation of phosphorylase, which leads to the stimulation of glycogenolysis.[5] The way in which cAMP promoted phosphorylase activation was elucidated by Krebs and Fisher[6] when they found that adrenaline stimulated a cascade of kinases. One of these kinases was directly stimulated by cAMP and this kinase was found to also phosphorylate many other proteins[7]. Therefore, it was renamed cAMP-dependent protein kinase or protein kinase A (PKA).[8] Initial biochemical studies of the PKA holo-enzyme structure showed that PKA consists of two regulatory subunits (R) and two catalytic subunits (C) that harbor the phosphotransferase activity.[9] The R subunits

dimerize through an N-terminal dimerization/docking domain followed by a linker containing an auto-inhibitory site for C and two tandem cAMP-binding domains that have low and high affinity for cAMP. The kinase is held in an inactive state when the two C subunits are associated with the R dimer (Figure 1a). The catalytic activity of PKA is induced by the cooperative binding of two cAMP molecules per R subunit, which causes the C subunit to be released and activated.

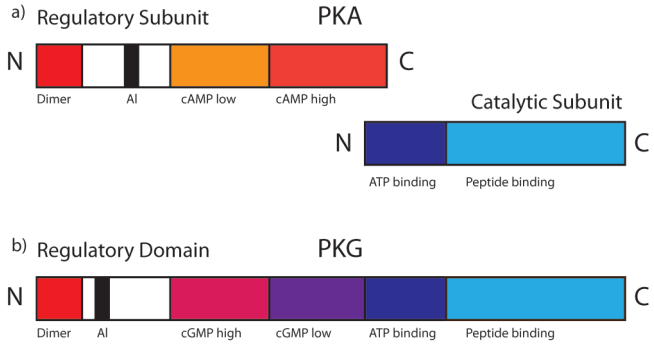

Figure 1 *Domain organization of a) PKA and b) PKG. Domains with high sequence homology between PKA and PKG are depicted in identical colors.*

PKA was identified in almost all the phyla of the animal kingdom.[10] In mammals three genes encode three isoforms of the C subunits (Cα, Cβ, Cγ) that show identical kinetic and physiological properties and four genes encode for four R subunits (RIα, RIβ, RIIα, RIIβ) that exhibit different cellular localization, cAMP binding affinities and tissue distributions. The cloning of cDNAs encoding the catalytic subunits allowed for the structural characterization of PKA.[11] In the cellular context, changes of the cAMP levels can happen in response to different agonists. These variations can result in diverse physiological responses, due to different activities of PKA pools.[12] These results, combined with the difference in cAMP affinity of the R subunits, led to the concept of compartmentalization of PKA signaling in the cell. Specificity of cAMP signaling in space and time is achieved by compartmentalization through A-kinase anchoring proteins (AKAPs). Already in 1982 Theurkauf et al. showed that PKA-RII co-purified with MAP2, however without appreciating it may well be the first example of an AKAP.[13] Two years later, Lohmann and colleagues identified a number of RII-binding proteins from bovine brain and heart and used the first iteration of the RII overlay technique, which is still widely used today and it is fundamental for the studies into AKAPs and compartmentalized cAMP signaling.[14] Subsequent in silico secondary structural analysis of MAP2 and other RII anchoring proteins identified common regions of approximately 14 residues, which display a high probability to form an amphipathic helix with hydrophilic charged residues aligned along one face and hydrophobic residues along the other face.[15] Since then several studies have been performed to understand the binding of the AKAP amphipathic helix to RI and RII

subunits.[16-18] From 1984, the AKAP family has grown to more than 50 very diverse members anchoring PKA along with many other signaling proteins such as protein phosphatases, phosphodiesterases, other kinases and substrates to defined intracellular locations. In this way their interdependent activities are locally restricted within the cell to achieve a high degree of signaling specificity towards the many different stimuli that depend on cAMP as their second messenger.

1.2 cGMP signaling and PKG

Since the discovery of cAMP, it became evident that other physiologically relevant cyclic nucleotides might also exist. In 1961 Smith and colleagues synthetized cGMP for the first time,[19] however only in 1963 it was deemed biologically relevant, when Ashman and Lipton detected and isolated endogenous cGMP from rabbit urine.[20] Interestingly, the circumstances around the study of cGMP were very different compared to cAMP as illustrated by Sutherland in his Nobel lecture:[21] "Then we had a function, and found a nucleotide (i.e. cAMP); now we have a nucleotide, and are trying to discover its function". In 1969 the enzyme responsible for the synthesis of cGMP was identified (guanylyl cyclase[22]). It showed different characteristics compared to the adenylyl cyclase, since it exists in both a soluble and a particulate form. It was not clear yet which extracellular stimuli induced the synthesis of cGMP and neither which metabolic pathways it regulated. Before the discovery of the endothelial-derived relaxant factor (EDRF) which later turned out to be the gaseous messenger nitric oxide (NO)[23] and the discovery of the atrial natriuretic peptide (ANP),[24] Kuo and Greengard found that a partially purified protein kinase from lobster tail was activated by both cAMP and cGMP. Afterwards they chromatographically separated these two activities and provided the first clear evidence of the cGMP-dependent protein kinase (cGKI, also known as PKG)[7] which was strongly activated by cGMP and only weakly activated by cAMP. After demonstration of the expression and activity of PKG in various tissues, and its purification using cAMP affinity capture[25] several studies were performed to determine PKG's amino acid sequence to reveal a large similarity to PKA[26] (Figure 1b). Lincoln and colleagues followed by the studies from Monken et al. determined that quaternary structure of PKG is composed by two monomers that dimerize at the N-termini.[27] A few years later, another study showed the existence of two isoforms of PKGI, α and β, that are encoded from the same gene through alternative splicing.[28] During the same year Wolfe and colleagues showed the high similarity of the two isoforms at the structural level, by sequencing the N-terminus.[29] A second family of PKG encoded by a different gene (PKGII), expressed mostly at the membrane, was discovered in rat and pig intestine.[30] In the years between 1989 and 1999 two different groups worked on the structure of the dimerization domains of PKGIα and PKGIβ with the conclusion that the two isoforms differ only in their N-terminal ~100 amino acids.[28,31] A successive study from Richie-Jannetta in 2003 led to the identification of the leucine/isoleucine zipper motif at the N-terminus of each PKGI monomer that provides for high-affinity homodimerization.[32] In PKGIα the leucine/isoleucine

zipper consists in 5 heptad repeats that are stabilized by hydrophobic residues and an extensive network of hydrogen bonds,[33] while in PKGIβ the leucine zipper includes 8 heptad repeats.[32,34] The differences in the N-terminal domains of the two isoforms raised the discussion that, as for PKA, the N-terminus might mediate PKG localization in the cell and be necessary for the interaction with PKG anchoring proteins (GKAPs). Several studies, albeit to a much lesser extent when compared with the AKAP field, were performed for the discovery of new GKAPs. Almost all known GKAPs are PKGI anchors, but also substrates, and they are known to bind specifically either to the α or the β isoform (e.g. MYPT1 or GKAP42 bind to PKGIα, while IRAG and TFII-I bind to PKGIβ). Up to today a common motif providing for the interaction of GKAPs with PKG has not been defined.

1.3 Ca^{2+}/Calmodulin dependent protein kinase

Sutherland and Krebs were interested to understand how the hormones glucagon and adrenaline break down glycogen to glucose in liver and muscle cells. They appreciated that different hormones stimulated the formation of cAMP from ATP via the activation of the adenylyl cyclases and that cAMP-formation led to the breakdown of glycogen to glucose by activating PKA. In the meantime Greengard and colleagues started to work on the molecular basis of synaptic transmission with the hypothesis that the same machinery is used by the endocrine system. Together with Schulman, Greengard demonstrated that phosphorylation of the synaptosomal membrane protein is dependent on the presence of the Ca^{2+} binding protein calmodulin (CaM).[35] CaM was previously shown to modulate the activities of cyclic nucleotide phosphodiesterases. Immediately after this discovery Sieghat and Greengard demonstrated that a Ca^{2+}/CaM protein kinase activity existed in brain membrane fractions and they showed that this particular activity was present in each animal tissue they examined.[36] In 1981, Kennedy and colleagues described different Ca^{2+}/calmodulin kinase activities,[37] and in 1983, different investigations showed the existence of two isoforms of CaM-dependent protein kinase, namely CaMKI and CaMKII.[38]

CaMKI is encoded by four genes (α, β, γ, and δ), with each gene producing at least one splice variant. All members of this family are monomeric and are between 38 and 42 kDa in size. Their activation depends on a sequence of events beginning with the binding of Ca^{2+}-loaded CaM, followed by phosphorylation of its activation loop by a Ca^{2+}/calmodulin-dependent protein kinase kinase.[39]

In mammals, the Ca^{2+}/CaM kinase type II is also encoded by four genes, α, β, γ, and δ.[40] Each of these isozymes has multiple splice variants leading to a large variety of CaMKII sequences. Activation of CaMKII takes place when the accumulating level of Ca^{2+}-saturated CaM binds to CaMKII resulting in the subsequent auto-phosphorylation at Thr286, which leads to a conformational change to open up the catalytic domain for substrate binding.

Conversely to CaMKI, that exists as a monomer six CaMKII monomers are assembled in two face-to-face rings of holoenzymes, resulting in a dodecameric spindle-like

structure.[41] Moreover monomers of different isozymes can coassemble, allowing for a large number of possible holoenzyme compositions.

1.4 Protein kinase C

A different and more broad concept of a second messenger dependent protein kinase was established when, in a 1977 pioneering study, Nishizuka and his collaborators identified a novel protein kinase from bovine cerebellum.[42] Not much later, the detailed properties of the pro-enzyme and its conversion to an active protein kinase form were reported and Nishizuka named this new enzyme protein kinase C (PKC).[43] In 1980 the same group demonstrated that the second messenger utilized by PKC is the membrane-associated factor diacylglycerol (DAG), placing this novel kinase downstream of receptor-stimulated phosphoinositide phosphatidylinositol 4,5 bisphosphate hydrolysis by phospholipase C.[44] The members of the PKC family have a single polypeptide chain and the structural organisation of the PKC gene family members is conserved throughout the classical (α, β, γ), novel (δ, ε, η, υ) and atypical (ζ, ι) isoforms. Together with PKA and PKG they all comprise a C-terminal serine/threonine protein kinase domain belonging to the AGC class of kinases.

1.5 Protein Tyrosine kinases

In 1978 two groups reported a particular kinase activity associated with the viral Src protein and both groups thought that this kinase phosphorylated its target proteins on threonine residues.[45] Two years later Hunter's research led to the surprising finding that v-Src phosphorylates tyrosine residues instead.[46] From that moment tyrosine phosphorylation became the thing to look for, since it was playing a big role in cancer, but also in a large number of crucial cellular functions. At the same time the Nobel prize laureate Stanley Cohen and his collaborators reported that the EGF-stimulated protein kinase phosphorylated threonine residues,[47] and that it resembled the kinase activity of Src. The EGF-stimulated kinase activity was then reinvestigated to reveal that also the EGF-stimulated kinase phosphorylates tyrosine residues.[48] The latest family of tyrosine kinases discovered are the JAK kinases, referring to Just Another Kinase. JAKs are also known as Janus kinases.[49] Today it is possible to divide the tyrosine kinases into two classes; (i) receptor tyrosine kinases (RTK), that are type I transmembrane proteins with the N-terminal extracellular domain binding to activating ligands and a cytoplasmic C-terminal catalytic domain, and (ii) the non-receptor tyrosine kinases (NRTK), which act as catalytic subunits of receptors which lack a kinase domain. Currently, 90 tyrosine kinases have been identified in the human genome of which 58 belong to the RTK class.

1.6 Protein Phosphatases

To construct a functional switch of signaling events, protein phosphorylation needs to be reversible and thus be counteracted by dephosphorylation. This is achieved by the interplay between protein kinases and protein phosphatases. The discovery of

serine/threonine protein phosphatases originated from the study of glycogen metabolism in skeletal muscle. In 1971 Krebs and Fischer discovered that the conversion of phosphorylase b to a involved a phosphorylation event, and it became obvious that the conversion of a to b was involving a protein phosphatase.
Antoniw et al. began to isolate the protein phosphatase that dephosphorylated and inactivated the phosphorylase kinase in skeletal muscle in 1973.[3] In 1975 he separated this protein into two enzymes, one relatively specific for the α-and one specific for the β-subunit of phosphorylase kinase, that were then termed α- and β-phosphorylase kinase phosphatase. In 1976 Glinsmann identified the proteins termed inhibitor 1 and inhibitor 2[50] and Nimmo showed that the protein phosphatase specific for the β-subunit of phosphorylase kinase isolated by Antoniw was inhibited by these two proteins.[51] The phosphatase was then renamed protein phosphatase1 (PP1) to reflect the fact that it had a broad specificity and tissue distribution. On the other hand the phosphatase that dephosphorylated the α subunit of phosphorylase kinase was insensitive to the inhibitors 1 and 2 and initially was termed protein phosphatase 2 (PP2). Later it was discovered that the PP2 class required different cations for its activation and afterward the PP2 were distinguished in PP2A (which does not require any bivalent cation for activation), PP2B (also known as Calcineurin) and PP2C, which are Ca^{2+}/calmodulin and Mg^{2+} dependent respectively.

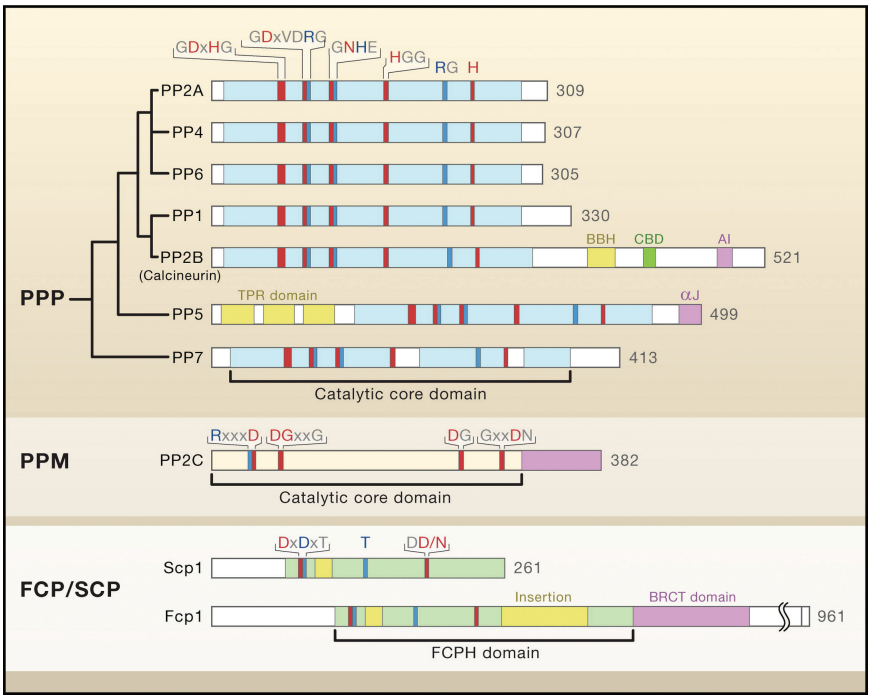

Figure 2 *A comprehensive overview of protein phosphatase families: (i) phosphoprotein phosphatases (PPPs), (ii) metal-dependent protein phosphatases (PPMs), and (iii) aspartate-based phosphatases. The catalytic core domains of each protein are indicated below the diagram. Residues that contribute to metal coordination and phosphate binding are colored in red and blue, respectively. The PPP family contains three characteristic sequence motifs within the conserved 30 kD catalytic domain: GDxHG, GDxVDRG, and GNHE (G, glycine; D, aspartic acid; x, any amino acid; H, histidine; V, valine; R, arginine; N, asparagine; E, glutamic acid). CBD, Ca^{2+}-calmodulin-binding motif; AI, autoinhibitory sequence. Figure adapted from Shi et al..*[52]

Today, the phosphatases that dephosphorylate serines and threonines are divided into three families: (i) the PPPs, including the signature phosphatases PP1, PP2A and PP2B, (ii) the PPM family, comprised of the Mg^{2+}-dependent protein phosphatases, including PP2C, and (iii) the aspartate-based phosphatases represented by FCP/SCP (Figure 2).[52] More recently, many other phosphatases have been discovered in the PPP family such as PP4, PP5, PP6, with a total of 12 genes encoding them.

Within the PPP family each PP1 holoenzyme consists of a catalytic subunit and a regulatory subunit,[53] while the PP2A core enzyme consists of a scaffold subunit (also known as the A or PR65 subunit) and a catalytic subunit. In turn, the PP2A core enzyme interacts with various regulatory subunits to assemble into a heterotrimeric holoenzyme. In both cases, the role of the regulatory subunits is to target substrate phosphoproteins to the phosphatase activity of PP2A.[54] Approximately 30 catalytic subunits of serine/threonine specific protein phosphatases are currently known; relatively little compared to the large number of serine/threonine protein kinases. Nev-

ertheless, for phosphatases, specificity is achieved via the large variety of regulatory subunits, leading to the formation of well over 500 protein phosphatase holoenzyme complexes in mammalian cells.

1.7 Breakdown of cyclic nucleotides: phosphodiesterases

After the discovery of cAMP and the identification of cGMP five years later, there was a need to understand the complete pathway of the two cyclic nucleotides and the role of proteins involved in their breakdown. Around that time the first phosphodiesterase (PDE) was purified and characterized by Butcher and Sutherland from bovine heart[55] and subsequently from several other tissues. In this study it was documented that this enzyme was capable of inactivating cAMP, and that caffeine had an inhibitory effect on its activity.

It was hypothesized that there should be different isoforms of PDEs, distinguished primarily by their substrate specificity and sensitivity to calcium-calmodulin (CaM). These isoenzymes were numbered according to their elucidation order. Beavo et al. differentiated the PDEs in the early 1970s in bovine and rat tissue.[56] Initially, three enzymes were identified and known as CaM-PDE, cAMP-PDE and cGMP-PDE, which were further characterized by the use of selective inhibitors for these enzymes.[57] Only in 1995, Beavo introduced the nomenclature for the PDE family.[58] PDEs exist as two classes (class I and class II) that can hydrolyze the cyclic nucleotides cAMP and cGMP into their 5'-monophosphate derivatives.[59] In mammals and flies, only class I enzymes have been identified, whereas yeast and protozoans contain both classes. A third class (class III) of PDEs which lack specificity for cAMP or cGMP was identified later.[60] Today there are 11 different PDE families known, comprised of 21 genes encoding proteins with an active (and conserved) PDE catalytic domain. Many of the PDEs contain amino-terminal subdomains and N-terminal hydrophobic regions that are important in subcellular localization and interaction with other signaling molecules (Figure 3).[61]

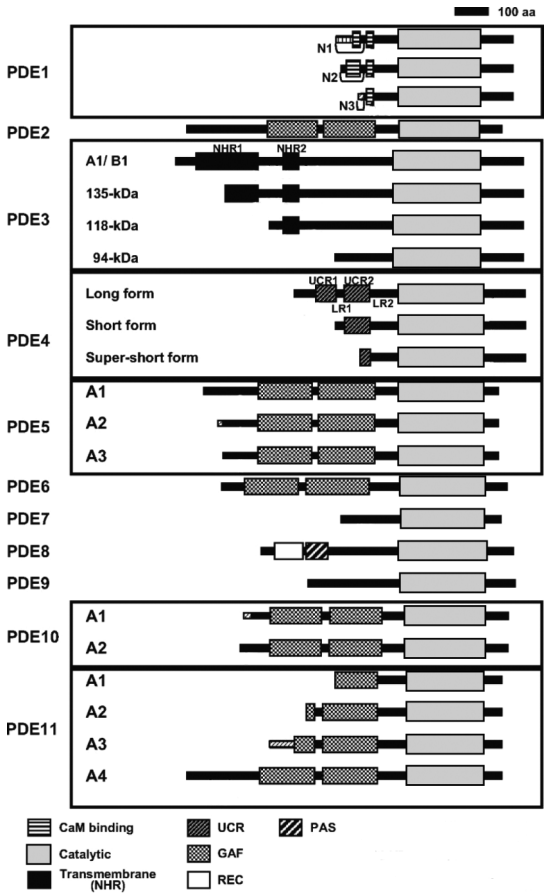

Figure 3 *Schematic representation of the eleven human PDE families. Representative members that constitute the 11 human PDE families are shown here. Each PDE protein is indicated by a thick line. N-terminal variation of PDE1A variants, PDE3 and PDE4 isoforms produced by alternative translation initiation, and splice variants of PDE5, PDE10, and PDE11 families, are boxed. Protein domains are represented by rectangles with patterns. Adapted from Omori et al..*[61]

1.8 Is there crosstalk between cAMP and cGMP?

The similar cyclic nucleotides cAMP and cGMP and their major targets, PKA and PKG, are widely distributed in nature, in particular in animal tissues.

Initial studies of these molecules suggested that cAMP and cGMP were freely distributed throughout the cell with a radius of action of about 220 μm.[62] The concept of cAMP signal compartmentalization as a means to achieve specificity was first introduced in 1981 by Brunton et al. In this pioneering work, it was demonstrated that the cAMP generated by stimulation of different Gs-coupled receptors in cardiac myocytes led to differential activation of the type-I and type-II isoforms of PKA.[63] Nevertheless the similarities between two cyclic nucleotides and their kinases gave

rise to speculations about the specificity for each of their own ligand and to the idea of cross reactivity.[64] In vitro, both cAMP and cGMP can activate PKG and PKA respectively, albeit at a concentration around a ~100-fold higher than the Ka reported for their 'own' kinase.[65] The tight localization of the kinases close to their own pools of cAMP/cGMP through anchoring proteins should largely minimize the cross activation event in vivo.

The complexity of molecular mechanisms that exist in the cell in order to have cAMP and cGMP signals compartmentalization became more clear only in recent years.

For example, the two second messengers regulate several processes such as cardiac function by the activation of PKA and PKG. It has been shown that they exert opposing influence on cardiac function, in part as a consequence of the opposite effects of PKA- and PKG- mediated phosphorylation on target proteins. This can be possible because of the strict compartmentalization of the kinases and their activating cyclic nucleotides.

Protein-protein interactions maintained by anchoring, adapter and scaffolding proteins provide the molecular glue that holds these signal transduction units together. This allowed the discovery of several anchoring proteins and the understanding of their molecular functions. Nevertheless still very little is known about the mechanisms of these proteins and more work needs to be done. The next chapters of this thesis will be focused on the characterization of the interactome of cyclic nucleotide signaling proteins.

2 TARGETED PROTEOMICS TO STUDY KINASE FUNCTION

The word proteomics was coined almost two decades ago in analogy to genomics and denotes the entire complement of proteins expressed in a specific state of an organism or a cell population.[66] In recent years, proteomics technologies have matured immensely through cumulative technological advances in instrumentation, sample preparation and computational analysis with the principal aim to understand how cells function.

A typical shotgun proteomics experiment, aimed to identify as many proteins in a sample as possible typically adopts a workflow consisting of sample preparation, liquid chromatography tandem mass spectrometry (LC-MS/MS) and data analysis. The relative low abundance of protein kinases and protein phosphorylation events necessitated the development of several techniques for more accurate identification of these proteins and their biochemical reactions. These are based either on fractionation, (e.g. ion exchange chromatography or hydrophilic interaction liquid chromatography) or specific enrichment strategies (Figure 4).

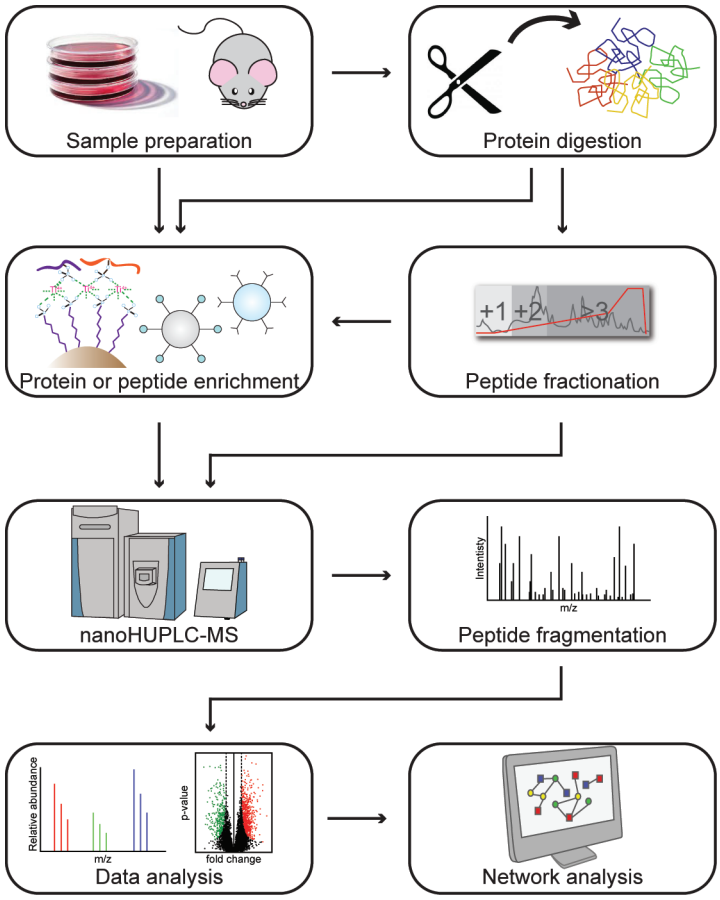

Figure 4 *A general proteomics workflow can be adapted according to particular research questions. In a typical proteomics workflow, proteins are extracted from cells or tissues and proteolytically digested. The peptides can be fractionated and/or subjected to enrichment for a particular PTM before nanoUPLC-MS/MS analysis. Acquired data are then analyzed with dedicated database search programs.*

A major limiting factor for in-depth, comprehensive proteomics profiling is the immense dynamic range of protein concentrations in a biological sample, which spans at least 10 to 12 orders of magnitude. In human plasma, for example, the 22 most abundant proteins are responsible for ~99% of the total mass of proteins, thus leaving thousands of proteins in the remaining 1%.

Current mass spectrometry equipment reaches maximally five orders of concentration depth. Therefore in order to analyze signaling events that may occur on less abundant proteins, more targeted approaches, focused on a specific protein class, pathway or a set of post-translational modifications (PTMs), are still essential. The isolation of selected "targets", such as protein complexes or peptides carrying PTMs yield a lot of additional information, essential for more detailed understanding of cellular function. These strategies are mainly focused on affinity chromatography or

antibody-based immunoprecipitation. The following paragraphs describe a selection of different "targeted" proteomics approaches to identify low abundant phosphopeptides, protein-drug interactions and protein-protein interactions.

2.1 Phosphopeptide enrichment (TiO^2/Ti^{4+}-IMAC)

Understanding how kinases (and phosphatases) regulate phosphorylation events is of particular importance since they are key regulators of protein activity, stability, localization etcetera. However, in a peptide mixture originating from a protein digest, the phosphorylated peptides are of much lower abundance and are therefore often masked by the vast majority of non-modified peptides. Hence, for an in-depth study of protein phosphorylation, enrichment steps ahead of the mass spectrometry analysis are necessary. Almost all developed general phosphopeptide enrichment strategies are based on ionic interaction of the phosphate moiety with a metal ion such as Fe^{3+}, Al^{3+} or Ga^{3+} immobilized on a stationary phase, known under the acronym IMAC for immobilized metal ion affinity chromatography.[67] In principle, the positive metal ion is chelated by an immobilized polydentate ligand to form multiple coordinated bonds towards the negatively charged phosphate moiety under acidic condition. Similarly, metal oxide affinity chromatography (MOAC) is based on porous metal dioxide microspheres that are used as a stationary phase to coordinate the negatively charged oxygen atoms of the phosphate (i.e. TiO_2[68], or ZrO_2[69]). Another strategy, SIMAC, which stands for sequential elution from IMAC, combines the strengths of both IMAC and TiO_2, allowing the enrichment of mono- and multi-phosphorylated peptides from highly complex samples.[70] All these techniques have unlocked the analysis of phosphorylation in a diverse range of studies,[71] however most of these conventional enrichment strategies have a bias towards peptides containing acidic residues. Only more recently another highly specific enrichment method was developed, Ti^{4+}-IMAC. This IMAC method proved to tackle the under-representation of basic phosphopeptides, bringing phosphopeptide enrichment to the next level.[72] A more recent work showed the high potential and the reproducibility of the use of single step Ti^{4+}-IMAC phosphopeptide enrichment to interrogate phosphosite abundance in a whole cell lysate.[73] In chapter 3 this approach will be applied for the quantification of phosphopeptides in a kinase knock-out mouse model.

2.2 The use of immunoprecipitation in (phospho)proteomics

Although the number of detected phosphorylated peptides is nowadays impressive, (some studies report over 20000 phosphosites), the current state-of-the-art general enrichment methodologies are still inclined to identify/quantify the more abundant phosphoproteins/peptides present in a sample.

The need to monitor specific kinase substrate motifs has led to the development of phosphosite specific antibodies. These have proven very useful in Western blotting over the last several decades.[74] In phospho-proteomics such antibodies could also prove useful. In such an approach however, a very tight specificity would limit their

effect, but when generated with a slightly broader specificity such antibodies could enrich for subsets of phosphopeptides with specific motifs or other characteristics. For example, tyrosine phosphorylation, which only comprises ~1% of all phosphorylations is typically underrepresented in large scale phosphoproteomics studies due its relative lower abundance. For this particular case, immunoprecipitation (IP) methodologies using antibodies with general phosphotyrosine specificity can be applied. Such methods have been developed for enrichment at both the protein and the peptide level. Initially both methods have been applied to study protein tyrosine phosphorylation.[75] The antibodies recognize phosphorylated tyrosine residues, with no apparent other sequence requirements. These have proved very successful to isolate tyrosine-phosphorylated proteins or peptides directly from a total cell/tissue lysate or a full protein digest respectively. Today, the peptide-based approach is preferred by most labs as this yields both protein and phoshposite-specific information. Careful evaluation has revealed that the results of this approach are largely complementary to the general phosphopeptide enrichment techniques described above.

More recently, the peptide-IP toolbox was expanded to phosphorylated serine and threonine motifs.[76,77] Different kinases recognize different AA motifs and the identification of responsible kinases for specific sites is still a big challenge for the field. Nevertheless the use of antibodies that selectively immunoprecipitate peptides containing the target sequences of particular basophilic kinases of interest, such as the PKA motifs[78] and AKT[76] is nowadays possible.

The use of antibodies can also be extended towards immunoprecipitation of a target protein and its interactors. This technique, also referred to as AP-MS or IP-MS, can be applied on the endogenous protein present in cell or tissue lysates, although it should be mentioned that the main drawback is the requirement of a very specific and clean antibody, which is not the case for most proteins. Some examples of immunoprecipitation are the GFP IP and the Strep-tag IP, where the proteins of interest are tagged with the green fluorescent protein (GFP)[79] or an eight-residues peptide sequence[80] respectively. The IPs are performed with a high specificity GFP antibody conjugate on a solid support, or streptavidin immobilized on a resin. Another example of immunoprecipitation is the tandem affinity purification (TAP-tag method), in which a particular protein of interest is expressed in cells with a TAP-tag. A general TAP-tag consists of two IgG binding domains of Protein A and a calmodulin binding peptide separated by a TEV protease cleavage site. Interacting proteins of the tagged protein can be identified after tandem affinity purification. The power of this methodology consist in the presence of two tags that can be enriched sequentially. In this way the pull down is cleaned up and experiences less contamination with background proteins, and only the proteins that interact with the bait are enriched. Typical drawbacks of a TAP-tag experiment can be related to the presence of the tag which can cause mislocation of the overexpressed proteins, away from the protein's endogenous targets. Misfolding due to the tag may also negate the binding of the endogenous interaction partners. In addition, it has only proved applicable in cell models.

2.3 Chemical proteomics

Chemical proteomics is a technique to study the interaction between small molecules and proteins. As such, it is very useful to identify small molecule target proteins under close to physiological conditions.[81,82] It can also be applied for resolving the makeup of protein complexes or to profile the presence of particular protein classes within different cell lines or tissues. Chemical proteomics approaches can be distinguished in two different main forms; (i) activity- and affinity-based protein profiling (ABPP),[83] which employs small molecules as probes to covalently capture a distinct class of proteins and (ii) affinity-chromatography based on immobilized small molecules, where immobilized (small) molecules such as enzyme inhibitors or small peptides[84-86] can be used for affinity enrichment of interacting proteins (Figure 5).

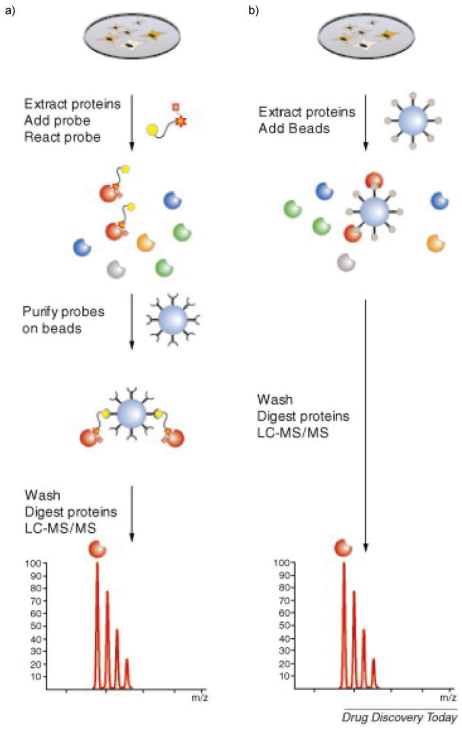

Figure 5 *a) Activity-based protein profiling workflow: after protein extraction, the lysate is incubated with a small molecular probe that covalently attaches to its targets. In the second step, probes and targets are purified using affinity chromatography before digestion and LC–MS/MS analysis. b) Affinity-chromatography based on immobilized small molecules. In this case the compounds of interest are modified and immobilized on a solid support. The immobilized drug is subsequently incubated with a lysate of choice to specifically purify target proteins that are then analyzed by LC–MS/MS. Figure adapted from Bantscheff et al..*[82]

Activity-based protein profiling via reactive probes designed specifically to bind to active sites of target enzymes was pioneered by the Cravatt laboratory. In this ap-

proach the reactive probe is typically fused to an affinity tag, such as biotin, via a linker. In principle, the small molecule probe is incubated with the biological sample and allowed to covalently attach to the proteins it has affinity for. Subsequently the formed probe-protein conjugates are captured using the affinity tag. Many probes have been developed for a variety of enzyme classes, including, proteases,[87] kinases,[88] phosphatases,[89] glycosidases,[90] histone deacetylases,[91] and deubiquitinating enzymes.[92] Moreover several probes have been synthetized with photo-activatable groups by which the probe binds covalently to its protein targets only when the sample is exposed to light with the proper wavelength. In this way, proteins and probe can be appropriately equilibrated in the dark before covalent coupling is induced. This reduces the binding of contaminants and optimizes the binding of specific targets to the probe.[91]

The affinity-chromatography approach depends on the immobilization of small molecules on a resin such as agarose beads. In this case no reactive group is required, since the compound of interest is first immobilized on a solid support and then incubated with a protein lysate to identify its targets. Different coupling chemistries and spacer lengths can be used to optimize binding conditions. Proteins are captured non-covalently and can be eluted from the affinity matrix by excess, free probe compound or denaturating conditions. Successful applications of the non-covalent approach include the selective enrichment of various kinases. One of the most successful uses of this technique is the application in drug selectivity profiling. To this effect, the resins are designed to bind tens to hundreds of proteins within the same protein class via their structurally related active sites. A nice example of this approach are the "kinobeads", where a set of 6 different non-selective kinase inhibitors were immobilized on the same resin. From different cell lines and tissues, close to 200 different kinases could be captured using these broad inhibitors as a general kinase bait. To profile the specificity of novel kinase inhibitors, the cell/tissue lysate was incubated with the novel lead compounds prior to kinase capture by the kinobeads. Quantitative MS was then used to profile which kinases were no longer captured by the beads in a dose-dependent manner. In this way it is possible to screen kinase inhibitor drug candidates in disease relevant human cells and even (diseased) tissue, i.e. in almost (patho)physiological conditions.[84] A similar approach was performed by Wissing and colleagues, where they used four different kinase-selective affinity resins with distinct target specificities to isolate a large variety of protein kinases.[93] Chemical proteomics can also be used for the identification of secondary interactors, i.e. proteins interacting with the primary protein target of the small molecule. For example, when capturing PKA with immobilized cAMP a large selection of AKAPs could be identified.[85] Aye et al. discovered that a substituted cAMP analog (8-AHA-2-OMe-cAMP) can distinguish between PKA-R type I and II and does not bind to PKG at all, allowing an even more focused interactome analysis of the two different PKA isoforms.[94] This method enabled the characterization of AKAPs that bind only to PKA-RI, i.e. SKIP[16] and smAKAP,[17] which were up to then not known to exist. The affinity based chemical proteomics setup is applied and further characterized in this

thesis to specifically study PKG, PKA and PDE interactomes.

3 MASS SPECTROMETRY

Mass spectrometry has earned a central role in proteomics for the identification of peptides and their originating proteins. Peptides can be identified based on the mass to charge ratio (m/z) of the precursor ion in combination with the m/z of the product ions obtained by fragmenting the precursor in MS/MS mode. In order to be introduced in the mass spectrometer the proteins or peptides must be converted to gas-phase ions without extensive degradation. This is made possible through soft ionization techniques such as electrospray ionization (ESI)[95] or matrix-assisted laser desorption ionization (MALDI).[96] Several types of mass analyzers with different characteristics such as mass range, analysis speed, resolution, dynamic range and sensitivity, exist. The mass spectrometers of major importance for proteomics include quadrupoles,[97] time-of-flight instruments,[98] ion traps,[99] Fourier transform ion cyclotron resonance machines (FT-ICR)[100] and the relatively newer Orbitrap.[101] The latter instrument was mostly used for the research described in this thesis.

3.1 Orbitrap mass spectrometer

The orbitrap mass analyzer is the most recently developed mass analyzer that employs orbital trapping as a novel method for m/z analysis. In 2000 Makarov designed the first Orbitrap where he proposed the principle of trapping ions based on the Kingdon trap[102] that was first described in 1923.

The Orbitrap, consists of an inner axial electrode surrounded by a barrel-shaped outer electrode. A constant electric potential is applied to both electrodes. Because opposing surfaces in the Orbitrap are nonparallel, the electric field between the two electrodes varies along the z-axis (quadro-logarithmic field) that forces the ions to circulate around the central electrode on stable trajectories while also oscillating along the z-axis with a frequency that depends only on the m/z (Figure 6). The ion oscillations in the orbitrap induce an image current on the outer electrodes that is recorded over time by a differential amplifier connected to the two halves. Because these frequencies are mass and charge dependent, fast Fourier transform (similar to FT-ICR signal processing[103]) can be used to convert time-domain signal into mass spectra with high resolution (routinely 60 000, going up to 450 000) and high mass accuracy (<2 ppm).

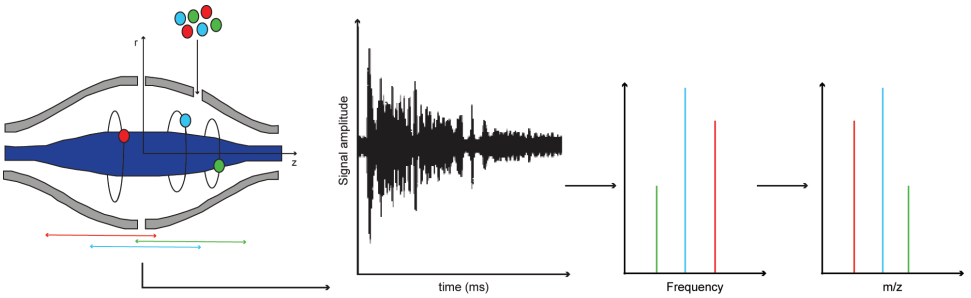

Figure 6 *Working principle of the Orbitrap mass analyzer: the ions move in spiral orbits around the inner electrode while their image current, which is recorded at the outer electrodes, is converted in frequency using Fourier transformation and subsequently converted in m/z values.*

External accumulation and injection of ions as confined packets turned out to be key challenges when coupling the Orbitrap analyzer to a continuous ion source. Today the hybrid LTQ-Orbitrap Velos,[104] and the more recent Orbitrap Elite[105] are ones of the most frequently used configurations in many proteomics labs, together with the newly developed hybrid Q-Orbitrap.[106]

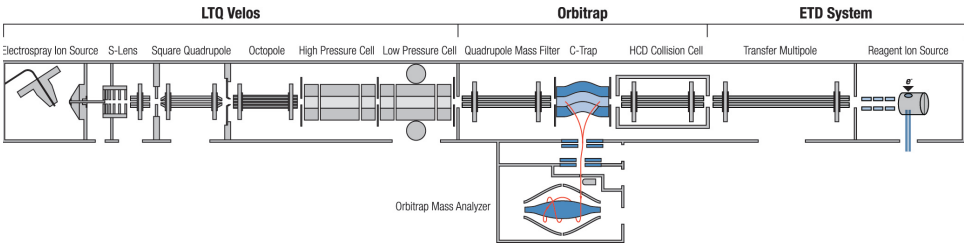

Figure 7 *Schematic overview of the hybrid LTQ-Orbitrap Velos instrument. Figure adapted from*[107].

The LTQ-Orbitrap Velos instrument consists of a dual-pressure ion trap, where two identical linear ion traps operate at different gas pressure regime. The first trap is held at higher pressure for improved trapping and fragmentation whereas the second trap is kept at lower pressure for enhanced scanning capabilities. The dual-pressure ion trap is coupled via a transfer multipole to the C-trap. From there, ions are sent in packages to the Orbitrap mass analyzer for the MS1 acquisition.
The fragmentation of the peptide ions can be done either in the ion trap, using collision induced dissociation (CID), or in the higher-energy collisional dissociation (HCD) chamber that is directly attached to the C-trap. A negative chemical ionization source, enabling electron transfer dissociation (ETD), can be mounted at the rear of the instrument.
The combination with different fragmentation techniques such as electron transfer dissociation (ETD[108]) or EThcD[109] makes the Orbitrap a versatile instrument for the

analysis of different types of samples (e.g. phosphorylated or glycosylated peptides, or bigger molecules such as intact proteins or protein complexes[110]).

4 QUANTITATIVE PROTEOMICS

Observing as many different proteins in a single cell type or tissue is a first qualitative step to obtain insight into a biological system under study. Since mass spectrometry is not quantitative by nature, different strategies have been developed to enable the comparison between different cell states, e.g. healthy versus diseased, or for the evaluation of the influence of systematic perturbation of the proteome. The quantification strategies can be divided into two groups namely absolute or relative quantitation. The first strategy is based on the introduction of a labelled standard (heavy synthetic peptides), often referred to as AQUA,[111] in each sample to determine the ratio between endogenous and standard peptide. Absolute quantification has been proposed also in a label free fashion in several studies, such as the top 3 method[112] (in which the protein abundance (e.g. in mg/mL) is calculated using the average intensity of the 3 most abundant peptide precursor ions identified) and the intensity based absolute quantification, also called iBAQ (in which the protein abundance is calculated as the sum of all the peptide precursor ions identified, normalized by the number of theoretically observable peptides).[113] The relative quantification can also be divided in two sub groups: label free and stable isotope labeling techniques. Both strategies are based on the comparison of physicochemically identical peptides from different origins (Figure 8).

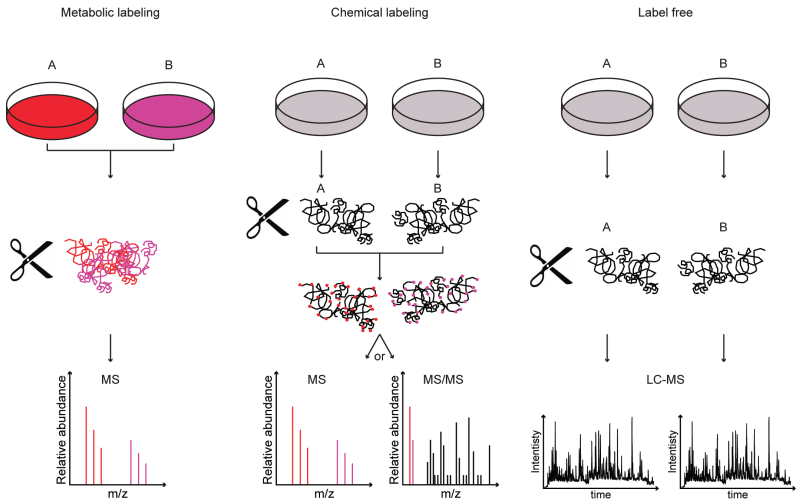

Figure 8 *Quantitative mass spectrometry-based proteomics strategies. A and B represent two experimental conditions to be quantitatively compared. Red and purple indicate the presence of light and heavy isotopes in the samples and in the resulting mass spectra. The quantification generally occurs by comparing precursor ion intensities in MS1 scan except for isobaric labeling, where reporter ions in the low mass region of the MS/MS spectra reflect the relative peptide abundances.*

4.1 Isotope labeling based quantification

Labeling in quantitative MS is based on the incorporation of different stable isotopes to distinguish between samples. Replacing isotopes introduces a difference in the mass of a compound that can be distinguished in the mass spectrometer, while minimally affecting chemical properties or biology. The most frequently used methods for the introduction of the heavy isotope (e.g. ^{2}H, ^{18}O, ^{15}N, ^{13}C) are described below.
One of the most commonly used metabolic labeling strategies is SILAC (Stable Isotope Labeling of Amino acid in Cell culture).[114] This strategy uses amino acids with specific heavy atoms that are incorporated into proteins during synthesis in the cell, and therefore allows the labeling of the entire proteome of cultured cells. In proteomics experiments heavy arginine and lysine are most often used since every tryptic peptide will then contain a label (except for C-terminal peptides). Even though the SILAC approach has been extended to whole animals[115] and towards the analysis of human tissue,[116] several factors are limiting its use. These include the cost and time for maintaining the model system on expensive media as well as the inability of certain cell lines and organisms to implement the labels. Another type of metabolic labeling is the use of ^{15}N, ^{13}C, and or ^{18}O instead of the naturally abundant ^{14}N, ^{12}C and ^{16}O isotopes. This type of labeling, is still used for the analysis of microorganisms such as bacteria and yeast, or to a lesser extent, higher multicellular organisms, such as Arabidopsis thaliana, C. elegans and D. melanogaster.[117] However this strategy is not commonly used in proteomics since the number of heavy isotopes vary from peptide to peptide thus complicating the subsequent data analysis. Chemical labeling after the biosynthesis of the proteins has become widely used in proteomics as well. There is a big variety in isotopic labels that can be introduced at different stages of the proteomics workflow. The most popular chemical labels target primary amines. For instance the isobaric tags termed tandem mass tag (TMT) and the isobaric tags for relative and absolute quantification (iTRAQ).[118] In both these comparable methods the differential tags are designed in such a way that in each condition the peptides have the exact same precursor mass and thus are indistinguishable at the MS1 level. Upon fragmentation of the labeled peptides, the isobaric tags fall apart and release their different reporter ions in the low mass region of the tandem mass spectrum. The benefit of this approach is its superior multiplexing capability of up to 10 samples, whereas most of the metabolic labeling approaches only allows up to 3 conditions to be compared. However, the MS/MS-based quantification of reporter ions suffers from the possibility of co-isolation and fragmentation of similar precursor ions that may distort the ratios of the peaks and negatively influencing the accuracy. This problem can be tackled with a multistage MS3-based approach, however at the expense of acquisition speed.[119]
Another method used for fast and largely complete labeling is stable isotope dimethyl labeling.[120] As for the methods described above, also here the primary amines of peptides, i.e. N-termini and lysine side chains, are labeled. Basically, formaldehyde and cyanoborohydride with a different number of ^{13}C and deuterium atoms are used to create dimethylated peptides with duplex and triplex reactions that introduce a mass

difference of 4 Da between each sample (Figure 9).

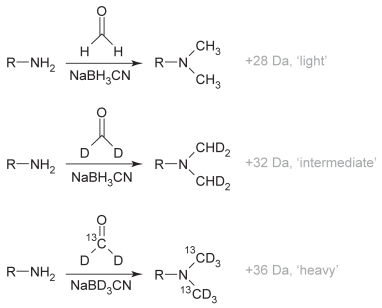

Figure 9 *Labeling scheme for stable isotope dimethyl labeling. The reaction is performed at neutral pH, and involves the formation of a Schiff base via the reaction of formaldehyde with primary amines which is then reduced by cyanoborohydride. Using different isotopomers of formaldehyde the added mass can be varied. Adapted from Boersema et al. Nature protocol, 2009.*

The features that make this technique attractive are the low cost reagents, its applicability to any type of biological sample, including human tissue and the application to a very broad range of protein quantities (from μg up to mg) with the same protocol. One of the limitations using this type of labeling is the slight difference in the chemical properties of the deuterium based labels and thus the labeled peptides, which can lead to small retention time shifts during LC-MS/MS analysis. This potentially compromises the accuracy of the quantification.[121]

4.2 Label-free quantification

Label free quantitative methods are based on the comparison of peptide abundances between different samples in separate LC-MS/MS runs without the use of stable isotope labels. This quantification technique can be divided into two methods: the first one, called spectral counting, is based on the consideration that the number of peptide spectrum matches (PSMs) obtained for each protein correlates with that protein's quantity in the sample. The second method, called intensity-based label-free quantification, employs the full scan signal response of intact peptides.[122]
Compared to the stable isotope labeling techniques, the label free quantification techniques have some particular advantages: (i) the number of conditions that can be analyzed is not predefined; (ii) the sample preparation is more straightforward, since it does not require any isotope labeling steps; (iii) this technique can be applied to samples from any kind of origin. The limitations reside in the increase of instrument analysis time (each sample is run separately), and in the requirement for very high reproducibility through the entire sample analysis pipeline (e.g. sample lysis and digestion variability) and at the LC-MS/MS level (e.g. peptide retention time shifts or

ionization variability).

4.3 Data analysis

Peptide fragment fingerprinting (PFF) is the MS approach widely used to identify peptide sequences through fragment ions. The acquired MS/MS spectra contain information concerning the peptide sequence and consequently protein identity. However, as single LC-MS/MS runs nowadays typically generate tens of thousands of spectra, manual interpretation of MS/MS data is no longer feasible. In order to assign spectra to peptides in a more automated way, the MS/MS spectra can be converted to a list of accurate masses and matched against theoretical spectra created from protein sequences of the organism being studied. These are generated from the gene-annotated genome sequence. To facilitate the database searching, several database search algorithms have been developed, such as Sequest,[123] Mascot,[124] and Andromeda.[125]
Depending on the experimental conditions, several parameters in a peptide database search are defined by the user. These include enzyme specificity, fixed and variable modifications e.g. phosphorylation, glycosylation and the mass tolerance, which depends on the MS system and settings that were used. Each search engines operates relatively similarly. First it generates in silico fragment masses for each peptide originating from a protein sequence present in the database within the limits of the setting defined by the user, as discussed above. It then matches the experimental precursor m/z to the list of hypothetical peptides. Then a hypothetical MS/MS spectrum is generated for these candidates and compared to the experimental MS/MS spectra. The best matching sequences to the spectrum are assigned with a score reflecting the similarity and thus confidence of identification. However, when matching tens of thousands spectra to millions of possible candidates the chance of obtaining random incorrect hits is quite high. The amount of random hits can be reduced by lowering the amount of possible sequence candidates by decreasing the mass tolerance for precursor and fragment matching and can be achieved by employing high accuracy mass analyzers. Even so, the amount of data will always result in false-positives. The reliability of peptide identification for large scale experiments can be estimated from a proportion of false positives presented in the results, also called false discovery rate (FDR). The most common strategy to measure FDR is to use a peptide database calculated from the actual sequences of proteins involved in the experiment concatenated with a reversed or randomized version of that same database. Typically an FDR of 1 % is accepted for large-scale proteomics experiments.[126]
Another major challenge in the data analysis is the confident localization of the phosphorylation sites. Phosphopeptide identification is feasible through sufficient peptide backbone fragments, however it can still be challenging to pinpoint the exact phosphosite when multiple serine, threonine and tyrosine residues are present. Unambiguous phosphosite localization is highly dependent on the presence of a series of fragment ions that carry the phosphate group. Previously, manual interpretation was the method of choice however with current numbers of identified phosphopeptides

exceeding the 10,000 mark in a typical high throughput experiment this is no longer possible. The absence of an algorithm that allows PTM site assignments in the most common used database search engines paved the way for the development of new PTMs computational scoring tools. These include the Ascore,[127] and the highly similar PTM score for CID fragmentation,[128] the SloMo[129] method, for ECD and ETD fragmentation, the Mascot delta (MD) ion score[130] and the recently developed phosphoRS,[131] which presently is uniquely compatible with CID, HCD, ETD and EThCD.

5 THESIS OUTLINE

Understanding the molecular mechanisms which regulate signal transduction is fundamental to the development of therapeutic molecules for the treatment of several diseases. In particular, signaling proteins, such as cyclic nucleotide dependent enzymes are the orchestrators of many tissue functions. As a consequence, their function and behavior are complex and dynamic, with constant activation and deactivation through protein modification, allowing the system to quickly achieve equilibrium where cell function is optimal to face the environmental conditions. This thesis describes the development of chemical-proteomics technology and the use of the most recent (phospho)proteomics techniques to increase our knowledge of cyclic nucleotide signaling pathways.

In particular cGMP and its related kinase are understudies compared to the cAMP and PKA, hence also the characterization of the direct PKG interactome and its downstream targets are not well known.

In **Chapter 2**, we describe a competitive chemical proteomics approach for the identification of new GKAPs. Among the proteins enriched we were able to identify a known GKAP, IRAG, and a new GKAP, the Huntingtin associated protein (HAP1). To confirm the interaction between HAP1 and PKGIβ we performed binding affinity assay using fluorescence anisotropy and mutations on the HAP1 region that binds to PKG. Moreover we docked the proposed GKAP binding domain of HAP1 onto PKGIβ to compare it with the known GKAPs, demonstrating that the proteins not only contain a similar domain but interact in a similar manner with PKG.

The importance of PKG cerebellar signaling is evaluated in **Chapter 3**, where a quantitative (phospho)proteomics approach is applied in a PKG knock-out mouse model. After the identification of several interesting differentially regulated (phospho) proteins a more targeted validation was performed using western blot and immunohistochemistry. The main observation in this study is that the loss of PKG induces regulation of several proteins associated with cyclic nucleotide and Ca^{2+} signaling pathways. These are then connected with the impaired motility and memory, that these knock-out mice present.

Understanding how kinase levels change in a relevant disease context, such as heart failure, can be achieved with chemical proteomics. **Chapter 4** illustrates the use of this technique, combined with label free mass spectrometry to identify the variation of PKA/AKAP levels and their localization during the evolution of cardiac remod-

eling in progression to heart failure. For this study we used a rat model of pressure overload.

Immobilized inhibitors on agarose beads are a good alternative for the use of cyclic nucleotides for the isolation of cAMP and cGMP regulated proteins other than PKA and PKG. **Chapter 5** focuses on the use of IBMX, an unspecific phosphodiesterase inhibitor, to capture various phosphodiesterases and their interactomes. The combination of our pull down with the use of specific PDEs inhibitors shed more light on the interactome of PDEs in HeLa cells.

REFERENCES

(1) Cori, C. F.; Schmidt, G.; Cori, G. T. *Science* **1939**, *89*. 464-5.
(2) Burnett, G.; Kennedy, E. P. *J Biol Chem* **1954**, *211*. 969-80.
(3) Cohen, P.; Antoniw, J. F. *FEBS Lett* **1973**, *34*. 43-7.
(4) Manning, G.; Whyte, D. B.; Martinez, R.; Hunter, T.; Sudarsanam, S. *Science* **2002**, *298*. 1912-34.
(5) Rall, T. W.; Sutherland, E. W. *J Biol Chem* **1958**, *232*. 1065-76.
(6) Fischer, E. H.; Krebs, E. G. *J Biol Chem* **1955**, *216*. 121-32.
(7) Kuo, J. F.; Greengard, P. *J Biol Chem* **1969**, *244*. 3417-9.
(8) Walsh, D. A.; Perkins, J. P.; Krebs, E. G. *J Biol Chem* **1968**, *243*. 3763-5.
(9) Reimann, E. M.; Walsh, D. A.; Krebs, E. G. *J Biol Chem* **1971**, *246*. 1986-95; Corbin, J. D.; Keely, S. L.; Soderling, T. R.; Park, C. R. *Adv Cyclic Nucleotide Res* **1975**, *5*. 265-79.
(10) Kuo, J. F.; Greengard, P. *Proc Natl Acad Sci U S A* **1969**, *64*. 1349-55.
(11) Uhler, M. D.; Carmichael, D. F.; Lee, D. C.; Chrivia, J. C.; Krebs, E. G.; McKnight, G. S. Proc Natl Acad Sci U S A **1986**, *83*. 1300-4; Johnson, D. A.; Akamine, P.; Radzio-Andzelm, E.; Madhusudan, M.; Taylor, S. S. *Chem Rev* **2001**, *101*. 2243-70.
(12) Zaccolo, M.; Pozzan, T. *Science* **2002**, *295*. 1711-5.
(13) Theurkauf, W. E.; Vallee, R. B. *J Biol Chem* **1982**, *257*. 3284-90.
(14) Lohmann, S. M.; DeCamilli, P.; Einig, I.; Walter, U. *Proc Natl Acad Sci U S A* **1984**, *81*. 6723-7.
(15) Carr, D. W.; Stofko-Hahn, R. E.; Fraser, I. D.; Bishop, S. M.; Acott, T. S.; Brennan, R. G.; Scott, J. D. *J Biol Chem* **1991**, *266*. 14188-92.
(16) Kovanich, D.; van der Heyden, M. A.; Aye, T. T.; van Veen, T. A.; Heck, A. J.; Scholten, A. *Chembiochem* **2010**, *11*. 963-71.
(17) Burgers, P. P.; Ma, Y.; Margarucci, L.; Mackey, M.; van der Heyden, M. A.; Ellisman, M.; Scholten, A.; Taylor, S. S.; Heck, A. *J. J Biol Chem* **2012**, *287*. 43789-97.
(18) Kinderman, F. S.; Kim, C.; von Daake, S.; Ma, Y.; Pham, B. Q.; Spraggon, G.; Xuong, N. H.; Jennings, P. A.; Taylor, S. S. *Mol Cell* **2006**, *24*. 397-408; Gold, M. G.; Lygren, B.; Dokurno, P.; Hoshi, N.; McConnachie, G.; Tasken, K.; Carlson, C. R.; Scott, J. D.; Barford, D. *Mol Cell* **2006**, *24*. 383-95.
(19) Drummond, G. I.; Perrott-Yee, S. *J Biol Chem* **1961**, *236*. 1126-9.
(20) Ashman, D. F.; Lipton, R.; Melicow, M. M.; Price, T. D. *Biochem Biophys Res Com-*

mun **1963**, *11*. 330-4.
(21) Sutherland, E. W. *Science* **1972**, *177*. 401-8.
(22) Hardman, J. G.; Sutherland, E. W. *J Biol Chem* **1969**, *244*. 6363-70.
(23) Ignarro, L. J.; Buga, G. M.; Wood, K. S.; Byrns, R. E.; Chaudhuri, G. *Proc Natl Acad Sci U S A* **1987**, *84*. 9265-9; Murad, F. *J Clin Invest* **1986**, *78*. 1-5.
(24) Kuno, T.; Andresen, J. W.; Kamisaki, Y.; Waldman, S. A.; Chang, L. Y.; Saheki, S.; Leitman, D. C.; Nakane, M.; Murad, F. *J Biol Chem* **1986**, *261*. 5817-23.
(25) Glass, D. B.; Krebs, E. G. *J Biol Chem* **1979**, *254*. 9728-38.
(26) Lincoln, T. M.; Dills, W. L., Jr.; Corbin, J. D. *J Biol Chem* **1977**, *252*. 4269-75.
(27) Monken, C. E.; Gill, G. N. *J Biol Chem* **1980**, *255*. 7067-70.
(28) Wernet, W.; Flockerzi, V.; Hofmann, F. *FEBS Lett* **1989**, *251*. 191-6.
(29) Wolfe, L.; Francis, S. H.; Corbin, J. D. *J Biol Chem* **1989**, *264*. 4157-62.
(30) de Jonge, H. R. *Adv Cyclic Nucleotide Res* **1981**, *14*. 315-33.
(31) Francis, S. H.; Corbin, J. D. *Crit Rev Clin Lab Sci* **1999**, *36*. 275-328.
(32) Richie-Jannetta, R.; Francis, S. H.; Corbin, J. D. *J Biol Chem* **2003**, *278*. 50070-9.
(33) Sharma, A. K.; Zhou, G. P.; Kupferman, J.; Surks, H. K.; Christensen, E. N.; Chou, J. J.; Mendelsohn, M. E.; Rigby, A. C. *J Biol Chem* **2008**, *283*. 32860-9.
(34) Casteel, D. E.; Smith-Nguyen, E. V.; Sankaran, B.; Roh, S. H.; Pilz, R. B.; Kim, C. *J Biol Chem* **2010**, *285*. 32684-8.
(35) Schulman, H.; Greengard, P. *Nature* **1978**, *271*. 478-9.
(36) Schulman, H.; Greengard, P. *Proc Natl Acad Sci U S A* **1978**, *75*. 5432-6; Sieghart, W.; Forn, J.; Greengard, P. *Proc Natl Acad Sci U S A* **1979**, *76*. 2475-9.
(37) Kennedy, M. B.; Greengard, P. *Proc Natl Acad Sci U S A* **1981**, *78*. 1293-7.
(38) Kennedy, M. B.; McGuinness, T.; Greengard, P. *J Neurosci* **1983**, *3*. 818-31; McGuinness, T. L.; Lai, Y.; Greengard, P.; Woodgett, J. R.; Cohen, P. *FEBS Lett* **1983**, *163*. 329-34.
(39) Zha, M.; Zhong, C.; Ou, Y.; Han, L.; Wang, J.; Ding, J. *PLoS One* **2012**, *7*. e44828; Hook, S. S.; Means, A. R. *Annu Rev Pharmacol Toxicol* **2001**, *41*. 471-505.
(40) Tombes, R. M.; Faison, M. O.; Turbeville, J. M. *Gene* **2003**, *322*. 17-31.
(41) Chao, L. H.; Stratton, M. M.; Lee, I. H.; Rosenberg, O. S.; Levitz, J.; Mandell, D. J.; Kortemme, T.; Groves, J. T.; Schulman, H.; Kuriyan, *J. Cell* **2011**, *146*. 732-45.
(42) Takai, Y.; Kishimoto, A.; Inoue, M.; Nishizuka, Y. *J Biol Chem* **1977**, *252*. 7603-9.
(43) Inoue, M.; Kishimoto, A.; Takai, Y.; Nishizuka, Y. *J Biol Chem* **1977**, *252*. 7610-6.
(44) Takai, Y.; Kishimoto, A.; Kikkawa, U.; Mori, T.; Nishizuka, Y. *Biochem Biophys Res Commun* **1979**, *91*. 1218-24.
(45) Collett, M. S.; Erikson, R. L. *Proc Natl Acad Sci U S A* **1978**, *75*. 2021-4; Levinson, A. D.; Oppermann, H.; Levintow, L.; Varmus, H. E.; Bishop, J. M. *Cell* **1978**, *15*. 561-72.
(46) Hunter, T.; Sefton, B. M. *Proc Natl Acad Sci U S A* **1980**, *77*. 1311-5.
(47) Carpenter, G.; King, L., Jr.; Cohen, S. *J Biol Chem* **1979**, *254*. 4884-91.
(48) Ushiro, H.; Cohen, S. *J Biol Chem* **1980**, *255*. 8363-5.
(49) Wilks, A. F.; Harpur, A. G.; Kurban, R. R.; Ralph, S. J.; Zurcher, G.; Ziemiecki, A. *Mol Cell Biol* **1991**, *11*. 2057-65.

(50) Huang, F. L.; Glinsmann, W. H. *Eur J Biochem* **1976**, *70*. 419-26.
(51) Cohen, P.; Nimmo, G. A.; Antoniw, J. F. *Biochem J* **1977**, *162*. 435-44.
(52) Shi, Y. *Cell* **2009**, *139*. 468-84.
(53) Cohen, P. T. *J Cell Sci* **2002**, *115*. 241-56.
(54) Eichhorn, P. J.; Creyghton, M. P.; Bernards, R. *Biochim Biophys Acta* **2009**, *1795*. 1-15.
(55) Butcher, R. W.; Sutherland, E. W. *J Biol Chem* **1962**, *237*. 1244-50.
(56) Beavo, J. A.; Hardman, J. G.; Sutherland, E. W. *J Biol Chem* **1970**, *245*. 5649-55.
(57) Hidaka, H.; Endo, T. *Adv Cyclic Nucleotide Protein Phosphorylation Res* **1984**, *16*. 245-59; Nicholson, C. D.; Challiss, R. A.; Shahid, M. *Trends Pharmacol Sci* **1991**, *12*. 19-27.
(58) Beavo, J. A. *Physiol Rev* **1995**, *75*. 725-48.
(59) Beavo, J. A.; Brunton, L. L. *Nat Rev Mol Cell Biol* **2002**, *3*. 710-8; Lugnier, C. *Pharmacol Ther* **2006**, *109*. 366-98.
(60) Richter, W. *Proteins* **2002**, *46*. 278-86.
(61) Omori, K.; Kotera, *J. Circ Res* **2007**, *100*. 309-27.
(62) Kasai, H.; Petersen, O. H. *Trends Neurosci* **1994**, *17*. 95-101.
(63) Brunton, L. L.; Hayes, J. S.; Mayer, S. E. *Adv Cyclic Nucleotide Res* **1981**, *14*. 391-7.
(64) Pelligrino, D. A.; Wang, Q. *Prog Neurobiol* **1998**, *56*. 1-18.
(65) Poppe, H.; Rybalkin, S. D.; Rehmann, H.; Hinds, T. R.; Tang, X. B.; Christensen, A. E.; Schwede, F.; Genieser, H. G.; Bos, J. L.; Doskeland, S. O.; Beavo, J. A.; Butt, E. *Nat Methods* **2008**, *5*. 277-8.
(66) Wilkins, M. R.; Pasquali, C.; Appel, R. D.; Ou, K.; Golaz, O.; Sanchez, J. C.; Yan, J. X.; Gooley, A. A.; Hughes, G.; Humphery-Smith, I.; Williams, K. L.; Hochstrasser, D. F. *Biotechnology (N Y)* **1996**, *14*. 61-5.
(67) Posewitz, M. C.; Tempst, P. *Anal Chem* **1999**, *71*. 2883-92; Villen, J.; Gygi, S. P. *Nat Protoc* **2008**, *3*. 1630-8.
(68) Pinkse, M. W.; Uitto, P. M.; Hilhorst, M. J.; Ooms, B.; Heck, A. J. *Anal Chem* **2004**, *76*. 3935-43.
(69) Kweon, H. K.; Hakansson, K. *Anal Chem* **2006**, *78*. 1743-9.
(70) Thingholm, T. E.; Jensen, O. N.; Robinson, P. J.; Larsen, M. R. *Mol Cell Proteomics* **2008**, *7*. 661-71.
(71) Huttlin, E. L.; Jedrychowski, M. P.; Elias, J. E.; Goswami, T.; Rad, R.; Beausoleil, S. A.; Villen, J.; Haas, W.; Sowa, M. E.; Gygi, S. P. *Cell* **2010**, *143*. 1174-89; Van Hoof, D.; Munoz, J.; Braam, S. R.; Pinkse, M. W.; Linding, R.; Heck, A. J.; Mummery, C. L.; Krijgsveld, *J. Cell Stem Cell* **2009**, *5*. 214-26.
(72) Zhou, H.; Low, T. Y.; Hennrich, M. L.; van der Toorn, H.; Schwend, T.; Zou, H.; Mohammed, S.; Heck, A. J. *Mol Cell Proteomics* **2011**, *10*. M110 006452; Zhou, H.; Ye, M.; Dong, J.; Corradini, E.; Cristobal, A.; Heck, A. J.; Zou, H.; Mohammed, S. *Nat Protoc* **2013**, *8*. 461-80.
(73) de Graaf, E. L.; Giansanti, P.; Altelaar, A. F.; Heck, A. J. *Mol Cell Proteomics* **2014**.
(74) Gronborg, M.; Kristiansen, T. Z.; Stensballe, A.; Andersen, J. S.; Ohara, O.; Mann, M.; Jensen, O. N.; Pandey, A. *Mol Cell Proteomics* **2002**, *1*. 517-27.
(75) Salomon, A. R.; Ficarro, S. B.; Brill, L. M.; Brinker, A.; Phung, Q. T.; Ericson,

C.; Sauer, K.; Brock, A.; Horn, D. M.; Schultz, P. G.; Peters, E. C. *Proc Natl Acad Sci U S A* **2003**, *100*. 443-8; Boersema, P. J.; Foong, L. Y.; Ding, V. M.; Lemeer, S.; van Breukelen, B.; Philp, R.; Boekhorst, J.; Snel, B.; den Hertog, J.; Choo, A. B.; Heck, A. J. *Mol Cell Proteomics* **2010**, *9*. 84-99; Rush, J.; Moritz, A.; Lee, K. A.; Guo, A.; Goss, V. L.; Spek, E. J.; Zhang, H.; Zha, X. M.; Polakiewicz, R. D.; Comb, M. J. *Nat Biotechnol* **2005**, *23*. 94-101.

(76) Moritz, A.; Li, Y.; Guo, A.; Villen, J.; Wang, Y.; MacNeill, J.; Kornhauser, J.; Sprott, K.; Zhou, J.; Possemato, A.; Ren, J. M.; Hornbeck, P.; Cantley, L. C.; Gygi, S. P.; Rush, J.; Comb, M. *J. Sci Signal* **2010**, *3*. ra64.

(77) Matsuoka, S.; Ballif, B. A.; Smogorzewska, A.; McDonald, E. R., 3rd; Hurov, K. E.; Luo, J.; Bakalarski, C. E.; Zhao, Z.; Solimini, N.; Lerenthal, Y.; Shiloh, Y.; Gygi, S. P.; Elledge, S. J. *Science* **2007**, *316*. 1160-6.

(78) Giansanti, P.; Stokes, M. P.; Silva, J. C.; Scholten, A.; Heck, A. J. *Mol Cell Proteomics* **2013**.

(79) Vermeulen, M.; Eberl, H. C.; Matarese, F.; Marks, H.; Denissov, S.; Butter, F.; Lee, K. K.; Olsen, J. V.; Hyman, A. A.; Stunnenberg, H. G.; Mann, M. *Cell* **2010**, *142*. 967-80.

(80) Schmidt, T. G.; Skerra, A. *Nat Protoc* **2007**, *2*. 1528-35.

(81) Rix, U.; Superti-Furga, G. *Nat Chem Biol* **2009**, *5*. 616-24.

(82) Bantscheff, M.; Scholten, A.; Heck, A. J. *Drug Discov Today* **2009**, *14*. 1021-9.

(83) Speers, A. E.; Cravatt, B. F. *Chembiochem* **2004**, *5*. 41-7.

(84) Bantscheff, M.; Eberhard, D.; Abraham, Y.; Bastuck, S.; Boesche, M.; Hobson, S.; Mathieson, T.; Perrin, J.; Raida, M.; Rau, C.; Reader, V.; Sweetman, G.; Bauer, A.; Bouwmeester, T.; Hopf, C.; Kruse, U.; Neubauer, G.; Ramsden, N.; Rick, J.; Kuster, B.; Drewes, G. *Nat Biotechnol* **2007**, *25*. 1035-44.

(85) Scholten, A.; Poh, M. K.; van Veen, T. A.; van Breukelen, B.; Vos, M. A.; Heck, A. J. *J Proteome Res* **2006**, *5*. 1435-47.

(86) Hanke, S.; Mann, M. *Mol Cell Proteomics* **2009**, *8*. 519-34.

(87) Saghatelian, A.; Jessani, N.; Joseph, A.; Humphrey, M.; Cravatt, B. F. *Proc Natl Acad Sci U S A* **2004**, *101*. 10000-5.

(88) Yee, M. C.; Fas, S. C.; Stohlmeyer, M. M.; Wandless, T. J.; Cimprich, K. A. *J Biol Chem* **2005**, *280*. 29053-9.

(89) Kumar, S.; Zhou, B.; Liang, F.; Wang, W. Q.; Huang, Z.; Zhang, Z. Y. *Proc Natl Acad Sci U S A* **2004**, *101*. 7943-8.

(90) Vocadlo, D. J.; Bertozzi, C. R. *Angew Chem Int Ed Engl* **2004**, *43*. 5338-42.

(91) Salisbury, C. M.; Cravatt, B. F. *Proc Natl Acad Sci U S A* **2007**, *104*. 1171-6.

(92) Ekkebus, R.; van Kasteren, S. I.; Kulathu, Y.; Scholten, A.; Berlin, I.; Geurink, P. P.; de Jong, A.; Goerdayal, S.; Neefjes, J.; Heck, A. J.; Komander, D.; Ovaa, H. *J Am Chem Soc* **2013**, *135*. 2867-70.

(93) Wissing, J.; Jansch, L.; Nimtz, M.; Dieterich, G.; Hornberger, R.; Keri, G.; Wehland, J.; Daub, H. *Mol Cell Proteomics* **2007**, *6*. 537-47.

(94) Aye, T. T.; Soni, S.; van Veen, T. A.; van der Heyden, M. A.; Cappadona, S.; Varro, A.; de Weger, R. A.; de Jonge, N.; Vos, M. A.; Heck, A. J.; Scholten, A. *J Mol Cell Cardiol*

2012, *52*. 511-8.
(95) Fenn, J. B.; Mann, M.; Meng, C. K.; Wong, S. F.; Whitehouse, C. M. Science 1989, 246. 64-71.
(96) Tanaka, K. Angew Chem Int Ed Engl 2003, 42. 3860-70; Hillenkamp, F.; Karas, M. *Methods in enzymology* **1990**, *193*. 280-95.
(97) Paul, W.; Steinwedel, H. Z *Naturforsch A* **1953**, *8*. 448-450.
(98) Stephens, W. E. *Phys Rev* **1946**, *69*. 691-691.
(99) Hager, J. W.; Le Blanc, J. C. Y. *J Chromatogr A* **2003**, *1020*. 3-9.
(100) Marshall, A. G.; Hendrickson, C. L. *Int J Mass Spectrom* **2002**, *215*. 59-75.
(101) Makarov, A. *Anal Chem* **2000**, *72*. 1156-62.
(102) Kingdon, K. H. *Phys Rev* **1923**, *21*. 408-418.
(103) Marto, J. A.; Guan, S.; Marshall, A. G. *Rapid Commun Mass Spectrom* **1994**, *8*. 615-20.
(104) Olsen, J. V.; Schwartz, J. C.; Griep-Raming, J.; Nielsen, M. L.; Damoc, E.; Denisov, E.; Lange, O.; Remes, P.; Taylor, D.; Splendore, M.; Wouters, E. R.; Senko, M.; Makarov, A.; Mann, M.; Horning, S. *Mol Cell Proteomics* **2009**, *8*. 2759-69.
(105) Michalski, A.; Damoc, E.; Lange, O.; Denisov, E.; Nolting, D.; Müller, M.; Viner, R.; Schwartz, J.; Remes, P.; Belford, M.; Dunyach, J. J.; Cox, J.; Horning, S.; Mann, M.; Makarov, A. *Mol Cell Proteomics* **2012**, *11*. O111.013698.
(106) Michalski, A.; Damoc, E.; Hauschild, J. P.; Lange, O.; Wieghaus, A.; Makarov, A.; Nagaraj, N.; Cox, J.; Mann, M.; Horning, S. *Mol Cell Proteomics* **2011**, *10*. M111 011015.
(107) Frese, C. K.; Altelaar, A. F.; van den Toorn, H.; Nolting, D.; Griep-Raming, J.; Heck, A. J.; Mohammed, S. *Anal Chem* **2012**, *84*. 9668-73.
(108) Syka, J. E.; Coon, J. J.; Schroeder, M. J.; Shabanowitz, J.; Hunt, D. F. *Proc Natl Acad Sci U S A* **2004**, *101*. 9528-33.
(109) Frese, C. K.; Zhou, H.; Taus, T.; Altelaar, A. F.; Mechtler, K.; Heck, A. J.; Mohammed, S. *J Proteome Res* **2013**, *12*. 1520-5.
(110) Rose, R. J.; Damoc, E.; Denisov, E.; Makarov, A.; Heck, A. J. *Nat Methods* **2012**, *9*. 1084-6.
(111) Gerber, S. A.; Rush, J.; Stemman, O.; Kirschner, M. W.; Gygi, S. P. *Proc Natl Acad Sci U S A* **2003**, *100*. 6940-5.
(112) Silva, J. C.; Gorenstein, M. V.; Li, G. Z.; Vissers, J. P.; Geromanos, S. J. *Mol Cell Proteomics* **2006**, *5*. 144-56.
(113) Schwanhausser, B.; Busse, D.; Li, N.; Dittmar, G.; Schuchhardt, J.; Wolf, J.; Chen, W.; Selbach, M. *Nature* **2011**, *473*. 337-42.
(114) Ong, S. E.; Blagoev, B.; Kratchmarova, I.; Kristensen, D. B.; Steen, H.; Pandey, A.; Mann, M. *Mol Cell Proteomics* **2002**, *1*. 376-86.
(115) Kruger, M.; Moser, M.; Ussar, S.; Thievessen, I.; Luber, C. A.; Forner, F.; Schmidt, S.; Zanivan, S.; Fassler, R.; Mann, M. *Cell* **2008**, *134*. 353-64.
(116) Geiger, T.; Cox, J.; Ostasiewicz, P.; Wisniewski, J. R.; Mann, M. *Nat Methods* **2010**, *7*. 383-5.
(117) Krijgsveld, J.; Ketting, R. F.; Mahmoudi, T.; Johansen, J.; Artal-Sanz, M.; Verrijzer, C. P.; Plasterk, R. H.; Heck, A. J. *Nat Biotechnol* **2003**, *21*. 927-31.

(118) Thompson, A.; Schafer, J.; Kuhn, K.; Kienle, S.; Schwarz, J.; Schmidt, G.; Neumann, T.; Johnstone, R.; Mohammed, A. K.; Hamon, C. *Anal Chem* **2003**, *75*. 1895-904; Ross, P. L.; Huang, Y. N.; Marchese, J. N.; Williamson, B.; Parker, K.; Hattan, S.; Khainovski, N.; Pillai, S.; Dey, S.; Daniels, S.; Purkayastha, S.; Juhasz, P.; Martin, S.; Bartlet-Jones, M.; He, F.; Jacobson, A.; Pappin, D. J. *Mol Cell Proteomics* **2004**, *3*. 1154-69.
(119) Ting, L.; Rad, R.; Gygi, S. P.; Haas, W. *Nat Methods* **2011**, *8*. 937-40.
(120) Boersema, P. J.; Raijmakers, R.; Lemeer, S.; Mohammed, S.; Heck, A. J. *Nat Protoc* **2009**, *4*. 484-94; Hsu, J. L.; Huang, S. Y.; Chow, N. H.; Chen, S. H. *Anal Chem* **2003**, *75*. 6843-52.
(121) Zhang, R.; Sioma, C. S.; Thompson, R. A.; Xiong, L.; Regnier, F. E. *Anal Chem* **2002**, *74*. 3662-9.
(122) Liu, H.; Sadygov, R. G.; Yates, J. R., 3rd. *Anal Chem* **2004**, *76*. 4193-201; Old, W. M.; Meyer-Arendt, K.; Aveline-Wolf, L.; Pierce, K. G.; Mendoza, A.; Sevinsky, J. R.; Resing, K. A.; Ahn, N. G. *Mol Cell Proteomics* **2005**, *4*. 1487-502.
(123) Eng, J. K.; McCormack, A. L.; Yates, J. R. *J Am Soc Mass Spectrom* **1994**, *5*. 976-89.
(124) Perkins, D. N.; Pappin, D. J.; Creasy, D. M.; Cottrell, J. S. *Electrophoresis* **1999**, *20*. 3551-67.
(125) Cox, J.; Neuhauser, N.; Michalski, A.; Scheltema, R. A.; Olsen, J. V.; Mann, M. *J Proteome Res* **2011**, *10*. 1794-805.
(126) Elias, J. E.; Gygi, S. P. *Nat Methods* **2007**, *4*. 207-14.
(127) Beausoleil, S. A.; Villen, J.; Gerber, S. A.; Rush, J.; Gygi, S. P. *Nat Biotechnol* **2006**, *24*. 1285-92.
(128) Olsen, J. V.; Blagoev, B.; Gnad, F.; Macek, B.; Kumar, C.; Mortensen, P.; Mann, M. *Cell* **2006**, *127*. 635-48.
(129) Bailey, C. M.; Sweet, S. M.; Cunningham, D. L.; Zeller, M.; Heath, J. K.; Cooper, H. J. *J Proteome Res* **2009**, *8*. 1965-71.
(130) Savitski, M. M.; Lemeer, S.; Boesche, M.; Lang, M.; Mathieson, T.; Bantscheff, M.; Kuster, B. *Mol Cell Proteomics* **2011**, *10*. M110 003830.
(131) Taus, T.; Kocher, T.; Pichler, P.; Paschke, C.; Schmidt, A.; Henrich, C.; Mechtler, K. *J Proteome Res* **2011**, 10. 5354-62.

Chapter 2

Huntingtin associated protein (HAP1) is a cGMP-dependent kinase anchoring protein (GKAP), specific for the cGMP-dependent protein kinase Iβ isoform

Eleonora Corradini[1,2], Pepijn P. Burgers[1,2], Michael Plank[1,2], Albert J.R. Heck[1,2,*], Arjen Scholten[1,2,3]

Published in Journal of Biological Chemistry 2015; Volume 290, issue 12, pages 7887-7896

[1] Biomolecular Mass Spectrometry and Proteomics, Bijvoet Center for Biomolecular Research and Utrecht Institute for Pharmaceutical Sciences, Science Faculty, Utrecht University, Padualaan 8, 3584 CH Utrecht, the Netherlands.

[2] Netherlands Proteomics Centre, Padualaan 8, 3584 CH Utrecht, the Netherlands

[3] Current address: Janssen, Pharmaceutical companies of Johnson&Johnson, Infectious diseases and vaccines, Newtonweg 1, 2333 CP, Leiden, The Netherlands.

ABSTRACT

Protein-protein interactions are important in providing compartmentalization and specificity in cellular signal transduction. Many studies have hallmarked the well-designed compartmentalization of the cAMP-dependent protein kinase (PKA) through its anchoring proteins (AKAPs). Much less data is available on the compartmentalization of its closest homolog, cGMP-dependent protein kinase (PKG), via its own anchoring proteins (GKAPs). For the enrichment, screening and discovery of (novel) AKAPs a plethora of methodologies is available, including our previously described chemical proteomics approach based on immobilized cAMP or cGMP. Although this method was demonstrated to be effective, each immobilized cyclic nucleotide did not discriminate in the enrichment for either PKA or PKG, and their secondary interactors. Hence, with PKG signaling components being less abundant in most tissues, it turned out to be challenging to enrich and identify GKAPs.

Here, we extend on this cAMP-based chemical proteomics approach, employing competitive concentrations of free cyclic nucleotides to isolate each kinase and its secondary interactors. Using this approach we identified Huntingtin associated protein 1 (HAP1) as a putative novel GKAP. Through sequence alignment with known GKAPs and secondary structure prediction analysis we defined a small sequence domain mediating the interaction with PKG Iβ, but not PKG Iα. In vitro binding studies and site directed mutagenesis further confirmed the specificity and affinity of HAP1 binding to the PKG Iβ N-terminus. These data fully support that HAP1 is a GKAP, anchoring specifically to the cGMP-dependent protein kinase isoform Iβ, and provide further evidence that also PKG spatio-temporal signaling is largely controlled by anchoring proteins.

INTRODUCTION

Signaling pathways are largely organized into complex and versatile transduction units, each tailored to respond optimally to a particular signal. These dynamic units consist of compartmentalized anchoring hubs harboring a combination of signaling proteins to ensure spatio-temporal control of signaling. One of the best characterized models for compartmentalization through protein-protein interactions is the large family of protein kinase A/A-kinase anchoring protein (PKA-AKAP) complexes. At present more than 40 mammalian genes encoding AKAPs are known, with each AKAP harboring specific isoforms of PKA, in addition to other signaling proteins such as phosphodiesterases and phosphatases.[1,2] Unique targeting domains on each AKAP direct PKA signaling modules towards specific subcellular compartments, thereby providing a mechanism that positions PKA in proximity of its.[3,4] PKA exists as a hetero-tetramer consisting of a regulatory subunit dimer (PKA-R) of which each PKA-R binds a catalytic subunit (PKA-C). The molecular basis of PKA-AKAP complexes is a hydrophobic groove formed at the dimerization interface of PKA-R. This constitutes a docking site for the hydrophobic edge of a small 3-4 turn amphipathic α-helix present in each AKAP.[5–7]

In mammalian cells, the three isoforms of cGMP-dependent protein kinase, also known as protein kinase G (PKG, cGK), are PKA's closest homologs.[8] The domain architecture of PKG is largely identical to PKA, except the fact that PKG exists as a homo-dimer in which regulatory and catalytic domains reside on a single subunit, and, more importantly, its molecular mechanism of dimerization is very different. At the N-terminus of PKG, the monomers are held together by a heptad repeat leucine zipper, while PKA-R dimerizes with a very different fold called the X-type 4-helix bundle. This suggests that, although PKA and PKG are close homologs, they differ entirely in the domains mediating their intracellular localization through binding to anchoring proteins. This difference in localization mechanism may well be the basis for the molecular segregation of cAMP and cGMP signaling in vivo.

Mammalian cells express three PKG isoforms: type I PKG (PKG I), which exists as two different splice variants of the same gene (PKG Iα and PKG Iβ)[9,10] and type II PKG (PKG II).[11] All the PKG isoforms share the same domain organization, with the earlier mentioned N-terminal dimerization domain, followed by a regulatory domain with an auto-inhibitory sequence, two cooperative cyclic nucleotide binding domains and a catalytic domain. Although being similar folds, the leucine zipper of the three PKG isoforms share only little sequence similarity, suggesting different localization behavior of the three isoforms. PKG localization via binding to G-kinase anchoring proteins (GKAPs) is mediated by its N-terminus, and the handful of GKAPs found thus far indeed show specificity for different PKG isoforms.[12–16] This is again similar to how AKAPs interact with respect to different isoforms of PKA regulatory subunits.[5,17,18]

In particular, MYPT1 and GKAP42 bind to PKG Iα,[19–21] IRAG and TFII-I are specific for PKG Iβ[12,22] while Rab11b forms a complex with PKG II.[23] Given the low number of GKAPs known, there is still no convincing definition of a common PKG I/GKAP binding domain. Therefore, it is essential to identify additional GKAPs, also to elucidate their binding mechanism(s) and study their role in vivo.

Over the years overlay assays and yeast two-hybrid screens have been used for the discovery of many new AKAPs[24,25] and some GKAPs,[21] with varying success. More recently chemical proteomics based mass spectrometry approaches provided an alternative to investigate kinase signaling.[26,27] Chemical proteomics enabled the discovery of new anchoring proteins while preserving the native structure of the proteins and their interactions with small molecules and scaffold proteins. Particularly immobilized cAMP on agarose beads played a pivotal role in the identification and characterization of several new AKAPs. However, all these studies focused on PKA and AKAPs,[18,28,29] and not on PKG and new GKAPs.

Due to the high similarity between both the second messenger molecules cAMP and cGMP and their main target sites on PKA and PKG the binding constants of cAMP and cGMP for PKG only differ by approximately 100-fold in favor of cGMP.[30] The same holds true for PKA and cGMP. Therefore, there has always been speculation about the occurrence of (in vivo) cross reactivity.[31] An argument against this hypothesis is the tight localization of the kinases via anchoring proteins close to their

designated pools of cAMP, or cGMP, which should largely minimize this event from occurring in vivo. In chemical proteomics experiments, in vitro enrichment by immobilized cAMP or cGMP leads to the simultaneous pull-down of both PKA and PKG, possibly due to the high local concentration of the cyclic nucleotide on the resin.
Here we describe an extension of our previously described cAMP based chemical proteomics method using in-solution competition with a low dose of free cAMP or cGMP which allows us to dissect PKA and PKG driven signaling complexes. Affinity purification followed by mass spectrometry analyses of these competed pull downs in rat lung tissue led to the selective enrichment of known GKAPs along with a putative novel GKAP candidate; the Huntingtin associated protein (HAP1). Follow-up experiments presented here, establish HAP1 as a novel GKAP and highlight the potential of our novel chemical proteomics methodology for discovery of GKAPs in other cells and tissue.

EXPERIMENTAL PROCEDURES

Cell Culture and Transfections

HEK293 and COS-7 cells were grown at 37° with 5% CO2 in Dulbecco's modified Eagle's medium containing 10% of fetal bovine serum and 0.1% Pen/Strep. HEK293 were grown to 80% confluence and then harvested with trypsin. Cells were washed in PBS, snap frozen in liquid nitrogen and kept at -80°C until use. COS-7 cells were grown to 70% confluence and transfected using PolyFect according to the manufacturer's protocol for the specific cell type (Qiagen).

Sample preparation and pull downs

HEK293 and COS-7 cells were lysed with a dounce homogenizer in ice cold PBS, supplemented with 0.1% Tween 20, protease and phosphatase inhibitors. Lysates were centrifuged at 20,000 ×g for 10 min at 4°C. Prior to the pull-down assay, ADP and GDP were added to the lysate to a final concentration of 10 mM. For the HEK293 the lysate was divided in three equal fractions of 10 mg. One was supplemented with cAMP (10 μM final concentration), one with cGMP (10 μM final concentration), while the third sample was used as control. The three samples were then incubated for 30 min at 4°C under agitation. 8-AHA-cAMP agarose beads (Biolog, Germany) were added to the lysates with a ratio of 1:100 (μL dried beads: μg protein), and incubated at 4°C for 2 hours. The 8-AHA-linked cAMP agarose beads have been described before and were chosen as they enable the pull-down of the PKA regulatory subunits, and exhibit somewhat lower affinity for PKA than other commercially available cAMP-coupled beads.[28] After the incubation the beads were washed three times with 1 ml of ice-cold lysis buffer containing the above mentioned concentrations of either free cAMP, or free cGMP, or normal lysis buffer for the control. Beads were subsequently washed three times with 1 ml ice-cold PBS before protein elution using SDS sample buffer at 95°C. The eluted proteins were separated on 4-12% SDS-PAGE (BIO-RAD) electrophoresis and subjected to in-gel digestion. Briefly the proteins were reduced dithiothreitol (Sigma Aldrich), alkylated with iodoacetamide (Sigma

Aldrich) and digested with sequencing-grade modified trypsin (Promega) prior to analysis with LC-MS/MS.[32]

Rat lung tissue

Lungs originated from 6 months old male Wistar rats were excorporated, frozen in liquid nitrogen and stored at -80°C until use. Protein isolation was achieved by cooling the tissues in liquid nitrogen followed by pulverization in a pre-cooled custom made steel mortar. The powdered tissues were then taken up in ice cold lysis buffer and 15 mg of protein lysate (1.5 times more than for the HEK293 lysate) was subjected to the same procedure as described above for the HEK293 cell lysates.

LC-MS/MS analysis

LC–MS/MS analysis was performed using an Agilent 1100 series liquid chromatography system equipped with an 20-mm Aqua C18 (Phenomenex, Torrance, CA) trapping column (packed in-house, i.d. 100 μm; resin 5 μm) and a 400 mm ReproSil-Pur C18-AQ analytical column (packed in-house, i.d. 50 μm; resin 3 μm). Trapping was performed at 5 μl min−1 solution A (0.6% acetic acid) for 10 min. Peptide elution was achieved with a linear gradient from 13 to 32% of solution B (80% acetonitrile, 0.6% acetic acid) in 60 min at a flow rate of 100 nl min^{-1} obtained by passively splitting the flow from 0.6 ml min^{-1}. Nanospray was achieved using a distally coated fused silica emitter (New Objective, Cambridge, MA; outer diameter 360 μm; i.d. 20 μm, tip i.d. 10 μm) biased to 1.8 kV. The LC system was coupled to an LTQ-Orbitrap Discovery or LTQ-Orbitrap Velos mass spectrometer (Thermo Electron, Bremen, Germany). Briefly, the mass spectrometer was operated in the data-dependent mode to automatically switch between MS and MS/MS acquisition. Survey full scan MS spectra were acquired from m/z 350 to m/z 1500 in the Orbitrap. The five most intense ions were fragmented in the linear ion trap using collision induced dissociation (CID) at a target value of 10 000. Peak lists were generated using Proteome Discoverer (version 1.3, Thermo Scientific, Bremen, Germany) using a standardized workflow. Peak lists, generated in Proteome Discoverer, were searched against the Swiss-Prot database (taxonomy Human, 20,407 protein entries or IPI rat 3.36, 42,689 protein entries) supplemented with frequently observed contaminants, using Mascot (version 2.3.02 Matrix Science, London, UK). The database search parameters were as follow: a mass tolerance of 50 ppm for the precursor ions and ±0.6 Da for the fragment ions. Enzyme specificity was set to Trypsin with allowing two missed cleavages. Carbarmidomethylation of cysteines was set as fixed modification and oxidation of methionine was used as variable modification. Search results were filtered by using a 5% FDR at the PSMs level.[33] In addition the results were filtered using the following criteria: (i) Mascot ion score of at least 20, (ii) a minimum of six amino acid residues per peptide, and (iii) maximum search engine rank of 1. The mass spectrometry proteomics data have been deposited to the ProteomeXchange Consortium (http://proteomecentral.proteomexchange.org)[34] via the PRIDE partner repository with the dataset identifier PXD001434.

The protein interactions from this publication have been submitted to the IMEx

(http://www.imexconsortium.org) consortium through IntAct[35] and assigned the identifier IM-23267.

DNA Constructs and Site-directed Mutagenesis

PKG Iα and PKG Iβ plasmids tagged with GFP were gifts from Robert Feil (Universität Tübingen, Tübingen, Germany) 36. The HAP1 and the shorter sequence HAP1 (a.a. 157-386), tagged with DsRed, were gifts from Edward Schmidt (Montana State University, Bozeman, MT) 37. The double site mutation (K567A/R568A) was introduced in the HAP1 plasmid using the QuickChange mutagenesis kit using the protocol provided by the manufacturer (Agilent Technologies, USA).

In vivo interaction studies

Transfections were performed in COS-7 cells. HAP1 was co-transfected with PKG Iα or PKG Iβ. The shorter version of HAP1 (a.a. 157-386) and the double point mutant of HAP1 were co-transfected with PKG Iβ. The cells were harvested 24–48 h post-transfection, and pull downs were performed on 4 mg of protein lysate as described above using 8AHA-cAMP agarose beads. After separation by SDS-PAGE the bound proteins were transferred onto PVDF membrane. Blots were incubated with rabbit anti-PKGI (Abcam, 1:1000) and mouse anti-Huntingtin associated protein 1 (HAP1, Novus biological, 1:5000). After several washes the blots were incubated with appropriate Cy3 and Cy5 labeled secondary antibodies (GE Healthcare) and detection was performed on a Typhoon 9400 imager (Amersham).

GKAP binding domain secondary structure prediction and docking study

Secondary structure prediction of IRAG, TFII-I and HAP1 domains that bind to PKG Iβ were obtained with the NetSurfP program 38. The PKG Iβ crystal structure of the N-terminus was retrieved from the PDB database (3NMD) and used with the predicted GKAP secondary structures for docking prediction.[39]

Fluorescence anisotropy

The dimer of the PKG Iβ leucine zipper (LZPKG Iβ 4-55), a kind gift from Dr. C. Kim, Baylor College of Medicine, Houston) was purified as described previously.[40] The GKAP interaction domains of IRAG (EAKLVSERFLTRRGRKSRSSPGESS, a.a. 164-188), HAP1 (QQLSNWQDAHSKRQQKQKVVPKDSP, a.a. 556-580) were tagged N-terminally with 5-carboxytetramethylrhodamine (5-TAMRA). A mutated version of the HAP1 peptide (QQLSNWQDAHSAAQQKQKVVPKDSP, a.a. 556-580) together with a scrambled peptide (EAQEELAWKIAKMIVSDIMQQAQY) were also tagged and used as controls. All peptides were synthesized at the peptide facility of the Netherland Cancer Institute (Amsterdam, Netherlands). Binding affinity assay between these peptides and the LZPKG Iβ dimeric domains were performed as described by us previously.[29]

RESULTS

Competitive chemical proteomics enables the selective identification of GKAPs

Previous chemical proteomics experiments based on various immobilized cAMP or cGMP analogs revealed not much specificity for either PKA or PKG.[41–43] Often, in cell lines PKG is expressed at a lower level when compared to PKA. Therefore, the search for novel GKAPs using chemical proteomics methodology is severely hampered by co-purification of the more abundant PKA-pathway components.

Here we investigated the use of in solution competition with free cAMP to compete for PKA binding to the resin while retaining binding of PKG and its putative binding partners. Since the affinity of cAMP for PKG is approximately 100-fold weaker than for PKA and vice versa for cGMP and PKA,[30] we sought to selectively occupy the cyclic-nucleotide binding motifs of either PKA or PKG prior to the pull-down performed by using the 8-AHA-linked cAMP agarose beads. Based on these data, we first aimed to identify this appropriate concentration of cAMP. In addition we also used different competing concentrations of cGMP to investigate the effect on isolating PKA pathway components. A concentration range of cAMP and cGMP was spiked into a HEK293 cell lysate and subsequently an 8-AHA-cAMP pull down was performed. A control experiment, without adding competing cyclic nucleotides was performed in parallel (Figure 1A). It could be deduced that the most effective concentration of cAMP/cGMP to compete off either PKA or PKG was 10 μM (Figure 1B). While in the control experiment, both PKA and PKG were captured, supplementing 10 μM cAMP to the lysate resulted in the complete abolishment of PKA-binding, while maintaining PKG association to the resin. In the reverse experiment, 10 μM cGMP resulted in the opposite effect; full abolishment of PKG binding without affecting PKA interactions (Figure 1B). To investigate this with more sensitivity, we performed in-gel digestion and mass spectrometry analysis of the Control and the two 10 μM cyclic nucleotide (cAMP and cGMP) gel lanes. This resulted in the cumulative identification of 246 proteins under these three different conditions, (i.e. no competition, supplemented with cAMP, or cGMP) (Supplemental Table 1A). In order to quantify the effectiveness of the competition, we quantitatively compared the number of peptide spectral matches (PSM) between the cAMP supplemented pull down and the cGMP supplemented pull down (Table 1). This quantitation revealed that PKA and all AKAPs were completely competed off the beads by 10 μM cAMP, while PKG binding was entirely retained (Table 1).When comparing to the control experiment, competing for binding of either PKA or PKG also increased our spectral and peptide coverage on the enriched kinase and its binding partners, and thus our depth of analysis on both sides of the experiment.

These experiments in HEK293 cells revealed that selectivity could be achieved in our pull-downs, as numerous AKAPs could be specifically pulled-down, albeit we did not identify any (putative) GKAPs in these experiments. Nevertheless, these data indicate that enriching for PKG while competing for PKA/AKAP binding is a promising tool to screen cells and tissues for novel putative GKAPs.

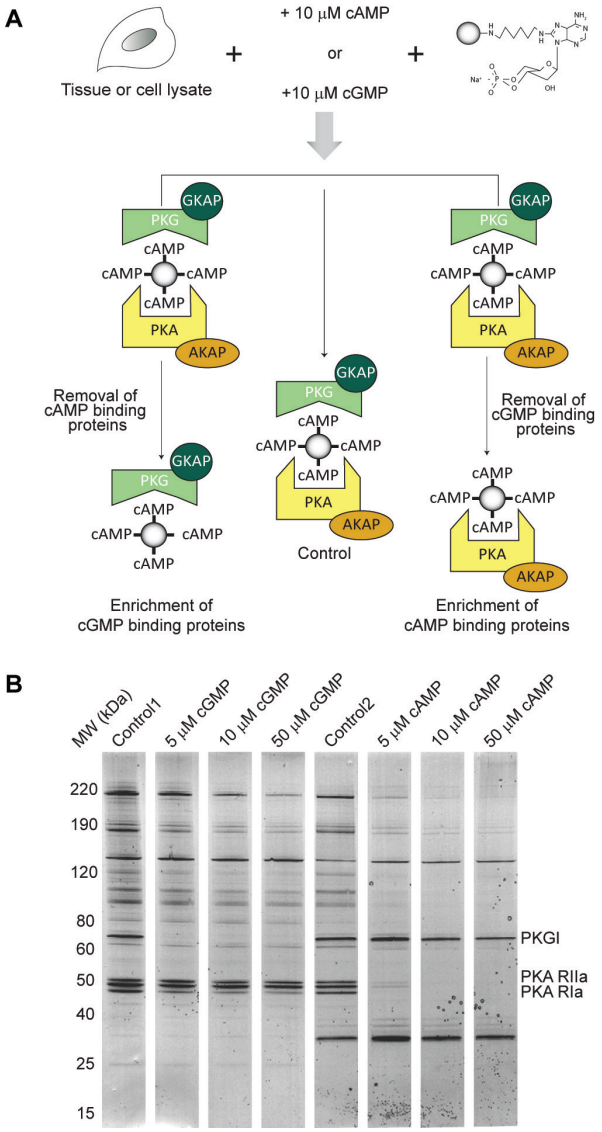

Figure 1. *A, Competitive chemical proteomics workflow used for the identification of new GKAPs. In the control no cyclic nucleotide is added to the lysate, whereas cAMP and cGMP are added to the lysate, to selectively enrich for PKG and its interactors and PKA and its interactors, respectively. B, Coomassie staining of the proteins pulled down by using 8-AHA-linked cAMP agarose beads in HEK293 cells with increasing amounts of cyclic nucleotide added to the lysate. Adding 10 μM of cGMP resulted in a complete removal of PKG. An alike scenario was observed for the pull downs performed in the presence of 10 μM cAMP, inducing that the PKA regulatory subunits and their interactors were competed off the beads.*

Following the optimization of the protocol in HEK293 cells, we extended our analysis to (rat) lung tissue, which attractively also has PKG present at a relatively high abundance. The setup was identical to the ones used for the HEK293 experiments (Figure 1A) such that again the pull downs supplemented with cAMP and cGMP could be quantitatively compared using spectral counts (Table 2).

Fortuitously, we were now able to selectively enrich not only PKG, but also a known GKAP, IRAG. Among the other proteins competed by 10 μM cGMP, and thus co-enriched with PKG (Supplemental Table 1B) we identified the Huntingtin associated protein (HAP1). HAP1 is involved in a protein complex with Huntingtin (Htt) and the type 1 inositol 1,4,5-trisphosphate receptor (InsP3R1) in an altered neuronal Ca^{2+} signaling pathway.[44] Interestingly, IRAG, and thus also PKG, are located nearby the InsP3R1 receptor, that upon phosphorylation by PKG, reduces the intracellular calcium release from intracellular storage sites.[12]

To further validate the interaction between HAP1 and PKG, HAP1 was co-expressed with either PKG Iα or PKG Iβ in COS-7 cells. Subsequently, a pull down using 8AHA-cAMP beads was performed. The proteins eluted from the beads were analyzed by SDS-PAGE and immunoblotting with antibodies against HAP1 and PKG I. These assays clearly revealed that HAP1 was not enriched by the cAMP-resin when co-expressed with PKG Iα while it was selectively enriched in the presence of PKG Iβ (Figure 2). This suggests that HAP1 and PKG Iβ are interacting in the context of the cell and that the interaction found in the proteomics studies is specific.

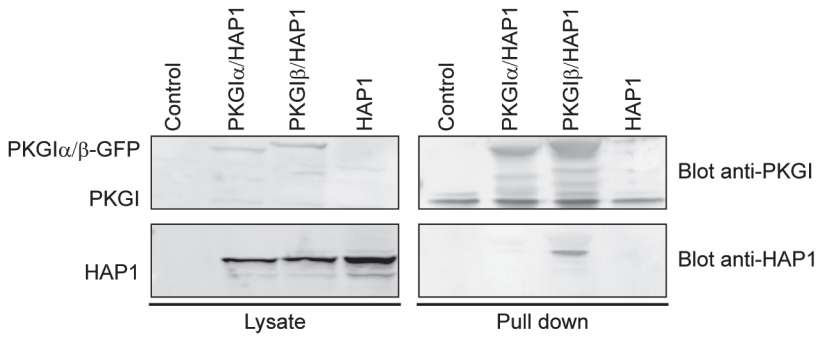

Figure 2. *HAP1 interacts specifically with the PKG Iβ isoform. Western blot analysis of pull downs performed in COS-7 cells co-expressing HAP1 alone or with either PKG Ia or PKG Iβ. The blots from the lysate show the expression of the proteins in the cells, while the pull down with the 8-AHA-linked cAMP agarose beads shows that HAP1 co-precipitates selectively with PKG Iβ.*

HAP1 harbors a domain with sequence similarity to known PKG Iβ selective GKAPs

As only the N-terminus is spliced differently between PKG Iα and PKG Iβ, it may harbor the basis for the observed GKAP isoform specificity. Ammendola et al. mapped the interaction between PKG Iβ and IRAG in detail,[45] while Casteel et al. identified the region in TFII-I interacting with PKG Iβ 22. Mutating basic residues

Accession	Gene name	Description	#Peptides Control	#PSMs Control	#Peptides +cAMP	#PSMs +cAMP	#Peptides +cGMP	#PSMs +cGMP
Q13976	PRKG1	cGMP-dependent protein kinase 1 α	34	97	40	118	2	2
Q12802	AKAP13	A-kinase anchoring protein 13	-	-	-	-	1	2
Q8WZA2	RAPGEF4	Rap guanine nucleotide exchange factor 4	6	8	2	2	5	7
Q5VU43	PDE4DIP	Myomegalin	9	17	-	-	7	10
Q9UKA4	AKAP11	A-kinase anchoring protein 11	9	22	-	-	11	15
Q9P0M2	AKAP7	A-kinase anchoring protein 7 gamma	2	6	-	-	7	17
P11137	MAP2	Microtubule-associated protein 2	1	1	-	-	11	21
P31321	PRKAR1B	cAMP-dependent protein kinase Iβ regulatory subunit	12	33	-	-	16	41
Q92667	AKAP1	A kinase anchoring protein 1	15	23	-	-	21	40
Q9Y2D5	AKAP2	A-kinase anchoring protein 2	2	8	-	-	9	42
Q99996	AKAP9	A-kinase anchoring protein 9	59	88	-	-	34	58
P10644	PRKAR1A	cAMP-dependent protein kinase type Iα regulatory subunit	35	150	1	1	38	178
P31323	PRKAR2B	cAMP-dependent protein kinase type IIβ regulatory subunit	25	111	-	-	38	281
P13861	PRKAR2A	cAMP-dependent protein kinase type IIα regulatory subunit	36	268	-	-	50	565

Table 1 *Specificity of primary and secondary cAMP and cGMP interacting proteins enriched by using 8AHA-cAMP beads in HEK293 lysates. The three columns represent the detection of proteins bound onto the beads, in the control lysates, and those supplemented with either 10 μM cAMP (+cAMP) or 10 μM cGMP (+cGMP). Listed are the numbers of unique peptides and peptide spectrum matches (PSMs) found for each protein in each of the experiments. Preferential cGMP targets are reported in green, while cAMP preferred targets are shown in orange.*

Accession	Gene name	Description	# Peptides Control	# PSM Control	# Peptides +cAMP	# PSMs +cAMP	# Peptides +cGMP	# PSMs +cGMP
IPI00231413.1	Hap1	Isoform A of Huntingtin-associated protein 1	2	4	1	10	-	-
IPI00870747.2	Prkg1	Cyclic GMP-dependent protein kinase	67	460	62	416	19	53
IPI00368515.3	Mrvi1	MRV integration site 1 homolog, e.g. IRAG	1	1	3	4	-	-
IPI00213019.1	Akap14	A-kinase anchoring protein 14	4	5	-	-	1	1
IPI00200327.4	Prkar1b	cAMP-dependent protein kinase type Iβ regulatory subunit	17	178	5	33	14	97
IPI00364348.6	Akap13	A kinase anchoring protein 13	19	29	-	-	1	3
IPI00213479.3	Akap1	A kinase anchoring protein 1	4	7	-	-	3	3
IPI00231770.5	Prkar1a	cAMP-dependent protein kinase type Iαregulatory subunit	41	543	17	96	37	313
IPI00215470.2	Akap5	A-kinase anchoring protein 5	37	420	13	72	28	331
IPI00196684.3	Prkar2a	cAMP-dependent protein kinase type IIα regulatory subunit	37	875	20	121	39	689
IPI00231053.1	Map2	Isoform MAP2d of Microtubule-associated protein 2	7	10	-	-	5	6
IPI00365600.3	Prkar2b	cAMP-dependent protein kinase type IIβ regulatory subunit	33	303	14	33	32	212
IPI00767226.1	Akap7	A-kinase anchoring protein 18, isoform delta	11	37	2	4	12	43
IPI00208697.4	Rapgef4	Rap guanine nucleotide exchange factor 4	26	66	2	3	16	52
IPI00948086.1	cg-nap	Centrosomal protein CG-NAP	228	763	17	20	128	362
IPI00560333.1	Akap9	Yotiao protein (Fragment)	21	58	-	-	6	19
IPI00948594.1	Prkacb	cAMP-dependent protein kinase catalytic subunit beta	7	19	1	1	10	22
IPI00200013.4	Prkaca	Isoform 1 of cAMP-dependent protein kinase catalytic subunit alpha	6	18	1	1	11	23
IPI00948267.1	Sphkap	180 kDa protein, new AKAP	25	79	1	1	10	34
IPI00779281.3	Akap11	A kinase anchoring protein 11	40	157	-	-	18	55

Table 2 *Specificity of primary and secondary cAMP and cGMP interacting proteins enriched by using 8AHA-cAMP beads in rat lung tissue lysates. The three columns represent the detection of proteins bound onto the bead, in the control lysates, and those supplemented with either 10 μM cAMP (+cAMP) or 10 μM cGMP (+cGMP). Listed are the number of unique peptides and peptide spectrum matches (PSMs) found for each protein in each of the experiments. Preferential cGMP targets are reported in green, while cAMP preferred targets are shown in orange. Within the preferred cGMP targets we identified Mrvi1 (IRAG), the known interactor of PKG Iβ and Hap1, the here presented putative novel GKAP.*

(into alanine) in the IRAG anchoring domain caused disruption in PKG binding, suggesting that electrostatic interactions play an important role in the PKG Iβ-GKAP interaction. In addition, the basic residues in the TFII-I binding domain interact with the acidic residues in the N-terminus of PKG Iβ. Although the anchoring domains of IRAG and TFII-I are known, two such domains make it not yet possible to clearly define a PKG binding motif using bioinformatics tools such as the hidden Markov model which successfully defined the PKA binding motif for several AKAPs.[28,46,47] Considering the fact that HAP1 binds only to the beta isoform of PKG, and knowing the anchoring sequences of IRAG and TFII-I, we aligned HAP1 with the binding domain of IRAG and TFII-I to screen for a region that showed at least a similar charge distribution. The alignment revealed the presence of a region rich in basic residues close to the C-terminus of HAP1 (AA565-580) with resemblance to the IRAG sequence, and to the TFII-I binding domain, albeit for the latter in a reverse configuration (Figure 3A), providing us the hypothesis that this could be the HAP1 anchoring motif to PKG Iβ. The alignment of the three protein sequences displays a clear pattern of basic residues that are involved in the interaction with PKG Iβ. BLAST analysis of this HAP1 domain revealed strong sequence conservation across several mammals, suggesting it to be important basic amino acid residues (Figure 3B).

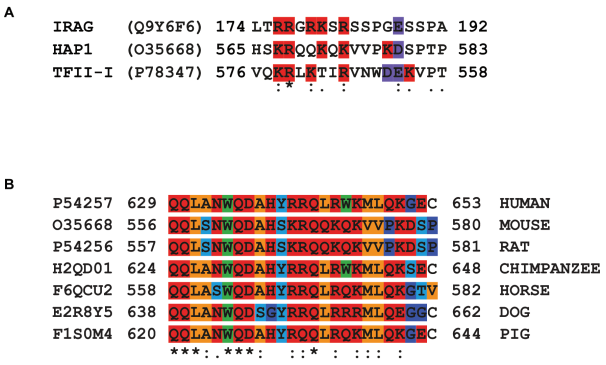

Figure 3. *A, Alignment of the established IRAG and the reverse TFII-I binding domain to PKG Iβ with the HAP1 region predicted to bind to PKG Iβ. These two sequences show a high degree of similarity regarding the position of the basic and acidic residues. The basic residues are highlighted in red, while the acidic residues are highlighted in purple. B, Sequence alignment of the human HAP1 region binding to PKG Iβ with various orthologues in other mammalian species. Similarity (:, .) and identity (*).The residues are color coded as follows: orange – aliphatic, red – polar, light blue – S/T/Y, green – bulky and blue – G/P.*

Docking of IRAG, TFII-I and HAP1 anchoring domains onto PKG Iβ

Recently the crystal structure of the leucine zipper of PKG Iβ (LZPKG Iβ) has been reported.[40] We used this structure to first model the binding of the two known Iβ specific GKAPs, IRAG and TFII-I, onto the N-terminus of PKG Iβ using molecular dynamic calculations by HADDOCK.[39] We then compared these results to the

docking of the proposed interaction site of HAP1. The modeling data suggested that TFII-I exhibits the strongest modeled affinity (HADDOCK score: -102 ±- 9) for PKG Iβ followed by HAP1 (-92 ± 5) and IRAG (-86 ± 1) (Figure 4A). As the anchoring domain of each GKAP is positioned a bit diagonally across the leucine zipper interface they do not make similar contacts on either monomer (Figure 4A). Nonetheless, the interaction sites of PKG Iβ with each GKAP studied here was identical: Glu27 and Glu31 on one monomer and Glu29, Asp33 and Asp36 (Figure 4B-D) on the other monomer of PKG Iβ's leucine zipper (LZPKG Iβ), moreover TFII-I shows an additional interaction with Asp26, as also reported by Casteel et al..[22] Our prediction shows not only that TFII-I has the strongest docking score but it is also bound backwards in sequence with respect to HAP1 and IRAG, in agreement with our (reverse) sequence alignment.

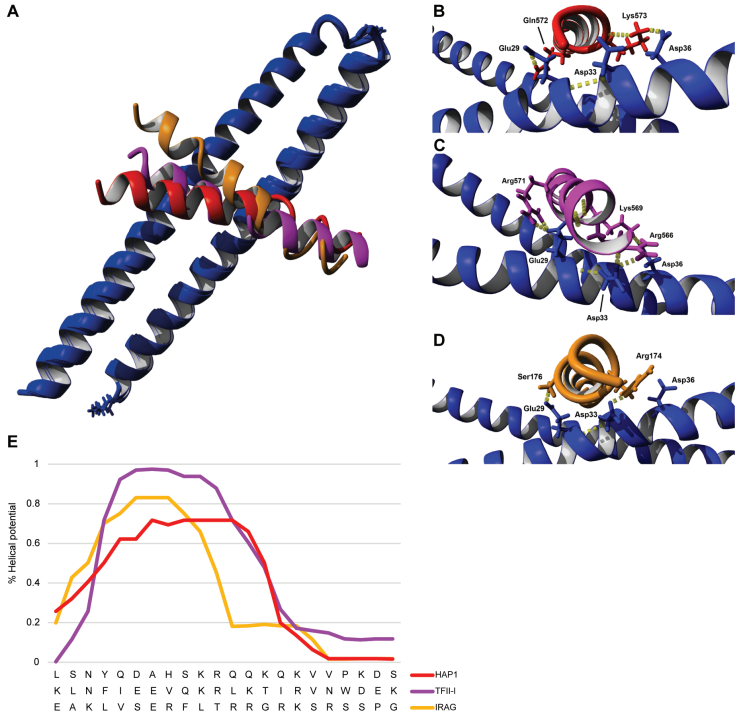

Figure 4. *Known and predicted GKAPs anchoring domains modeled onto the surface of PKG Iβ. A, The overlay of HAP1(red), TFII-I (purple), and IRAG (yellow) shows an alike binding mode to the leucine zipper domain of PKG Iβ (blue). None of the GKAPs anchoring domains shows a full helical structure. Close up view of B, HAP1, C, TFII-I and D, IRAG interacting with the dimerization domain of PKG Iβ. The interactions take place at Glu29 and Asp36 of PKG with the positive charged residues of the GKAPs. E, Helicity prediction of the PKG Iβ binding domain of HAP1, TFII-I and IRAG. The plot shows how the helical potential decreases after the KR/RR residues in all the protein sequences (residues 572/571, 567/568 and 175/176 respectively). Mutation of the basic residues can influence the helical potential of the proteins and be part of the cause of the disruption of the binding of the GKAPs to PKG Iβ.*

Interaction of HAP1 with the leucine zipper of PKG Iβ takes place at the C-terminus of HAP1

To firmly establish that the HAP1 region at the C-terminus interacts with the N-terminus of PKG Iβ as suggested by HADDOCK we performed in vitro binding affinity assays. We probed the binding between LZPKG Iβ and the 25 residue long 5-TAMRA tagged GKAP anchoring sequences of HAP1 (QQLSNWQDAHSKRQQKQKVVPKDSP), IRAG (EAKLVSERFLTRRGRKSRSSPGESS), a scrambled peptide (EAQEELAWKIAKMIVSDIMQQAQY) and the anchoring sequence of HAP1 with the Lys12 and Arg13 mutated into alanine (QQLSNWQDAHSAAQQKQKVVPKDSP) as control peptides using fluorescence anisotropy. The in vitro assay, carried out in triplicate, clearly demonstrated the high-affinity binding of HAP1 peptide fragment to the N-terminal domain of PKG Iβ (Figure 5A) with a K_d of around 15 nM, i.e. in the range of that of the peptide used for IRAG (positive control, 25 nM), while the scrambled peptide (negative control) and the mutated HAP1 peptide did not bind to PKG Iβ (Figure 5B), in line with the modeling data.

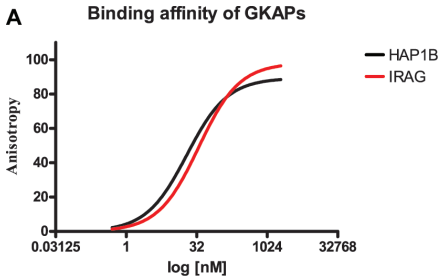

B

	K_d(nM)			
	HAP1	IRAG	HAP1 MUT	Scrambled
LZPKGIβ	13 ± 4	26 ± 6	nd	nd

Figure 5. *A, Binding affinity of HAP1 peptide (black) mimicking its proposed anchoring domain to the leucine zipper of PKG Iβ by fluorescence anisotropy. IRAG peptide binding to PKG Iβ was used as positive control. The peptides were tagged with 5-TAMRA, excitation at 535 nm and emission at 580 nm. B, K_d values and relative standard deviations (n=3).*

After establishment of the putative anchoring domain in vitro, we sought to verify that the HAP1 region from residue 556 to 580 is essential for the binding to PKG Iβ also in cellular context. Following an approach similar to Casteel et al., determining the residues involved in the binding of IRAG and TFII-I to PKG Iβ, we decided to create a double mutant of the HAP1 construct to show that the interaction of HAP1 with the N-terminus of PKG Iβ relies on particular electrostatic interactions. Therefore, we mutated two consecutive basic residues, K567A and R568A, in the HAP1 anchoring domain. Also a truncated version of HAP1 lacking the C-terminus (amino acid 157-386) was used. PKG Iβ was co-expressed either with HAP1 (control), mutated HAP1 (K567A and R568A) or truncated HAP1 in COS-7 cells. Subsequently a cAMP pull down was performed (Figure 6). The double mutated HAP1 and the truncated version of HAP1 did not bind to PKG Iβ, further establishing that the basic

amino acid stretch located at the C-terminus of HAP1 is crucial for binding to PKG (Figure 6). All these data combined leads us to the conclusion that HAP1 is a novel genuine GKAP, with the same specificity and docking sites as the related GKAPs IRAG and TFII-I.

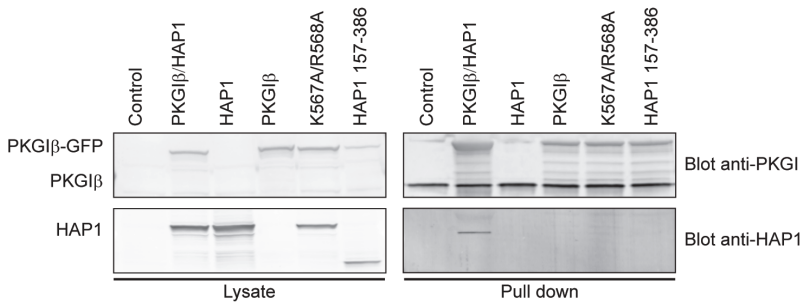

Figure 6. *PKG Iβ binds exclusively to HAP1 harboring the predicted anchoring domain. Western blot analysis of lysates and proteins pulled down with the 8-AHA-linked cAMP agarose beads in COS-7 cells co-expressing PKG Iβ-GFP plasmid with I) the HAP1-DSRed construct (Control), II) the HAP1-DSRed bearing the double mutation K567A/R568A and III) the C-terminal truncated HAP1-DSRed construct (HAP1 157-386). Pull downs were performed also in non-transfected cells and cells transfected with only PKG Iβ or HAP1 as negative controls.*

DISCUSSION

Although there is clear proof that they do exist, evidence for protein scaffolds involved in spatio-temporal cGMP/PKG I signaling is still scarce. Here, by using an efficient competitive chemical proteomics approach we identified a new GKAP expressed in mammalian (rat) lung tissue. The used affinity capture method is based on cAMP and cGMP-coupled resins that were previously shown to enrich both PKA and PKG, and their respective interactors. This is caused by the high concentration of the immobilized cyclic nucleotide (6 mM) on the agarose bead, needed to achieve efficient pull down results.[28] Such concentrations exceed the physiological cyclic nucleotide concentration by at least three orders of magnitude,[48] as well as the K_a for both PKA and PKG.[30] Therefore, here we set out to use a specific elution protocol with free cyclic nucleotides to selectively isolate the interactome of PKG. After optimization of the protocol in HEK293 cells, we were able to extend it to rat tissue and enrich for and identify HAP1 as a putative GKAP, along with the known GKAP IRAG.

The few described GKAPs are often found to interact selectively with one of the two isoforms of PKG I,[12,19,21,49] and that the specificity depends on the charge distribution at the PKG I N-terminus. Indeed, Casteel et al. investigated in detail how PKG Iβ interacts with its GKAPs, TFII-I and IRAG, showing that the presence of the negatively charged residues (Asp26, Glu27, Glu29, and Glu31) on PKG Iβ N-terminus is crucial for the interaction with the positively charged residues on the GKAPs.[22]

The N-terminal domain of PKG Iα contains a highly charged sequence with basic residues, with the consequent different overall charge distribution and topology, when compared to the PKG Iβ isoform. Still, also the positively charged residues on PKG Iα (Lys37 and Lys39) in the LZ domain are essential for the formation of the complex with the PKG Iα specific GKAP MYPT1.[13]

These differences between the two isoforms with the opposite charge state distribution may be the origin of the specificity of GKAPs for a single PKG I isoform. An additional proof of the relative importance of the charge distribution on the LZ domain of PKG determining the interaction with GKAPs has been published recently.[23] PKG II shows a completely different amino acid sequence and charge distribution when compared to the PKG I isoforms, and the crystal structure of the PKG II leucine zipper-Rab11b complex shows that PKG II binds to Rab11b mainly through Van der Waals forces instead of electrostatic interactions.

Here we demonstrated that HAP1, similarly to the previously discovered GKAPs, is selective for a single isoform, being PKG Iβ. Using molecular modeling, we hypothesize how the negatively charged residues on PKG Iβ may interact with a positively charged sequence in the known GKAPs (IRAG and TFII-I) to accommodate the binding. With these data as a starting point, and the crystal structure of the PKG Iβ N-terminal leucine zipper,[40] we used HADDOCK to perform docking studies with the HAP1 binding sequence and compared it to the two known PKG Iβ specific GKAPs. After overlaying the three docking studies we propose that TFII-I binds backwards in comparison with IRAG and HAP1. This is further supported by the alignment of TFII-I with IRAG and HAP1, where there is much more consensus for the reverse TFII-I sequence (Figure 3A). Our modeling results reveal that the interactions of each GKAP with PKG Iβ take place in a similar manner. Indeed the Glu29, Asp33 and Asp36 on one PKG I monomer interact with Gln572 and Lys573 on HAP1 (Figure 4B), with Arg566, Lys569 and Arg571 on TFII-I (Figure 4C) and with Arg174 and Ser176 on IRAG (Figure 4D).

The presence and order of these basic residues in this region of HAP1, structurally align with those present in the PKG Iβ binding domain of IRAG and TFII-I (Figure 3A and 4). A quite surprising result was that neither of the GKAP anchoring sequences displayed a full helix as each of them contains a small knick. Indeed, the helical potential of each GKAP, obtained from the secondary structure prediction,[38] decreases radically after the initial KR/RR sequence (Figure 4E). We hypothesize that, besides the change in charge bearing amino acids, the mutations we made onto the HAP1 sequence, may increase the helical potential of the sequence stretch, which would then further disturb the binding of the GKAPs to PKG. Through the double mutation of Lys567 and Arg568 to alanine or the deletion of HAP1 C-terminus, we showed that this region is essential for binding to PKG Iβ.

Summarizing, the here presented chemical proteomics - mass spectrometry based approach is a valid method for the identification of novel PKG anchoring proteins directly in any cell or tissue lysate. Defining HAP1 as a novel GKAP, anchoring specifically to the cGMP-dependent protein kinase isoform Iβ, provides further proof

for the fact that PKG spatio-temporal signaling is, in analogy to that for its sister kinase PKA, principally controlled by a wide family of known and yet to be discovered G-kinase anchoring proteins.

ACKNOWLEDGMENTS

We thank Prof. Dr. Robert Feil (Universität Tübingen, Tübingen, Germany) for providing the PKG Iα and PKG Iβ constructs. We would also like to thank Dr. Edward Schmidt (Montana State University, Bozeman, MT) for supplying us the HAP1 constructs and Dr. C. Kim, Baylor College of Medicine, Houston) for donating us the LZPKG Iβ. Part of this research was performed within the framework of the PRIME-XS project, grant number 262067, funded by the European Union 7th Framework Program and the Netherlands Organization for Scientific Research (NWO) supported large scale proteomics facility Proteins@Work (project 184.032.201) embedded in the Netherlands Proteomics Centre.

REFERENCES

(1) Welch, E. J.; Jones, B. W.; Scott, J. D. *Mol Interv* **2010**, *10*, 86–97.
(2) Stangherlin, A.; Zaccolo, M. J. *Cardiovasc. Pharmacol.* **2011**, *58*, 345–353.
(3) Wong, W.; Scott, J. D. *Nat. Rev. Mol. Cell Biol.* **2004**, *5*, 959–970.
(4) Skroblin, P.; Grossmann, S.; Schafer, G.; Rosenthal, W.; Klussmann, E. *Int. Rev. Cell Mol. Biol.* **2010**, *283*, 235–330.
(5) Carr, D. W.; Stofko-Hahn, R. E.; Fraser, I. D.; Bishop, S. M.; Acott, T. S.; Brennan, R. G.; Scott, J. D. *J. Biol. Chem.* **1991**, *266*, 14188–14192.
(6) Kim, C.; Xuong, N. H.; Taylor, S. S. *Science* (80-.). **2005**, *307*, 690–696.
(7) Kinderman, F. S.; Kim, C.; von Daake, S.; Ma, Y.; Pham, B. Q.; Spraggon, G.; Xuong, N. H.; Jennings, P. A.; Taylor, S. S. *Mol. Cell* **2006**, *24*, 397–408.
(8) Francis, S. H.; Corbin, J. D. *Crit. Rev. Clin. Lab. Sci.* **1999**, *36*, 275–328.
(9) Wernet, W.; Flockerzi, V.; Hofmann, F. *FEBS Lett.* **1989**, *251*, 191–196.
(10) Wolfe, L.; Francis, S. H.; Corbin, J. D. *J. Biol. Chem.* **1989**, *264*, 4157–4162.
(11) De Jonge, H. R. *Adv. Cyclic Nucleotide Res.* **1981**, *14*, 315–333.
(12) Schlossmann, J.; Ammendola, A.; Ashman, K.; Zong, X.; Huber, A.; Neubauer, G.; Wang, G. X.; Allescher, H. D.; Korth, M.; Wilm, M.; Hofmann, F.; Ruth, P. *Nature* **2000**, *404*, 197–201.
(13) Sharma, A. K.; Zhou, G. P.; Kupferman, J.; Surks, H. K.; Christensen, E. N.; Chou, J. J.; Mendelsohn, M. E.; Rigby, A. C. *J. Biol. Chem.* **2008**, *283*, 32860–32869.
(14) Richie-Jannetta, R.; Francis, S. H.; Corbin, J. D. *J. Biol. Chem.* **2003**, *278*, 50070–50079.
(15) French, P. J.; Bijman, J.; Edixhoven, M.; Vaandrager, A. B.; Scholte, B. J.; Lohmann, S. M.; Nairn, A. C.; de Jonge, H. R. *J. Biol. Chem.* **1995**, *270*, 26626–26631.
(16) Yuasa, K.; Yamagami, S.; Nagahama, M.; Tsuji, A. *Biochem Biophys Res Commun* **2008**, *374*, 522–526.

(17) Gold, M. G.; Lygren, B.; Dokurno, P.; Hoshi, N.; McConnachie, G.; Tasken, K.; Carlson, C. R.; Scott, J. D.; Barford, D. *Mol. Cell* **2006**, *24*, 383–395.
(18) Kovanich, D.; van der Heyden, M. A.; Aye, T. T.; van Veen, T. A.; Heck, A. J.; Scholten, A. *Chembiochem* **2010**, *11*, 963–971.
(19) Vo, N. K.; Gettemy, J. M.; Coghlan, V. M. *Biochem. Biophys. Res. Commun.* **1998**, *246*, 831–835.
(20) Surks, H. K.; Mochizuki, N.; Kasai, Y.; Georgescu, S. P.; Tang, K. M.; Ito, M.; Lincoln, T. M.; Mendelsohn, M. E. *Science* (80-.). **1999**, *286*, 1583–1587.
(21) Yuasa, K.; Omori, K.; Yanaka, N. *J. Biol. Chem.* **2000**, *275*, 4897–4905.
(22) Casteel, D. E.; Boss, G. R.; Pilz, R. B. *J. Biol. Chem.* **2005**, *280*, 38211–38218.
(23) Reger, A. S.; Yang, M. P.; Koide-Yoshida, S.; Guo, E.; Mehta, S.; Yuasa, K.; Liu, A.; Casteel, D. E.; Kim, C. *J. Biol. Chem.* **2014**.
(24) Lohmann, S. M.; Walter, U.; Miller, P. E.; Greengard, P.; De Camilli, P. *Proc. Natl. Acad. Sci. U. S. A.* **1981**, *78*, 653–657.
(25) Alto, N. M.; Soderling, J.; Scott, J. D. *J. Cell Biol.* **2002**, *158*, 659–668.
(26) Bantscheff, M.; Scholten, A.; Heck, A. J. *Drug Discov. Today* **2009**, *14*, 1021–1029.
(27) Rix, U.; Superti-Furga, G. *Nat. Chem. Biol.* **2009**, *5*, 616–624.
(28) Scholten, A.; Poh, M. K.; van Veen, T. A.; van Breukelen, B.; Vos, M. A.; Heck, A. J. *J. Proteome Res.* **2006**, *5*, 1435–1447.
(29) Burgers, P. P.; Ma, Y.; Margarucci, L.; Mackey, M.; van der Heyden, M. A.; Ellisman, M.; Scholten, A.; Taylor, S. S.; Heck, A. J. *J. Biol. Chem.* **2012**, *287*, 43789–43797.
(30) Poppe, H.; Rybalkin, S. D.; Rehmann, H.; Hinds, T. R.; Tang, X. B.; Christensen, A. E.; Schwede, F.; Genieser, H. G.; Bos, J. L.; Doskeland, S. O.; Beavo, J. A.; Butt, E. *Nat. Methods* **2008**, *5*, 277–278.
(31) Pelligrino, D. A.; Wang, Q. *Prog. Neurobiol.* **1998**, *56*, 1–18.
(32) Shevchenko, A.; Jensen, O. N.; Podtelejnikov, A. V; Sagliocco, F.; Wilm, M.; Vorm, O.; Mortensen, P.; Boucherie, H.; Mann, M. *Proc Natl Acad Sci U S A* **1996**, *93*, 14440–14445.
(33) Elias, J. E.; Gygi, S. P. *Nat. Methods* **2007**, *4*, 207–214.
(34) Vizcaino, J. A.; Cote, R. G.; Csordas, A.; Dianes, J. A.; Fabregat, A.; Foster, J. M.; Griss, J.; Alpi, E.; Birim, M.; Contell, J.; O'Kelly, G.; Schoenegger, A.; Ovelleiro, D.; Perez-Riverol, Y.; Reisinger, F.; Rios, D.; Wang, R.; Hermjakob, H. *Nucleic Acids Res.* **2013**, *41*, D1063–D1069.
(35) Orchard, S.; Ammari, M.; Aranda, B.; Breuza, L.; Briganti, L.; Broackes-Carter, F.; Campbell, N. H.; Chavali, G.; Chen, C.; del-Toro, N.; Duesbury, M.; Dumousseau, M.; Galeota, E.; Hinz, U.; Iannuccelli, M.; Jagannathan, S.; Jimenez, R.; Khadake, J.; Lagreid, A.; Licata, L.; Lovering, R. C.; Meldal, B.; Melidoni, A. N.; Milagros, M.; Peluso, D.; Perfetto, L.; Porras, P.; Raghunath, A.; Ricard-Blum, S.; Roechert, B.; Stutz, A.; Tognolli, M.; van Roey, K.; Cesareni, G.; Hermjakob, H. *Nucleic Acids Res.* **2014**, *42*, D358–D363.
(36) Feil, R. *Circ. Res.* **2002**, *90*, 1080–1086.
(37) Prigge, J. R.; Schmidt, E. E. *BMC Mol. Biol.* **2007**, *8*, 76.
(38) Petersen, B.; Petersen, T. N.; Andersen, P.; Nielsen, M.; Lundegaard, C. *BMC*

Struct. Biol. **2009**, *9*, 51.
(39) De Vries, S. J.; van Dijk, M.; Bonvin, A. M. *Nat. Protoc.* **2010**, *5*, 883–897.
(40) Casteel, D. E.; Smith-Nguyen, E. V; Sankaran, B.; Roh, S. H.; Pilz, R. B.; Kim, C. *J. Biol. Chem.* **2010**, *285*, 32684–32688.
(41) Aye, T. T.; Soni, S.; van Veen, T. A.; van der Heyden, M. A.; Cappadona, S.; Varro, A.; de Weger, R. A.; de Jonge, N.; Vos, M. A.; Heck, A. J.; Scholten, A. *J. Mol. Cell. Cardiol.* **2012**, *52*, 511–518.
(42) Scholten, A.; van Veen, T. A.; Vos, M. A.; Heck, A. J. *J. Proteome Res.* **2007**, *6*, 1705–1717.
(43) Wong, J. W.; McRedmond, J. P.; Cagney, G. *Proteomics* **2009**, *9*, 40–50.
(44) Tang, T. S.; Tu, H.; Chan, E. Y.; Maximov, A.; Wang, Z.; Wellington, C. L.; Hayden, M. R.; Bezprozvanny, I. *Neuron* **2003**, *39*, 227–239.
(45) Ammendola, A.; Geiselhoringer, A.; Hofmann, F.; Schlossmann, J. *J. Biol. Chem.* **2001**, *276*, 24153–24159.
(46) Hundsrucker, C.; Skroblin, P.; Christian, F.; Zenn, H. M.; Popara, V.; Joshi, M.; Eichhorst, J.; Wiesner, B.; Herberg, F. W.; Reif, B.; Rosenthal, W.; Klussmann, E. *J. Biol. Chem.* **2010**, *285*, 5507–5521.
(47) Burgers, P. P.; van der Heyden, M. A.; Kok, B.; Heck, A. J.; Scholten, A. *Biochemistry* **2014**.
(48) Eigenthaler, M.; Nolte, C.; Halbrugge, M.; Walter, U. Eur. *J. Biochem.* **1992**, *205*, 471–481.
(49) Casteel, D. E.; Zhuang, S.; Gudi, T.; Tang, J.; Vuica, M.; Desiderio, S.; Pilz, R. B. *J. Biol. Chem.* **2002**, *277*, 32003–32014.

Chapter 3

Alterations in the cerebellar (phospho)proteome of a cGMP-dependent protein kinase knockout mouse

Eleonora Corradini[1, 2], Raghavan Vallur[3, 4, 5], Linsey M. Raaijmakers[1, 2], Susanne Feil[3], Robert Feil[3], Albert J.R. Heck[1, 2], Arjen Scholten[1, 2]

Published in Molecular & Cellular Proteomics 2014; Volume 13, issue 8, pages 2004-2016

[1] Biomolecular Mass Spectrometry and Proteomics, Bijvoet Center for Biomolecular Research and Utrecht Institute for Pharmaceutical Sciences, Science Faculty, Utrecht University, Padualaan 8, 3584 CH Utrecht, the Netherlands.

[2] Netherlands Proteomics Centre, Padualaan 8, 3584 CH Utrecht, the Netherlands

[3] Interfakultäres Institut für Biochemie, Universität Tübingen, Tübingen, Germany.

[4] Graduate School for Cellular and Molecular Neuroscience, Universität Tübingen, D-72074 Tübingen, Germany

[5] German Center for Neurodegenerative diseases (DZNE), D-72076 Tübingen, Germany

ABSTRACT

The cyclic nucleotide cGMP plays an important role in learning and memory, but its signaling mechanisms in the mammalian brain are not fully understood. Using mass spectrometry-based proteomics we evaluate how the cerebellum adapts its (phospho) proteome in a knockout mouse model of the cGMP-dependent protein kinase type I (cGKI, also known as PKG-I). Our data reveal that a small subset of proteins in the cerebellum (~3% of the quantified proteins) becomes substantially differentially expressed in the absence of cGKI. More changes are observed at the phosphoproteome level, with hundreds of sites being differentially phosphorylated between wild-type and knockout cerebellum. Most of these phosphorylated sites do not represent known cGKI substrates. An integrative computational network analysis of the data indicated that the differentially expressed proteins and proteins harboring differentially phosphorylated sites largely belong to a tight network in the Purkinje cells of the cerebellum involving important cGMP/cAMP signaling nodes (e.g., PDE5 and PKA-RIIβ) and Ca^{2+} signaling (e.g. SERCA3). In this way, removal of cGKI could be linked to impaired cerebellar long-term depression at Purkinje cell synapses. In addition, we could identify a set of novel putative (phospho)proteins to be considered in this network. Overall, our data improve our understanding of cerebellar cGKI signaling and suggest novel players in cGKI-regulated synaptic plasticity.

INTRODUCTION

Knockout (KO) mouse models represent powerful methods for studying the physiological relevance of a protein. However, to appreciate the effects of KO-induced perturbations on the entire system, systems-wide molecular characterization is needed, as for instance provided by (phospho)proteomics. Recent technological and methodological advancements now allow the mapping of protein expression, at least in cell cultures, close to completion.[1] More challenging, proteomics is also increasingly used to attempt systems-wide proteome characterizations in tissue. This has led to semi-quantitative[2] and quantitative[3] reasonably comprehensive proteome data of selected tissues, both in humans and animal models. More recently proteomics has also been applied for the in-depth profiling of perturbations in the proteome occurring in KO models. For instance, de Graaf et al.[4] used an in depth proteomic approach to identify the proteins changing by DNA damage induced pre-mature aging, using a KO mouse model lacking the excision repair cross-complementing group 1 gene. Another recent study used a mouse model lacking apolipoprotein E in order to identify biomarker candidates for coronary artery disease.[5]

Adaptation and/or perturbations in the proteome caused by a KO can lead to changes in protein expression, but at least equally likely, also to rewiring of signaling networks, through changes in post-translational modifications, such as protein phosphorylation. The application of (phospho)proteomics technology on KO or knock-in models is therefore also extremely relevant, albeit even more challenging. Hilger et al.,[6] combined proteomics and phosphoproteomics on a cell line, wherein a phosphatase had

been knocked-out. To perform such experiments in a more (disease) relevant context, we should invest in functional, tissue-based phosphoproteomics approaches. A few examples of such approaches have very recently been reported. Lundby et al.[7] globally assessed phosphorylation events downstream of systemic adrenergic stimulation in mouse cardiac tissue. We recently reported on the use of a cardiac delimited CaMKII inhibited knock-in mouse to probe for substrates using a focused kinase-inhibition directed approach.[8] Moreover, a mouse model lacking nitric oxide synthase,[9] as a system of interest for Alzheimer's disease, was recently studied by (phospho)proteomics. Here we explore how mature state-of-the-art (phospho)proteomics technology is to monitor the adaptation at the proteome level of the mouse cerebellum in a mouse line deficient for cGMP-dependent protein kinase type I (cGKI, also known as PKG-I), a kinase that plays an important role in synaptic plasticity, motor learning, and other brain functions.[10] The cGMP-dependent protein kinases are serine/threonine kinases that act as key mediators of nitric oxide (NO) signaling, as well as of the natriuretic peptide pathway.[11] In mammals, cGKs are encoded by two different genes: prkg1 coding for cGKI and prkg2 coding for cGKII.[12] The prkg1 gene encodes two cGKI isoforms, cGKIα and cGKIβ,[13] which differ in their N-terminal leucine zipper and auto-inhibitory domain. cGKI regulates cardiovascular functions such as smooth muscle and cardiac contractility;[12] in the nervous system it modulates synaptic plasticity in the hippocampus[14] and cerebellum.[15]

In the mammalian brain, more than 250 protein kinases are expressed, but only a few of these kinases are currently known to contribute to learning and memory. In particular, cGKIα is highly expressed in cerebellar Purkinje cells (PCs).[16] Long-term depression (LTD) is an activity-dependent reduction in the efficacy of synaptic transmission and occurs at the PC synapses. Both a pharmacological approach using enzyme inhibitors[17] and a conditional PC-specific cGKI-KO[18] showed that cGKI plays a role in cerebellar LTD. Several proteins have been identified in the past years to be cGKI substrates *in vitro* or in cultured cells,[11] but only a small portion of these have been confirmed to be cGKI substrates *in vivo*. Therefore, the understanding of cGKI signaling and function depends strongly on the identification of novel in vivo substrates and signaling partners. In this perspective, the currently described approach allows us to discover potentially novel cGKI signaling routes and substrates directly in relevant cerebellar tissue. Our study reveals that cGKI-KO leads to differential expression in the cerebellum of a specific group of proteins, of which many are closely connected to cGMP-cGKI signaling. More changes are observed at the phosphoproteome level, with the regulation of phosphorylation of a few hundred proteins. In particular, we hypothesize that some of the down-regulated phosphoproteins, but certainly not all, may be putative substrates of cGKI.

EXPERIMENTAL PROCEDURES

Mouse model

cGKI-KO mice carrying a null mutation of the prkg1 gene, also termed cGKI$^{L-/L-}$

mice, were generated as described previously.[19] Six-week-old female wild-type (WT) and cGKI-KO mice on a 129/Sv background were sacrificed, and cerebella were dissected and snap frozen with liquid nitrogen and stored at -80°C until use.

Sample preparation

Frozen cerebella were lysed by sonication in lysis buffer consisting in 10 mL of 8 M urea in 50 mM ammonium bicarbonate, 1 tablet of protease inhibitors (Complete mini EDTA-free mixture, Roche Applied Science) and 1 tablet of phosphatase inhibitor mixture (PhosSTOP, Roche Applied Science).

After centrifugation (20,000 x g for 10 min at 4°C), the protein concentration of the supernatant was measured using the Bradford assay and ~1 mg of proteins for each condition was subjected to digestion. Protein reduction and alkylation were performed using a final concentration of 2 mM dithiothreitol and 4 mM iodoacetamide, respectively. Proteins were first digested for 4 h at 37°C with Lys-C (enzyme/substrate ratio 1:100). The second digestion was performed over night at 37°C with trypsin (enzyme/substrate ratio 1:100) in 2 M Urea. The resulting peptides were chemically labeled using stable isotope dimethyl labeling as described before.[20]

Strong cation exchange

Three biological replicates were performed. One WT littermate was used as "Internal Standard" (IS) in all the biological replicates and was labeled with the "Light" (L), while the cGKI-KO mice and the other WT littermates were labeled respectively with "Intermediate" (I) and "Heavy" (H). The labeling efficiency was measured for all the samples and was higher than 95%. The 3 different labeled samples were reconstituted in 10% formic acid (FA) and mixed in a 1:1:1 ratio, prior fractionation using strong cation exchange (SCX) as described previously.[21]

Briefly, the SCX was performed using a Zorbax BioSCX-Series II column (0.8 mm inner diameter X 50 mm length, 3.5 μm). SCX solvent A consisted of 0.05% FA in 20% acetonitrile (ACN) and solvent B of 0.05% FA, 0.5 M NaCl in 20% ACN. The SCX gradient was as follows: 0-0.01 min (0-2% B); 0.001-8.01 min (2-3% B); 8.01-18.01 min (3-8% B); 18.01-28 min (8-20% B); 28-38 min (20-40% B); 38-44 min (40-100% B); 44-48 min (100% B); and 48-50 min (100-0% B), at a flow rate of ~40 μl/min. A total of 45 fractions were collected after injection of ~300 μg of labeled peptides and dried down in a vacuum centrifuge prior LC-MS/MS analysis.

Ti^{4+}-IMAC enrichment

After protein digestion the cGKI-KO mice cerebella were labeled "Heavy" and the WT littermates were labeled "Intermediate". The labeling efficiency was measured and then the samples were mixed in a 1:1:1 ratio by using the same WT "internal standard" labeled "Light" in all the 3 biological replicates. ~300 μg of the peptide mixtures were subjected to phosphopeptide enrichment using Ti^{4+}-IMAC material as described previously 22. Briefly, the mixtures of labeled samples were dried to completion and reconstituted in 80% ACN, 6% trifluoroacetic acid (TFA) and loaded onto the Ti^{4+}-IMAC columns. After washing with 50% ACN, 0.5% TFA, 200 mM NaCl and 50% ACN, 0.1% TFA consecutively, the phosphopeptides were eluted first

with 10% ammonia and then with 80%ACN, 2% FA and were dried to completion in a vacuum centrifuge.

Liquid chromatography and mass spectrometry (SCX and Ti^{4+}-IMAC)

After reconstitution in 10% FA, 5% dimethyl sulfoxide, the SCX fractions containing doubly charged peptides were analyzed using nano flow reverse phase liquid chromatography on a Proxeon Easy-nLC 1000 (Thermo Scientific) coupled to a Q-Exactive mass spectrometer (Thermo, San Jose, CA). The SCX fractions containing triply charged peptides were analyzed on a LTQ-Orbitrap Velos or an Orbitrap Elite (Thermo, San Jose, CA). Depending on the SXC UV trace, 0.5-10% of each fraction was injected. Densely populated 2+ and 3+ fractions were injected twice to minimize under-sampling of the mass spectrometer.

Peptides were separated on an in-house made 50 cm column, 75 μm inner diameter packed with 1.8 μm C18 resin (Agilent Zorbax SB-C18) at a constant temperature of 40°C, connected to an Orbitrap mass spectrometer (Thermo Scientific) through a nanoelectrospray ion source. The injected peptides were first trapped with a double fritted trapping column (Dr Maisch Reprosil C18, 3 μm, 2 cm x 100 μm) at a pressure of 800 bar with 100% solvent A (0.1 % formic acid in water) before being chromatographically separated by a linear gradient of buffer B (0.1% formic acid in acetonitrile) from 7% up to 30% in 150 min at a flow rate of 150 nl/min.

The enriched phosphopeptides were chromatographically separated with 150 min gradient as described previously and analyzed on a LTQ-Orbitrap Elite.

Nanospray was achieved with an in-house pulled and gold coated fused silica capillary (360 μm outer diameter, 20 μm inner diameter, 10 μm tip inner diameter) and an applied voltage of 1.7 kV. Full-scan MS spectra (from m/z 350 to 1500) were acquired in the orbitrap with a resolution of 35,000 for the Q-Exactive and 30,000 for the Orbitrap Velos and Elite. Up to ten most intense ions above the threshold of 500 counts were selected for fragmentation. HCD fragmentation was performed when using the Q-Exactive with a data dependent mode, as previously described.[22] For the fragmentation using the Velos or Elite instrument, a decision tree method was used as described previously.[23]

Data analysis: SCX

For each raw data file recorded by the mass spectrometer, peak lists were generated using Proteome Discoverer (version 1.3, Thermo Scientific, Bremen, Germany) using a standardized workflow. Peak lists, generated in Proteome Discoverer, were searched against a Swiss-Prot database (version 2.3.02, taxonomy Mus musculus, 32402 protein entries) supplemented with frequently observed contaminants, using Mascot (version 2.3.02 Matrix Science, London, UK). The database search was performed by using the following parameters: a mass tolerance of 50 ppm for the precursor masses and ±0.6 Da for CID/ETD fragment ions and ±0.05 Da for HCD fragments. Enzyme specificity was set to Trypsin with 2 missed cleavages allowed. Carbarmidomethylation of cysteines was set as fixed modification, oxidation of methionine, dimethyl labeling (L, I, H) of lysine residues and N termini were used as variable modifications.

Percolator was used to filter the PSMs for <1% false discovery-rate. Triplex dimethyl labeling was used as quantification method,[24] with a mass precision of 2 ppm for consecutive precursor mass scans. A retention time tolerance of 0.5 min was used to account for the potential retention time shifts due to deuterium. To further filter for high quality data we used the following parameters: high confidence peptide spectrum matches, minimal Mascot score of 20, minimal peptide length of 6 and only unique rank 1 peptides. For the identification and quantitation of the proteins, only unique peptides were considered. To estimate if the proteins were significantly regulated, t-test based statistics were applied only to the proteins quantified in all the biological replicates with at least one quantified unique peptide passing the above-mentioned filtering criteria. Multiple testing correction was applied by using a permutation-based false discovery rate method in Perseus[25] (number of randomization=250, FDR=0.1, s0=0.3), and only the proteins with a ratio of cGKI-KO/ IS/ WT/IS (cGKI-KO/ WT) ≥ 1.7-fold were considered regulated.

Data analysis: Ti^{4+}-IMAC

For the phosphopeptide analysis after Ti^{4+}-IMAC enrichment the same parameters as for the SCX analysis were used and phosphorylation (S, T, Y) was used as variable modification. Percolator was used to filter the PSMs for <1% false discovery-rate. Phosphorylation sites were localized by applying phosphoRS (pRS) (v2.0).[26] Triplex dimethyl labeling was used as quantification method, with a mass precision for the 2 ppm for consecutive precursor mass scan. A retention time tolerance of 0.5 min was used to account effect of deuterium on retention time. To further filter for high quality data we used the following parameters: high confidence peptide spectrum matches, minimal Mascot score of 20, minimal peptide length of 6, only unique rank 1 peptide and the search rank 1 peptide.

Only the ratios of the peptides with the same amino acid sequence, the same number of phosphorylation sites and identical phosphosite localization in the three biological replicates were averaged. Normalization of the protein ratios obtained in the corresponding biological replicate was used. The cGKI-KO/WT ratios were then subjected to a Significance B test. The phosphopeptides that showed an on/off situation in the cGKI-KO or in the WT were manually quantified by giving them an arbitrary value of 100 or 0.01 for extreme up- or down-regulation, which corresponds to the maximum allowed fold change in the used Proteome Discoverer settings. The significantly changing phosphopeptides were subjected to network analysis using STRING.[27] Two different queries were performed for the up- and down-regulated phosphopeptides, with the following parameters for the active prediction methods: experiments, databases and neighborhood, required confidence (score): high. The obtained networks were implemented with the kinases using the network analysis environment Cytoscape v.2.8.2[28] using the PhosphoSitePlus plugin. The phosphosites that showed a connection with one or more kinases were manually matched against the database repository PhosphoSitePlus.[29]

The mass spectrometry proteomics data have been deposited to the ProteomeX-

change Consortium (http://proteomecentral.proteomexchange.org) via the PRIDE partner repository[30] with the dataset identifier PXD000502.

Western blot analysis

After separation by SDS-PAGE the proteins were transferred onto PVDF membrane. Blots were incubated with rabbit anti-cGKI[31] (1:5000); mouse anti-Huntingtin associated protein 1 (HAP1, Novus biological, 1:5000); rabbit anti-sarcoplasmic/endoplasmic reticulum calcium ATPase 3 (SERCA3, Thermo Fisher, 1:2000), goat anti-cAMP-dependent protein kinase type II-beta regulatory subunit (PKARIIβ, Santa Cruz, 1:500); rabbit anti- cGMP-specific 3',5'-cyclic phosphodiesterase (PDE5, Cell Signaling, 1:1000), or mouse anti-glyceraldehyde-3-phosphate dehydrogenase (GAPDH, GeneTex, 1:2000). After several washes the blots were incubated with appropriate horseradish peroxidase-labeled secondary antibodies and developed with the ECL reagent (GE Healthcare). Proteins were quantified using the program ImageQuantTL 1D v. 7.0 (GE Healthcare).

Immunohistochemistry on paraffin sections

Cerebella were fixed overnight at 4°C using 2% formaldehyde and 0.2% glutaraldehyde in PBS. Subsequently the tissues were dehydrated with an ethanol gradient and embedded in paraffin. 10 µm sections were cut, dried overnight, deparaffinized, and rehydrated. Endogenous peroxidase was blocked using peroxidase blocking solution (300 µl 30% H2O2 and 130 µl 10% CH3OH/PBS in a final volume of 1 ml PBS) for 20 minutes at room temperature. Then, antigen retrieval using the heating method was performed and the sections were incubated overnight at 4°C with primary antibodies: rabbit anti-cGKI (1:500)[31] or rabbit anti-SERCA3 (Thermo Fisher, 1:100). Then the sections were incubated with biotinylated secondary antibody (1:200) for 1 hour followed by the ABC complex (Vectastain ABC kit, Vector Laboratories) for 30-40 minutes at room temperature and color was developed using the diaminobenzidine peroxidase substrate. Sections were mounted with Shandon Immu-Mount (Thermo Fischer Scientific) and images were obtained under 20x magnification using an Axioskop (Zeiss).

Immunofluorescence staining of frozen sections

Cerebella were perfusion-fixed using 4% paraformaldehyde in PBS. After dissection the tissues were incubated in the same fixative at 4°C overnight. The cerebella were washed twice with PBS, passed through a sucrose gradient (10%, 20%, and 30%) and embedded in O.C.T. compound (VWR International GmbH). 10 µm sections were cut at -20°C and dried. Sections were incubated at 4°C overnight with rabbit anti-PDE5 (1:500).[32] Then sections were incubated with secondary antibody (Alexa 488, goat anti-rabbit; 1:200) for 1 hr at room temperature and mounted with Shandon Immu-Mount (Thermo Fischer Scientific). Images were obtained under 16x magnification using an Axiovert 200 (Zeiss).

RESULTS

Alterations in the cerebellar proteome of cGKI-KO mice

We first performed an in-depth quantitative proteomics screen on the cerebellum of cGKI-KO mice and compared these in a biological triplicate experiment with their WT littermates with identical genetic background. After dissection, the cerebellar tissues were processed as schematically described in Figure 1A and in the materials and methods. One of the WT mice was used as "internal standard" and multiplexed with three biological replicate comparisons (WT vs. cGKI-KO). We used triplex dimethyl stable isotope labeling as described previously to enable us to quantitatively profile the proteome in three samples simultaneously.[20] After trypsin digestion, the internal standard was tagged with the light dimethyl label. In all the biological replicates, the cGKI-KO mice were labeled as medium while the WT mice were labeled as heavy. These three peptide mixtures were fractionated using SCX and consecutively analyzed by reverse phase high-resolution LC-MS/MS using an Orbitrap employing methods essentially as described before.[23] We identified a total of 6981 cerebellar proteins (Supplemental Figure 1A) of which 6210 (89%) could be quantified (Figure 1B, Supplemental Figure 1B and Supplemental Table 1A). Amongst these proteins, more than 95% were quantified with more than one unique peptide (Supplemental Figure 1C). To strengthen the statistics, and reliability, we only considered the proteins for which we obtained both an Intermediate/Light (cGKI-KO/IS) and a Heavy/Light (WT/IS) ratio in all three replicates (3755) (Supplemental Table 1B). To compare the protein expression levels, we applied a t-test to the logarithmic ratios of the cGKI-KO and the WT mice, by using the Perseus software package.[25] After the application of multiple testing corrections, only the significantly regulated proteins with a minimum ratio of cGKI-KO/WT of at least 1.7-fold were considered as differential.

Out of 3755 proteins robustly quantified, 86 proteins showed an up-regulation while 30 proteins were significantly down-regulated (Table 1). As expected, the knocked-out cGKI was the top-down regulated protein.

To put these 116 proteins in functional perspective, we manually scrutinized the literature to better understand the role of these regulated proteins in the cerebellum and their putative role in LTD. Noticeably, we found many of the regulated proteins either linked to cGMP or cAMP signaling. This group contained the cyclic nucleotide degrading phosphodiesterases PDE5 (cGKI-KO/WT= 0.5), PDE1B (cGKI-KO/WT= 2.0), and PDE1C (cGKI-KO/WT= 0.5), the cAMP-dependent protein kinase type II-beta regulatory subunit, PKARIIβ (cGKI-KO/WT= 2.3), and its anchoring scaffolds AKAP5 (cGKI-KO/WT= 2.6), and SPHKAP (cGKI-KO/WT=0.6). In addition, we observed regulation of several neurotransmitter receptors (i.e. GRIN2B, mGluR7, and VGluT2), ion channels/transporters (i.e. SERCA3, CA2D1 and KCNA4), and signal transduction enzymes (i.e. the already mentioned cyclic nucleotide kinases, but also IP3KA, CaMKIV, CaMKV, LYN and CDK14). In summary, the adaptation to the cGKI-KO at the global proteome level is not enormous, as only 3% of the quantified proteins appear substantially differentially expressed. However,

many of the differentially expressed proteins are involved in cyclic nucleotide signaling and/or play a role in synaptic transmission.

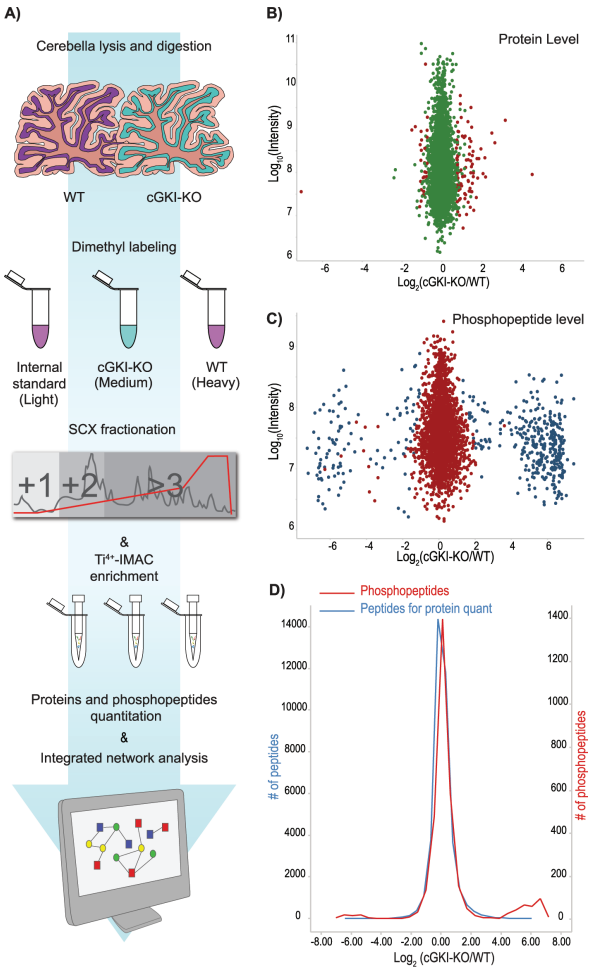

Figure 1. *A) Proteomics workflow. After dissection, the cerebella from WT and cGKI-KO mice were lysed in 8 M urea and digested with Lys-C and trypsin. Internal standard, KO and WT peptides were labeled using stable isotope dimethyl labeling and mixed in a 1:1:1 ratio. To enhance proteome coverage, sample complexity was reduced by fractionating the resulting peptide mixtures using strong cation exchange (SCX). The same samples were used for phosphoproteome analysis, using phosphopeptide enrichment by Ti^{4+}-IMAC. All the (phospho)peptide mixtures were analyzed by UHPLC-MS/MS. After protein and phosphopeptide quantitation the data were subjected to network analysis. B) MA-plot of proteins quantified in all three biological replicates (the proteins that showed significant changes after statistical analysis are reported in red). C) MA-plot of the quantified phosphopeptides in all the biological replicates after Ti^{4+}-IMAC enrichment (the phosphopeptides that showed significant regulation using significance B testing are reported in blue). D) Density curves of observed peptide ratios used for the protein quantitation (blue) and for the phosphopeptides quantified after Ti^{4+}-IMAC enrichment. The peptides and the phosphopeptides show a tight distribution with more extreme differentials observed at the phosphopeptide level.*

Accession	Gene name	Description	cGKI-KO/ WT	St.Dev	# Unique peptides
Q60590	Orm1	Alpha-1-acid glycoprotein 1	23.45	1.46	5
Q91X72	Hpx	Hemopexin	9.27	2.46	22
Q8K0E8	Fgb	Fibrinogen beta chain	6.21	0.90	22
Q8VCM7	Fgg	Fibrinogen gamma chain	5.75	1.57	20
Q8CGV2	Tph2	Tryptophan 5-hydroxylase 2	6.08	3.81	11
Q3UHL1	Camkv	CaM kinase-like vesicle-associated protein	4.67	1.00	11
P06909	Cfh	Complement factor H	4.24	1.08	18
Q5DTY9	Kctd16	BTB/POZ domain-containing protein KCTD16	4.54	1.30	5
Q9R111	Gda	Guanine deaminase	3.46	0.71	10
O35668	Hap1	Huntingtin-associated protein 1	3.52	0.20	7
O08677	Kng1	Kininogen-1	3.50	0.75	13
Q9QUG9	Rasgrp2	RAS guanyl-releasing protein 2	3.46	0.85	6
P01029	C4b	Complement C4-B	3.16	1.11	8
Q8K3E5	Ahi1	Jouberin	3.05	0.43	25
P97467	Pam	Peptidyl-glycine alpha-amidating monooxygenase	3.15	0.91	12
P50153	Gng4	Guanine nucleotide-binding protein G(I)/G(S)/G(O) subunit gamma-4	3.09	0.84	1
P20918	Plg	Plasminogen	3.04	0.93	15
Q61704	Itih3	Inter-alpha-trypsin inhibitor heavy chain H3	2.90	0.56	11
Q61147	CERU	Ceruloplasmin	3.00	0.87	22
Q91ZP9	Necab2	N-terminal EF-hand calcium-binding protein 2	3.19	1.17	5
Q91XV3	Basp1	Brain acid soluble protein 1	3.02	0.67	14
P11276	Fn1	Fibronectin	2.79	0.65	30
P01027	C3	Complement C3	2.92	0.99	54
Q921I1	TRFE	Serotransferrin	2.84	0.81	38
Q9DB26	Phyhd1	Phytanoyl-CoA dioxygenase domain-containing protein 1	2.84	0.81	2
Q91WP6	Serpina3n	Serine protease inhibitor A3N	2.85	0.65	3
Q8BHH2	Rab9b	Ras-related protein Rab-9B	2.91	1.21	4
Q8CHT1	Ngef	Ephexin-1	2.65	0.59	3
Q61423	Kcna4	Potassium voltage-gated channel subfamily A member 4	2.71	0.89	1
Q03517	Scg2	Secretogranin-2	2.73	0.48	19
O35526	Stx1a	Syntaxin-1A	2.62	0.44	11
Q9CZS1	Aldh1b1	Aldehyde dehydrogenase X, mitochondrial	2.64	0.42	7
D3YVF0	Akap5	A-kinase anchor protein 5	2.52	0.42	7
Q60673	Ptprn	Receptor-type tyrosine-protein phosphatase-like N	2.75	0.83	6
Q9WTR5	Cdh13	Cadherin-13	2.54	0.52	9
Q9WUC3	Ly6h	Lymphocyte antigen 6H	2.52	0.06	4
Q01097	Grin2b	Glutamate [NMDA] receptor subunit epsilon-2	2.41	0.50	5
Q9QXV0	Pcsk1n	ProSAAS	2.59	0.53	9
Q68ED2	Grm7	Metabotropic glutamate receptor 7	2.37	1.01	4
P06728	Apoa4	Apolipoprotein A-IV	2.37	0.87	14
Q3TW96	Uap1l1	UDP-N-acetylhexosamine pyrophosphorylase-like protein 1	2.45	0.87	8
P16460	Ass1	Argininosuccinate synthase	2.32	0.18	8

Accession	Gene name	Description	cGKI-KO/ WT	St.Dev	# Unique peptides
P31324	Prkar2b	cAMP-dependent protein kinase type II-beta regulatory subunit	2.27	0.32	13
Q68FM6	Elfn2	Protein phosphatase 1 regulatory subunit 29	2.25	0.26	5
P19221	THRB	Prothrombin	2.34	0.88	7
O54901	Cd200	OX-2 membrane glycoprotein	2.32	0.50	3
Q61838	A2m	Alpha-2-macroglobulin	2.19	0.62	39
P48320	Gad2	Glutamate decarboxylase 2	2.20	0.37	14
Q921X9	Pdia5	Protein disulfide-isomerase A5	2.32	0.96	3
P80560	Ptprn2	Receptor-type tyrosine-protein phosphatase N2	2.09	0.27	16
P29699	Ahsg	Alpha-2-HS-glycoprotein	2.31	1.23	4
Q61247	Serpinf2	Alpha-2-antiplasmin	2.06	0.68	5
Q01065	Pde1b	Calcium/calmodulin-dependent 3',5'-cyclic nucleotide phosphodiesterase 1B	2.09	0.58	12
Q8BLR2	Cpne4	Copine-4	2.08	0.53	5
P31650	Slc6a11	Sodium- and chloride-dependent GABA transporter 3	1.97	0.28	11
Q60771	Cldn11	Claudin-11	2.04	0.66	3
Q8R5A6	Tbc1d22a	TBC1 domain family member 22A	2.01	0.67	7
Q62188	Dpysl3	Dihydropyrimidinase-related protein 3	1.90	0.08	17
P49025	Cit	Citron Rho-interacting kinase	1.94	0.45	15
O54990	Prom1	Prominin-1	1.91	0.46	4
Q2M3X8	Phactr1	Phosphatase and actin regulator 1	1.85	0.41	5
Q9R226	Khdrbs3	KH domain-containing, RNA-binding, signal transduction-associated protein 3	1.98	0.79	3
O35495	Cdk14	Cyclin-dependent kinase 14	1.96	0.63	2
P84075	Hpca	Neuron-specific calcium-binding protein hippocalcin	1.86	0.49	5
Q8R5M8	Cadm1	Cell adhesion molecule 1	1.83	0.19	7
P70392	Rasgrf2	Ras-specific guanine nucleotide-releasing factor 2	1.90	0.56	7
Q5XG69	Fam169a	Protein FAM169A	1.80	0.13	9
P70699	Gaa	Lysosomal alpha-glucosidase	1.79	0.37	14
Q61553	Fscn1	Fascin	1.75	0.12	15
P07356	Anxa2	Annexin A2	1.78	0.21	15
Q80TL4	Kiaa1045	Protein KIAA1045	1.77	0.39	13
O89026	Robo1	Roundabout homolog 1	1.76	0.13	5
O08532	Cacna2d1	Voltage-dependent calcium channel subunit alpha-2/delta-1	1.80	0.42	21
Q5RJG7	Ispd	2-C-methyl-D-erythritol 4-phosphate cytidylyltransferase-like protein	1.73	0.03	4
O35633	Slc32a1	Vesicular inhibitory amino acid transporter	1.73	0.16	10
Q8BLE7	Slc17a6	Vesicular glutamate transporter 2	1.73	0.37	7
Q9EQF6	Dpysl5	Dihydropyrimidinase-related protein 5	1.73	0.11	26
A2ALU4	Shroom2	Protein Shroom2	1.73	0.18	15
O55091	Impact	Protein IMPACT	1.82	0.54	13
Q61599	Arhgdib	Rho GDP-dissociation inhibitor 2	1.74	0.35	6
P36552	Cpox	Coproporphyrinogen-III oxidase, mitochondrial	1.70	0.22	8
Q3UUG6	Tbc1d24	TBC1 domain family member 24	1.70	0.02	9

Accession	Gene name	Description	cGKI-KO/ WT	St.Dev	# Unique peptides
Q66L44	Dos	Protein Dos	1.69	0.10	3
Q922J6	Tspan2	Tetraspanin-2	1.69	0.14	3
Q8BR92	Palm2	Paralemmin-2	1.69	0.13	9
Q9CX80	Cygb	Cytoglobin	1.68	0.19	10
Q8BYJ6	Tbc1d4	TBC1 domain family member 4	0.63	0.05	16
Q99JP6	Homer3	Homer protein homolog 3	0.61	0.11	21
Q69ZX8	Ablim3	Actin-binding LIM protein 3	0.60	0.04	12
Q8BYR5	Cadps2	Calcium-dependent secretion activator 2	0.60	0.08	34
P08414	Camk4	Calcium/calmodulin-dependent protein kinase type IV	0.61	0.09	21
Q8R071	Itpka	Inositol-trisphosphate 3-kinase A	0.58	0.07	20
Q6NSW3	Sphkap	A-kinase anchor protein SPHKAP	0.60	0.09	26
Q91ZH7	Abhd3	Abhydrolase domain-containing protein 3	0.58	0.10	6
Q9QUR8	Sema7a	Semaphorin-7A	0.58	0.07	12
Q0VEJ0	Cep76	Centrosomal protein of 76 kDa	0.59	0.13	19
Q9JJZ2	Tuba8	Tubulin alpha-8 chain	0.57	0.07	7
P25911	Lyn	Tyrosine-protein kinase Lyn	0.56	0.11	7
Q3UH99	Shisa6	Protein shisa-6 homolog	0.56	0.11	11
P18653	Rps6ka1	Ribosomal protein S6 kinase alpha-1	0.58	0.12	17
Q6WQJ1	Dagla	Sn1-specific diacylglycerol lipase alpha	0.54	0.10	14
Q64338	Pde1c	Calcium/calmodulin-dependent 3',5'-cyclic nucleotide phosphodiesterase 1C	0.53	0.10	5
Q5F226	Fat2	Protocadherin Fat 2	0.56	0.19	37
Q8QZT2	CA096	Uncharacterized protein C1orf96 homolog	0.53	0.11	7
Q80YX1	Tnc	Tenascin	0.50	0.03	45
P55088	Aqp4	Aquaporin-4	0.51	0.25	2
Q64518	Atp2a3	Sarcoplasmic/endoplasmic reticulum calcium ATPase 3	0.52	0.20	23
Q8CG03	Pde5a	cGMP-specific 3',5'-cyclic phosphodiesterase	0.54	0.16	9
Q9ERY9	ORF11	Probable ergosterol biosynthetic protein 28	0.53	0.20	3
Q9EQK7	Icmt	Protein-S-isoprenylcysteine O-methyltransferase	0.54	0.24	3
Q9ERQ8	Ca7	Carbonic anhydrase 7	0.49	0.11	4
Q64444	Ca4	Carbonic anhydrase 4	0.52	0.19	8
P06537	Nr3c1	Glucocorticoid receptor	0.49	0.21	6
P68433	Hist1h3a	Histone H3.1	0.40	0.03	5
P62806	Hist1h4a	Histone H4	0.35	0.01	9
P0C605	Prkg1	cGMP-dependent protein kinase 1	0.01	0.00	11

Table 1 *Proteins differentially expressed in mouse cerebellum upon cGKI knockout.*

Validation of the proteomics results by Western blot analysis and immunostaining of tissue sections

We decided to verify some of these results by Western blot analysis, when good antibodies were available (Figure 2A). Three cerebellar tissues for each condition (i.e. KO versus WT) were analyzed and the protein levels quantified from the blot (Figure 2B).

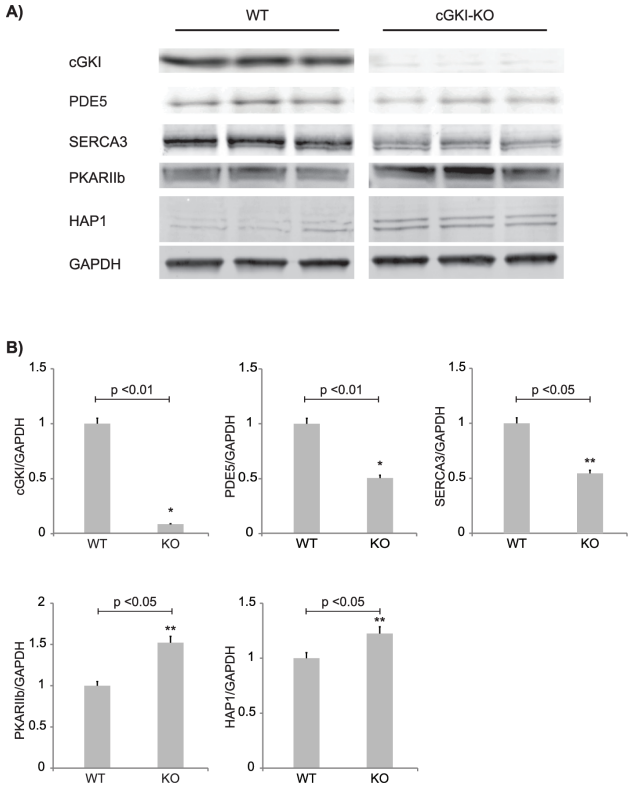

Figure 2 *Confirmation of regulated proteins. A) Western blot analysis of selected significantly regulated proteins and B) their relative quantification. Data values were normalized using GAPDH (30 μg lysate). The data are given as the mean±S.E.M. (n=3 per condition). Significant changes are indicated; * = p< 0.05 and ** p< 0.01.*

These data confirmed the absence of cGKI in cGKI-KO cerebellum and indicated a lower expression of cGMP-specific phosphodiesterase PDE5 and the calcium pump SERCA3 in cGKI-deficient cerebellum, while PKARIIβ and the Huntingtin associated protein 1 (HAP1) showed an increased expression in the KO cerebellum. All these results are consistent with our proteomics results. However, with MS-based proteomics and the Western blot analysis it is hardly possible to say if the down-regulation of a protein is related to a global change or to an event localized to a particular cell type or region within the cerebellum. Therefore, we next performed immunohistochemistry and immunofluorescence staining of cerebellar sections for cGKI, SERCA3, and PDE5 (Figure 3).

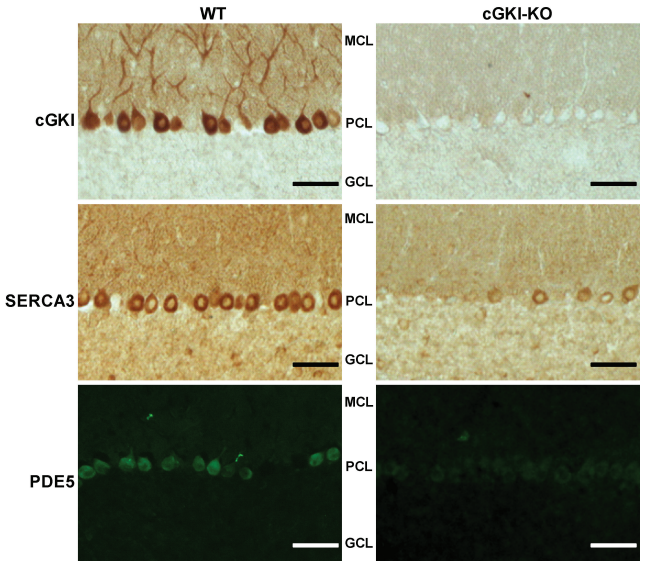

Figure 3 *Cellular localization of cGKI-KO induced regulated proteins. Immunohistochemical (top and middle panel) and immunofluorescence (bottom panel) stainings showing the localization of cGKI, SERCA3 and PDE5 in the cerebella of WT and cGKI-KO mice (scale bar, 50 μm). cGKI (top panel) is highly expressed in the PCs of WT mice, wherein SERCA3 and PDE5 are also co-expressed. As compared to WT mice, SERCA3 (middle panel) and PDE5 (bottom panel) are down-regulated in PCs of cGKI-KO mice. MCL, PCL, and GCL denotes molecular, Purkinje, and granular cell layer, respectively.*

These images clearly indicate that cGKI, SERCA3 and PDE5 are co-expressed in the PCs of WT mice, whereas SERCA3 and PDE5 expression levels are diminished in the cGKI-KO PCs. Thus, the Western blot results, combined with the immunostaining of cerebellar sections, confirmed the data obtained from our MS-based proteomics approach for these selected proteins. These findings provide also confidence to the remainder of reported differentially expressed proteins.

Alterations in the cerebellar phosphoproteome of cGKI-KO mice

Since cGKI is a protein kinase, we next globally profiled altered phosphorylation patterns as a consequence of the proteome rewiring induced by the cGKI deletion. cGKI, like its closest relative PKA, targets serine or threonine phosphorylation sites in its substrates within a basic consensus motif $[R/K_{2\text{-}3}]X[K][S/T]$.[33] Therefore, we used an adapted Ti^{4+}-IMAC-based phosphopeptide enrichment strategy shown to be suited for basic kinase motifs.[22] For the phosphopeptide enrichment, the same cerebella were used as for the proteome analysis (Figure 1A). A total of 3690 unique phosphopeptides could be identified after running the enriched phosphopeptide fractions, of which 3271 could be quantified. 2859 of these quantified phosphopeptides were identified with reasonable definite site localization (pRS ≥75%)[26] (Supplemental Table 2A). Within the localized phosphopeptides 1696 could be quantified in at least two out of three replicates, whereas 1163 were quantified in just one replicate

(Supplemental Figure 2A and 2B). The average of the quantified phosphopeptides (cGKI-KO/WT) from the three biological replicates was subjected to Significance B using the Perseus package, in order to define the cut-off for significant regulation. Since the animal model that we used lacks cGKI we had to consider that several phosphorylation sites could show an on/off regulation. We manually scrutinized the MS spectra of the peptides that showed intensity in only one of the two conditions, before giving them an arbitrary value of 100 or 0.01, which corresponds to the maximum allowed fold-change in the software settings. Using these parameters, a total of 345 and 113 phosphopeptides, originating from 296 phosphoproteins, were considered to be up- or down-regulated, respectively (Figure 1C).

Global evaluation of the quantitative data showed more changes at the phosphopeptide level in comparison to the protein level, nevertheless when the phosphopeptides are compared to the peptides used for the protein quantitation, they show overall a similar and very tight distribution (Figure 1D).

To visualize how the signaling network in the cerebellum adapted to the cGKI-KO we evaluated all these 296 phosphoproteins against protein and interactome databases, such as STRING.[27] The proteins showing increased phosphorylation were found to be enriched in Ca^{2+} transporters and receptors (i.e. GRID2, CCG7, and SLC32A1), enzyme modulators (i.e. PP14A and MYPT1), G-protein modulators (i.e. SRGAP3 and RIMS1) and cytoskeletal proteins (i.e. CTNNA2, NCAM and VCL). For proteins showing decreased phosphorylation in the cGKI-KO cerebellum we identified various proteins such as kinases (i.e. GSK3β), enzyme modulators (i.e. AMPKb1) and structural proteins (i.e. NEFH and NEM). To further complete the picture of the changes observed in the phosphopeptides which did not show any connection in the networks, we implemented the networks with the possible upstream kinases, identified in our proteomics dataset, and assigned, when possible, the right putative kinases to each regulated phosphosite.

The up-regulated network (Figure 4A) clearly shows a set of phosphosites that are not directly linked to the KO kinase cGKI, but are thought to be phosphorylated by different kinases, such as PKA, casein kinase 2 (CKIIA1) and CaMKII. Notably, we identified one of the sites, which mediates protein kinase C beta (PKCβ) activity (Thr-642) to be up-regulated in the cGKI-KO mice. PKCβ activity is regulated through three distinct phosphorylation events that occur at Thr500, at Thr-642 through auto-phosphorylation and at the carboxy-terminal site at Ser-660.[34] The up-regulation of the phosphorylated site in the cGKI-KO mice, could implicate an increased activity of PKCβ in absence of cGKI, potentially to compensate for its lack.

Interestingly, several proteins involved in the regulation of cell survival showed regulated phosphorylations on specific sites reported to be critical for apoptosis. For example, the up-regulation of the phosphorylated Ser-1040 of MAP3K5 suppresses its pro-apoptotic function.[35] On the other side, the down-regulation of the phosphorylation at Ser-116 of PEA-15, a downstream effector of PKC, AKT and CaMKII (Figure 4B), blocks ERK's translocation to the nuclei and therefore cell proliferation.[36] Also the Glycogen synthase kinase 3β (GSK3β) showed a down-regulation of phos-

phorylation at Ser-389. Thornton et al.[37] showed that phosphorylation of GSK3β by p38 MAPK on Ser-389, deactivates the kinase, in brain, and that it is potentially linked to cell survival.

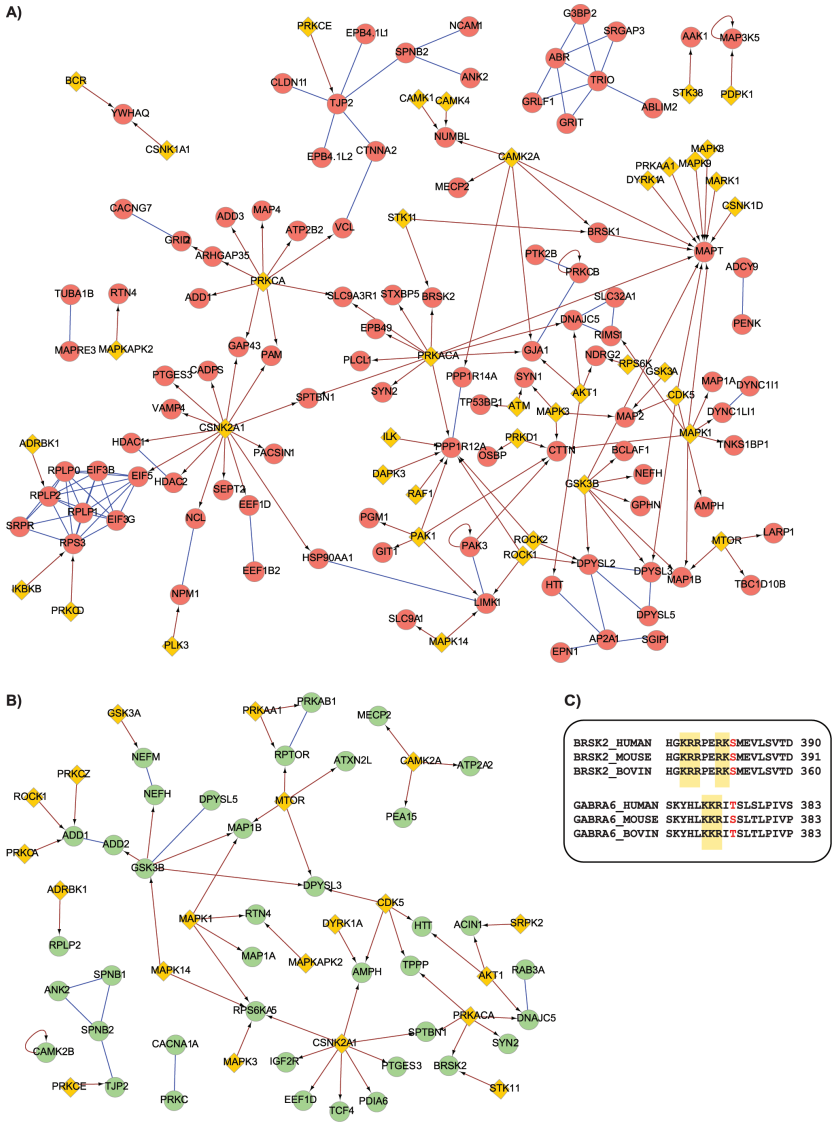

Figure 4 *Interaction network of cGKI-KO affected phosphoproteins. Interaction network for the observed differential phosphorylated proteins. A) When the phosphosites were higher in the cGKI-KO mice they are given in red and B) when lower in green. Evidence of protein-protein interactions (blue lines) were retrieved from the STRING database. The networks were implemented with kinases (yellow diamonds) using the PhosphoSitePlus plugin in Cytoscape. Each phosphorylation was manually checked in the PhosphoSitePlus database and connected with its (known) kinase (arrows). C) Alignment of the putative cGKI phosphorylation sites, for BRSK2 and Gabra6 in different species implicates a putative role of their phosphorylation in cerebellum.*

We hypothesized that we could potentially observe cGKI substrates as being "completely" down-regulated in the cGKI-KO mice. Therefore, we screened within the down-regulated phosphopeptides, for peptides harboring a cGKI-linked basic consensus motif. We observed only two, one on the serine/threonine-protein kinase BRSK2 (BRSK2) and the other on the gamma-aminobutyric acid receptor subunit alpha-6 (Gabra6) which are both involved in neural polarization. The phosphorylated sequences in these two proteins show an elevated amount of lysine/arginine residues, N-terminal to the phosphorylation site, implying that they may be cGKI substrates. Moreover, multiple alignments of both BRSK2 and Gabra6 from different species show that the putative cGKI phosphorylation sites as well as the preceding basic residues are well conserved, implying a possible functional role of the two proteins, when phosphorylated (Figure 4C).

Combined proteome and phosphoproteome data provide a link to LTD

In a recent review, Collingridge et al.[38] proposed an overview of the intricate protein signaling networks involved in the regulation of LTD, both in the hippocampus and cerebellum. Using the knowledge retained from the BioGRID and STRING protein-protein interaction databases,[39] we observed that we could clearly put our data in the context of LTD. We were able to identify several connections between observed regulated proteins and phosphoproteins involved in cGMP-cGKI signaling and playing a role in cerebellar plasticity (figure 5A). We identified, for instance, in our cGKI-KO (phospho)proteome dataset a highly interconnected network between cGKI, inositol 1,4,5-trisphosphate receptor type 1 (Itpr1), Huntingtin (Htt), the Huntingtin associated protein 1 (HAP1), and its direct interactor Jouberin (AHI1). HAP1 was recently found to form a complex with the Htt and the Itpr1 to regulate the concentration of cytoplasmic Ca^{2+}.[40] Furthermore Itpr1 might be a substrate of cGKI and activation of cGKI regulates cytoplasmic Ca^{2+} through the inositol 1,4,5-trisphosphate receptor-associated cGMP kinase substrate (IRAG) in smooth muscle.[41] This could imply that the Ca^{2+} regulation operates through a similar mechanism in cerebellum. Based on these findings we could link our data clearly to the network described to be highly involved in LTD (Figure 5B).

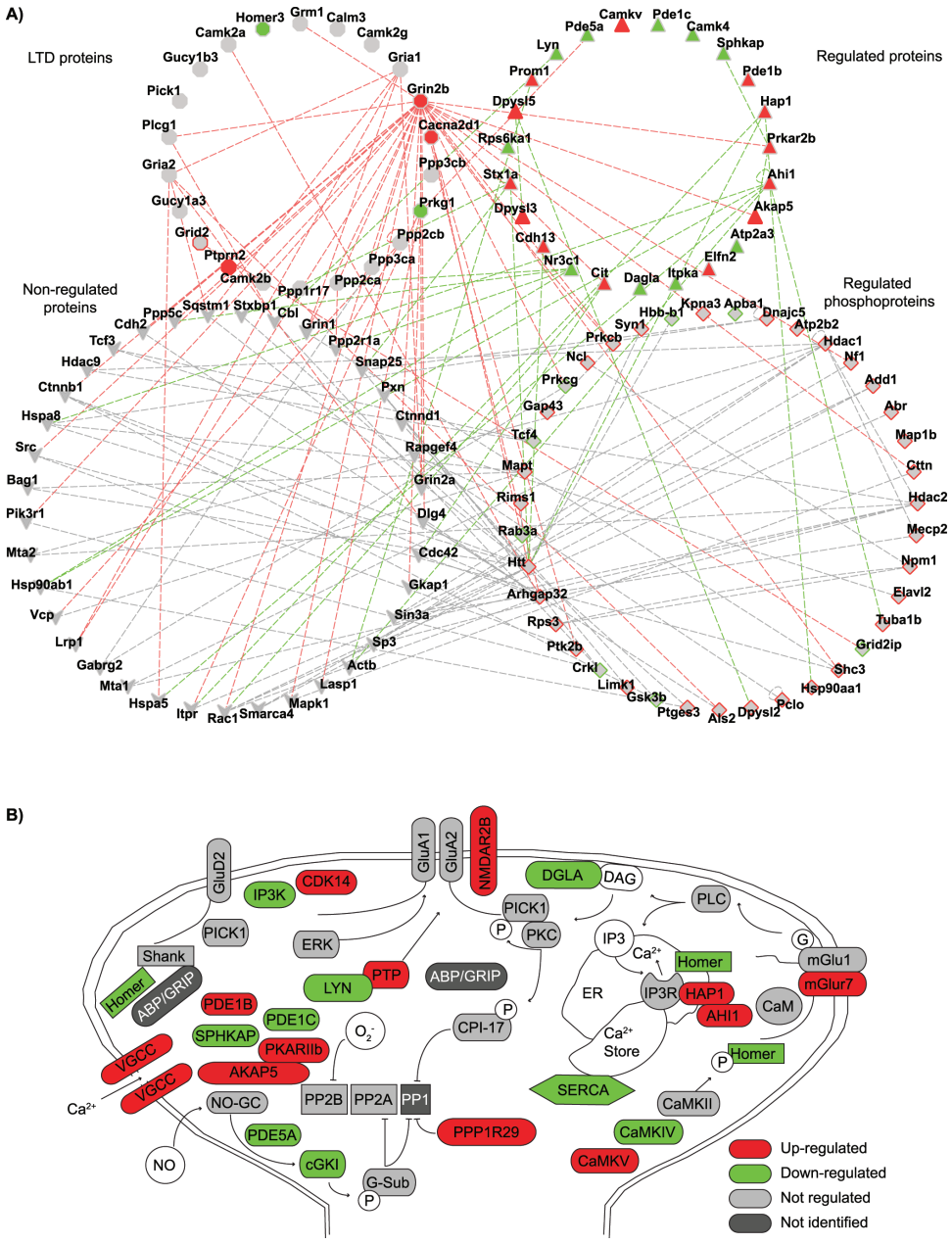

Figure 5 *Integrative computational network analysis reveals implication of altered proteins in LTD. A) Protein-protein interaction network of the combined proteomics and phosphoproteomics datasets B) Signaling network modulating LTD in the cerebellum, superimposed with the current quantitative proteomics and phosphoproteomics data, and additional more recent literature. Figure is adapted from Collingridge et al..*[38] *Red means up-regulated, green down-regulated in cGKI-KO cerebellum.*

DISCUSSION

In the past years many studies have been carried out at the molecular biology and physiological level to try to understand the exact role of cGMP and cGKI in the PCs for the regulation of LTD and cerebellar learning.

In this study we have started to add much more molecular detail towards this interesting field by investigating the changes that occur at the proteome and phosphoproteome level of the cerebellum in a cGKI-deficient mouse model. Using this approach we have identified a specific subset of proteins that are significantly changed in expression in the cGKI-KO as compared with the WT littermates.

Within the down-regulated proteins, PDE5 drew our attention, since it plays an important role in the cGMP pathway. The down-regulation of PDE5 in the PCs may be explained as a compensatory mechanism for the lack of cGKI action. Attempting to increase the levels of cGMP is a logical response and the down-regulation of the cGMP-degrading enzyme, PDE5 (Figure 3),[11] a logical strategy to achieve this. In line with this observation, several studies revealed that tissues lacking cGKI show an elevated concentration of cGMP.[42,43] The absence of cGKI and an increase of the cGMP level could lead to the activation of other kinases, such as PKA,[42] or PKC.[44] PKCIIβ, indeed, in our dataset, shows a high regulation at the phosphorylation level of the activation loop site (Figure 4B).

Moreover, other proteins that could be involved in LTD in the cerebellum show an increased protein expression in the absence of cGKI, such as the protein phosphatase 1 regulatory subunit (PPP1R29). PPP1R29 functions to inhibit the activity of protein phosphatase 1 and 2 A (PP1 and PP2). Together with PPP1R29, a protein termed G-substrate also blocks PP1 activity after it has been phosphorylated by cGKI.[45]

Although we were not able to identify the activation phosphosites of G-substrate at Thr72 and Thr123, we observed that the expression of G-substrate in our biological replicates did show a decreasing trend in the cGKI-KO cerebella (cGKI-KO/WT =0.58, Supplemental Table 1).

This fact could explain the higher level of the phosphatase regulatory subunit; in fact, in accordance with the general accepted view, the inhibition of PP1 enhances the phosphorylation of the AMPA receptor and its subsequent internalization, with induction of LTD. In view of these results, it is tempting to hypothesize that, in absence of an adequate level of G-substrate, PPP1R29 is highly expressed, to ensure the occurrence of, at least, a low level of LTD in the cGKI-KO cerebellum.

Ca^{2+} regulation is fundamental in the nervous system and we could quantify significant changes at the protein level of the Ca^{2+} pump SERCA3 (Figure 3) and of HAP1 that regulates the cytosolic Ca^{2+} concentration in a complex with the Itpr1 and Htt (Figure 2). The altered expression of Ca^{2+} signaling proteins in cGKI-KO cerebellum is in line with the known function of cGKI in the regulation of the intracellular Ca^{2+} level in cardiovascular cells.[41] These results warrant a more detailed analysis of a potential cross-talk of cGKI and Ca^{2+} signaling in cerebellar PCs.

The combination of proteomics and immunostaining of brain sections gave more information on the localization of the proteins in the cerebellum. It is in fact necessary

to understand whether the proteins that change in expression are expressed in PCs and/or in other areas of the cerebellum.
We hypothesize that many of the peptides that show a regulation might be phosphorylated by other kinases that are more active in the cGKI-KO, or are direct substrates of cGKI. Furthermore, we were able to identify two potential cGKI phosphorylation substrates (BRKS2 and Gabra6) that showed a down regulated ratio in the cGKI-KO mice (Figure 4C).
Overall, we were able to identify significant changes of the cerebellar (phospho)proteome upon genetic ablation of cGKI. As a first validation we found perturbations on proteins that are involved in synaptic plasticity, such as ion transporters, signal transduction enzymes and neurotransmitter receptors.
The combination of the protein-protein interaction results with the current literature on cerebellar LTD allowed us to highlight the signaling mechanisms that could modulate synaptic plasticity and cerebellar learning. Moreover, we were able to identify new putative cGKI substrates that can shed more light on the cGMP-cGKI signaling pathways in the cerebellum.

ACKNOWLEDGMENTS

This work was in part supported by the PRIME-XS project, Grant Agreement Number 262067, funded by the European Union Seventh Framework Program. The Netherlands Proteomics Centre, embedded in The Netherlands Genomics Initiative is acknowledged for funding. Shabaz Mohammed, Teck Yew Low and Harm Post are acknowledged for technical assistance. We thank Dr. Sergei Rybalkin and Dr. Joe Beavo for providing the anti-PDE5 antibody used for immunofluorescence staining of frozen sections.

REFERENCES

(1) Geiger, T.; Wehner, A.; Schaab, C.; Cox, J.; Mann, M. *Mol Cell Proteomics* **2012**, *11*. M111 014050; Munoz, J.; Low, T. Y.; Kok, Y. J.; Chin, A.; Frese, C. K.; Ding, V.; Choo, A.; Heck, A. J. *Mol Syst Biol* **2011**, *7*. 550; Nagaraj, N.; Kulak, N. A.; Cox, J.; Neuhauser, N.; Mayr, K.; Hoerning, O.; Vorm, O.; Mann, M. *Mol Cell Proteomics* **2012**, *11*. M111 013722.
(2) Kislinger, T.; Cox, B.; Kannan, A.; Chung, C.; Hu, P.; Ignatchenko, A.; Scott, M. S.; Gramolini, A. O.; Morris, Q.; Hallett, M. T.; Rossant, J.; Hughes, T. R.; Frey, B.; Emili, A. *Cell* **2006**, *125*. 173-86; Huttlin, E. L.; Jedrychowski, M. P.; Elias, J. E.; Goswami, T.; Rad, R.; Beausoleil, S. A.; Villen, J.; Haas, W.; Sowa, M. E.; Gygi, S. P. *Cell* **2010**, *143*. 1174-89; Aye, T. T.; Scholten, A.; Taouatas, N.; Varro, A.; Van Veen, T. A.; Vos, M. A.; Heck, A. *J. Mol Biosyst* **2010**, *6*. 1917-27.
(3) Geiger, T.; Velic, A.; Macek, B.; Lundberg, E.; Kampf, C.; Nagaraj, N.; Uhlen, M.; Cox, J.; Mann, M. *Mol Cell Proteomics* **2013**, *12*. 1709-22.
(4) de Graaf, E. L.; Vermeij, W. P.; de Waard, M. C.; Rijksen, Y.; van der Pluijm, I.; Hoogenraad, C. C.; Hoeijmakers, J. H.; Altelaar, A. F.; Heck, A. J. *Mol Cell Proteomics*

2013, *12*. 1350-62.
(5) Jing, L.; Parker, C. E.; Seo, D.; Hines, M. W.; Dicheva, N.; Yu, Y.; Schwinn, D.; Ginsburg, G. S.; Chen, X. *Proteomics* **2011**, *11*. 2763-76.
(6) Hilger, M.; Bonaldi, T.; Gnad, F.; Mann, M. *Mol Cell Proteomics* **2009**, *8*. 1908-20.
(7) Lundby, A.; Andersen, M. N.; Steffensen, A. B.; Horn, H.; Kelstrup, C. D.; Francavilla, C.; Jensen, L. J.; Schmitt, N.; Thomsen, M. B.; Olsen, J. V. *Sci Signal* **2013**, *6*. rs11.
(8) Scholten, A.; Preisinger, C.; Corradini, E.; Bourgonje, V. J.; Hennrich, M. L.; van Veen, T. A.; Swaminathan, P. D.; Joiner, M. L.; Vos, M. A.; Anderson, M. E.; Heck, A. J. *J Am Heart Assoc* **2013**, *2*. e000318.
(9) Hoos, M. D.; Richardson, B. M.; Foster, M. W.; Everhart, A.; Thompson, J. W.; Moseley, M. A.; Colton, C. *J Proteome Res* **2013**.
(10) Kleppisch, T.; Feil, R. *Handb Exp Pharmacol* **2009**. 549-79.
(11) Francis, S. H.; Busch, J. L.; Corbin, J. D.; Sibley, D. *Pharmacol Rev* **2010**, *62*. 525-63.
(12) Lohmann, S. M.; Vaandrager, A. B.; Smolenski, A.; Walter, U.; De Jonge, H. R. *Trends Biochem Sci* **1997**, *22*. 307-12.
(13) Wernet, W.; Flockerzi, V.; Hofmann, F. *FEBS Lett* **1989**, *251*. 191-6.
(14) Kleppisch, T.; Wolfsgruber, W.; Feil, S.; Allmann, R.; Wotjak, C. T.; Goebbels, S.; Nave, K. A.; Hofmann, F.; Feil, R. *J Neurosci* **2003**, *23*. 6005-12.
(15) Ito, M. *Physiol Rev* **2001**, *81*. 1143-95.
(16) Hofmann, F.; Sold, G. *Biochem Biophys Res Commun* **1972**, *49*. 1100-7; Lohmann, S. M.; Walter, U.; Miller, P. E.; Greengard, P.; De Camilli, P. *Proc Natl Acad Sci U S A* **1981**, *78*. 653-7.
(17) Hartell, N. A. *Neuroreport* **1994**, *5*. 833-6.
(18) Feil, R.; Hartmann, J.; Luo, C.; Wolfsgruber, W.; Schilling, K.; Feil, S.; Barski, J. J.; Meyer, M.; Konnerth, A.; De Zeeuw, C. I.; Hofmann, F. *J Cell Biol* **2003**, *163*. 295-302.
(19) Wegener, J. W.; Nawrath, H.; Wolfsgruber, W.; Kuhbandner, S.; Werner, C.; Hofmann, F.; Feil, R. *Circ Res* **2002**, *90*. 18-20.
(20) Boersema, P. J.; Raijmakers, R.; Lemeer, S.; Mohammed, S.; Heck, A. J. *Nat Protoc* **2009**, *4*. 484-94.
(21) Gauci, S.; Helbig, A. O.; Slijper, M.; Krijgsveld, J.; Heck, A. J.; Mohammed, S. *Anal Chem* **2009**, *81*. 4493-501.
(22) Zhou, H.; Ye, M.; Dong, J.; Corradini, E.; Cristobal, A.; Heck, A. J.; Zou, H.; Mohammed, S. *Nat Protoc* **2013**, *8*. 461-80.
(23) Frese, C. K.; Altelaar, A. F.; Hennrich, M. L.; Nolting, D.; Zeller, M.; Griep-Raming, J.; Heck, A. J.; Mohammed, S. *J Proteome Res* **2011**, *10*. 2377-88.
(24) Kovanich, D.; Cappadona, S.; Raijmakers, R.; Mohammed, S.; Scholten, A.; Heck, A. J. *Anal Bioanal Chem* **2012**, *404*. 991-1009.
(25) Cox, J.; Mann, M. *Nat Biotechnol* **2008**, *26*. 1367-72.
(26) Taus, T.; Kocher, T.; Pichler, P.; Paschke, C.; Schmidt, A.; Henrich, C.; Mechtler, K. *J Proteome Res* **2011**, *10*. 5354-62.
(27) Szklarczyk, D.; Franceschini, A.; Kuhn, M.; Simonovic, M.; Roth, A.; Minguez, P.; Doerks, T.; Stark, M.; Muller, J.; Bork, P.; Jensen, L. J.; von Mering, C. *Nucleic Acids*

Res **2011**, *39*. D561-8.
(28) Cline, M. S.; Smoot, M.; Cerami, E.; Kuchinsky, A.; Landys, N.; Workman, C.; Christmas, R.; Avila-Campilo, I.; Creech, M.; Gross, B.; Hanspers, K.; Isserlin, R.; Kelley, R.; Killcoyne, S.; Lotia, S.; Maere, S.; Morris, J.; Ono, K.; Pavlovic, V.; Pico, A. R.; Vailaya, A.; Wang, P. L.; Adler, A.; Conklin, B. R.; Hood, L.; Kuiper, M.; Sander, C.; Schmulevich, I.; Schwikowski, B.; Warner, G. J.; Ideker, T.; Bader, G. D. *Nat Protoc* **2007**, *2*. 2366-82.
(29) Hornbeck, P. V.; Kornhauser, J. M.; Tkachev, S.; Zhang, B.; Skrzypek, E.; Murray, B.; Latham, V.; Sullivan, M. *Nucleic Acids Res* **2012**, *40*. D261-70.
(30) Vizcaino, J. A.; Cote, R. G.; Csordas, A.; Dianes, J. A.; Fabregat, A.; Foster, J. M.; Griss, J.; Alpi, E.; Birim, M.; Contell, J.; O'Kelly, G.; Schoenegger, A.; Ovelleiro, D.; Perez-Riverol, Y.; Reisinger, F.; Rios, D.; Wang, R.; Hermjakob, H. *Nucleic Acids Res* **2013**, *41*. D1063-9.
(31) Valtcheva, N.; Nestorov, P.; Beck, A.; Russwurm, M.; Hillenbrand, M.; Weinmeister, P.; Feil, R. *J Biol Chem* **2009**, *284*. 556-62.
(32) Shimizu-Albergine, M.; Rybalkin, S. D.; Rybalkina, I. G.; Feil, R.; Wolfsgruber, W.; Hofmann, F.; Beavo, J. A. *J Neurosci* **2003**, *23*. 6452-9.
(33) Dostmann, W. R.; Nickl, C.; Thiel, S.; Tsigelny, I.; Frank, R.; Tegge, W. *J. Pharmacol Ther* **1999**, *82*. 373-87.
(34) Keranen, L. M.; Dutil, E. M.; Newton, A. C. *Curr Biol* **1995**, *5*. 1394-1403.
(35) Fujii, K.; Goldman, E. H.; Park, H. R.; Zhang, L.; Chen, J.; Fu, H. *Oncogene* **2004**, *23*. 5099-104.
(36) Krueger, J.; Chou, F. L.; Glading, A.; Schaefer, E.; Ginsberg, M. H. *Mol Biol Cell* **2005**, *16*. 3552-61.
(37) Thornton, T. M.; Pedraza-Alva, G.; Deng, B.; Wood, C. D.; Aronshtam, A.; Clements, J. L.; Sabio, G.; Davis, R. J.; Matthews, D. E.; Doble, B.; Rincon, M. *Science* **2008**, *320*. 667-70.
(38) Collingridge, G. L.; Peineau, S.; Howland, J. G.; Wang, Y. T. *Nat Rev Neurosci* **2010**, *11*. 459-73.
(39) Stark, C.; Breitkreutz, B. J.; Reguly, T.; Boucher, L.; Breitkreutz, A.; Tyers, M. *Nucleic Acids Res* **2006**, *34*. D535-9.
(40) Tang, T. S.; Tu, H.; Chan, E. Y.; Maximov, A.; Wang, Z.; Wellington, C. L.; Hayden, M. R.; Bezprozvanny, I. *Neuron* **2003**, *39*. 227-39.
(41) Hofmann, F.; Feil, R.; Kleppisch, T.; Schlossmann, J. *Physiol Rev* **2006**, *86*. 1-23.
(42) Sausbier, M.; Schubert, R.; Voigt, V.; Hirneiss, C.; Pfeifer, A.; Korth, M.; Kleppisch, T.; Ruth, P.; Hofmann, F. *Circ Res* **2000**, *87*. 825-30.
(43) Massberg, S.; Sausbier, M.; Klatt, P.; Bauer, M.; Pfeifer, A.; Siess, W.; Fassler, R.; Ruth, P.; Krombach, F.; Hofmann, F. *J Exp Med* **1999**, *189*. 1255-64.
(44) Kumazoe, M.; Sugihara, K.; Tsukamoto, S.; Huang, Y.; Tsurudome, Y.; Suzuki, T.; Suemasu, Y.; Ueda, N.; Yamashita, S.; Kim, Y.; Yamada, K.; Tachibana, H. *J Clin Invest* **2013**, *123*. 787-99.
(45) Aitken, A.; Bilham, T.; Cohen, P.; Aswad, D.; Greengard, P. *J Biol Chem* **1981**, *256*. 3501-6.

SUPPLEMENTAL INFORMATION

Supplemental tables are available as excel files via internet at http://www.mcponline.org/

Supplemental Table 1
Supplemental Table 2

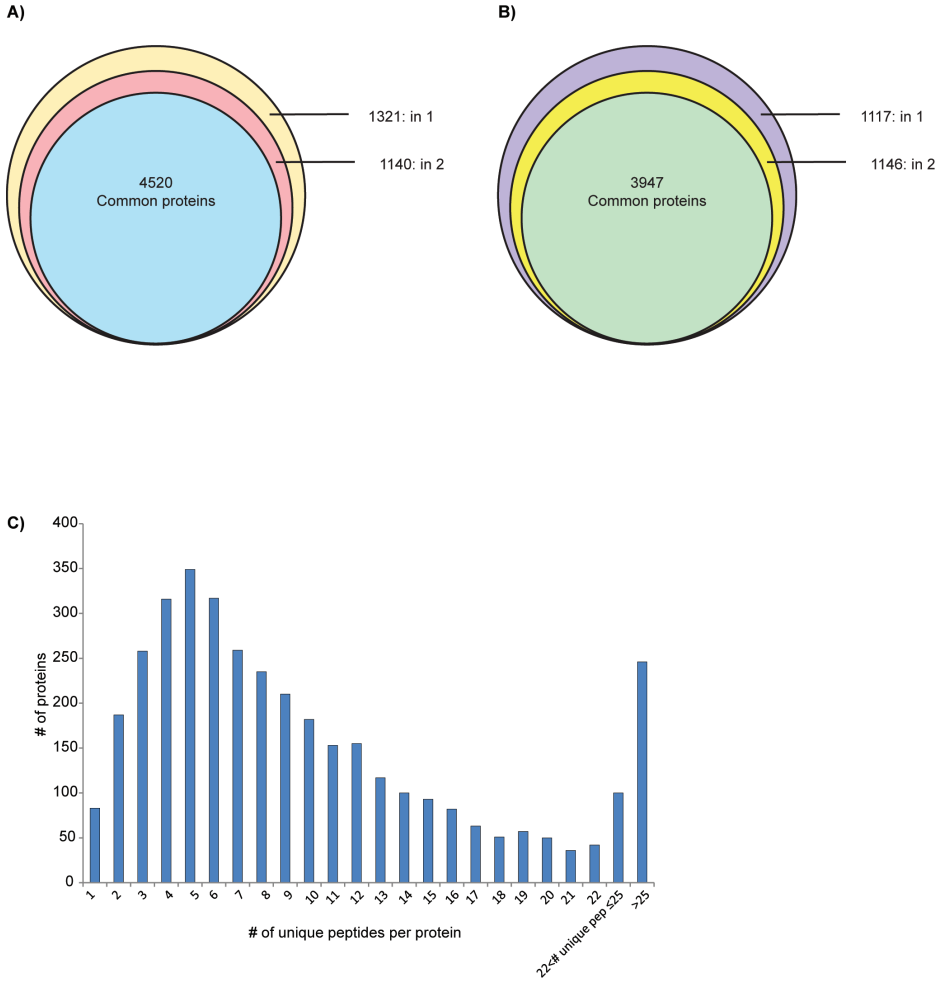

Supplemental Figure 1. *Identified and quantified proteins in all the biological replicates. A) A total of 6981 proteins were identified in all the 3 biological replicates, of which 89% B) were quantified. The proteins quantified in all three biological replicates (60% of all the quantified proteins, 3755) were considered for statistical analysis and follow up experiments. C) Number of unique peptides quantified per protein.*

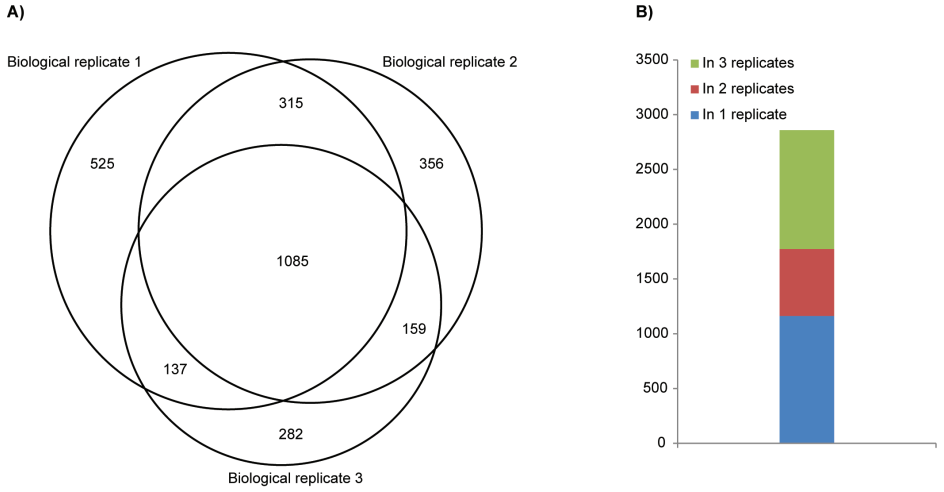

Supplemental Figure 2. *Quantified phosphopeptides in all the biological replicates. A) Overlap between the quantified phosphopeptides with localized phosphosites (pRS> 75%) in the three biological replicates. B) Within the localized phosphopeptides, 1085 phosphopeptides were quantified in all the biological replicates, 611 in two out of three replicates and 1163 quantified only in one out of three replicates.*

Chapter 4

Timed alterations in anchored cAMP signaling and arrhythmogenesis in a rat model with progression to heart failure.

S. Soni[1,2], E. Corradini[2,3], M. Boulaksil[1,4], R. van der Nagel[1], B.G. Kok[1], P. Puchalska[5], M.F. Bierhuizen[1], J.M.T de Bakker[1], H.V.M van Rijen[1], A.J.R. Heck[2,3], A. Scholten[2,3], M. A. Vos[1], T.A.B. van Veen[1]

Manuscript under review

[1] Dept of Medical Physiology, Division of Heart & Lungs, University Medical Centre Utrecht, Yalelaan 50 3584 CM, Utrecht, The Netherlands

[2] Biomolecular Mass Spectrometry and Proteomics, Bijvoet Center for Biomolecular Research and Utrecht Institute for Pharmaceutical Sciences, Science Faculty, Utrecht University, Padualaan 8, 3584 CH Utrecht, the Netherlands.

[3] Netherlands Proteomics Centre, Padualaan 8, 3584 CH Utrecht, the Netherlands

[4] Department of Cardiology, Radboud Univeristy Medical Center, Nijmegen, The Netherlands

[5] Department of Analytical Chemistry, University of Alcalá, Ctra. Madrid-Barcelona Km. 33.600, 28871 Alcalá de Henares (Madrid), Spain

ABSTRACT

Aims: Pathophysiological progression to Heart Failure (HF) occurs in different phases and encompasses alterations in β-adrenergic signaling. Detailed information concerning temporal changes in 1) the components of ventricular remodeling and associated arrhythmias, and 2) the PKA-AKAP (Protein kinase A-A kinase anchoring protein) interaction profile is lacking.

Methods: Rats were subjected to transverse aortic constriction (TAC) or Sham surgeries. Epicardial mapping was performed to test arrhythmogenicity. Using cAMP coated beads, proteomic analysis of the cAMP interactome was performed to study temporal changes in the PKA-AKAP profile during progression to HF.

Results: TAC groups were classified as T4 (4 weeks, compensated), T12 (transition phase) and T16 (early HF) based on; echo-based morphology and contractility, hypertrophy and CaMKII- δ levels. At T4, sustained polymorphic ventricular tachycardias (pVT) were induced in 8/13 T4 and 0/13 in Sham rats. Arrhythmias were associated with increased cardiac fibrosis, Connexin43 heterogeneity and dispersion of conduction. At T4, phosphorylation of various PKA substrates was increased, whereas it was reduced at T12 and T16. Proteomic analysis showed a highest association with the cAMP-beads of PKA-Regulatory (PKA-R) subunits and cGMP pathway components (PDE2A & PKGIα) at T12 and a decrease at T16. As secondary interactors, AKAPs (dAKAP1, AKAP18δ, AKAP11 and SPHKAP) showed a highest association with PKA-R subunits at T4 and all values decreased towards T16.

Conclusion: The early stage with compensated hypertrophy (T4) shows arrhythmias while phosphorylation status of PKA substrates is up possibly by increased PKA-AKAP interactions. The T12 group showed maximal association of PKA-R subunits and a 50% mortality, whereas T16 displayed decreases, which could be the first signs of exhaustion of the downstream components of cAMP driven signaling.

INTRODUCTION

Heart failure (HF) is the "common" endpoint of several cardiac diseases. During progression to HF, a number of cardiac adaptation processes take place, collectively called ventricular remodeling, that underlie the stage dependent "phenotype".[1] After the initial insult, the subsequent stages can be separated in asymptomatic compensated hypertrophy New York Association (NYHA) I, the stage of transition in which symptoms become apparent (NYHA II), the symptomatic stage where patients require more intensive therapy (NYHA III) as compared to those in the first two classes, and finally the maladaptive phase of end stage HF (NYHA IV).

Sequential investigations regarding the different aspects of remodeling in each of these subsequent phases, including their arrhythmogenic consequences, are scarce and often limited to a specific stage only. An example is the chronic Atrio-Ventricular block dog model, in which beneficial contractile and structural remodeling leading to compensated hypertrophy is accompanied by electrical remodeling and predisposition to arrhythmias,[2] indicating that the enhanced arrhythmic susceptibility is an early

phenomenon. This was recently confirmed in a rat model of pressure overload (TAC) that was temporarily followed for 3 months and showed 25% mortality at 3 weeks and 50% mortality at 6 weeks.[3]

Besides the "arrhythmic phenotype", the subsequent effects of persistently elevated neurohumoral signals on its downstream targets have not been fully elucidated in a time-lined fashion. An important contributing factor is the β-adrenergic receptor pathway,[4] that when persistently elevated in its activity triggers development of HF. Upon β-adrenergic stimulation and a rise in intracellular cAMP, cAMP binds to the regulatory subunit of cAMP-dependent protein kinase A (PKA-R). Following that, the catalytic subunits (PKA-C) are released from the PKA-R dimer in order to phosphorylate their targets in a space and time dependent manner.[5] To achieve this in an organized fashion, PKA is guided by a wide variety of A-kinase anchoring proteins (AKAPs).[6] In-vitro and In-vivo studies using peptides competing at the interaction domain have shown the importance of these PKA-AKAP interactions in maintenance of normal cardiac function and that disruptions of PKA-AKAP interactions significantly impair PKA substrate phosphorylation.[7-9]

For long, de-sensitization and down regulation of β adrenergic receptors has been considered as one of the most prominent causes for impaired cardiac function in HF.[10] More recently, in end-stage HF, we also detected decreased levels of PKA-R subunits and alterations in several PKA-AKAP interactions although it still remains to be elucidated whether a causative relationship exists between these alterations and the degree of HF.[11] The levels of the second messenger cAMP and the catalytic activity of PKA are, however, known to remain unchanged in end stage human HF.[8] In the current study, using a rat model of pressure overload, we hypothesized that a decrease in PKA substrate phosphorylation is attributed to a spatial reorganization of PKA-AKAP complexes during progressive remodeling of cardiac contractile performance. In addition, we investigated whether an increase in the propensity for ventricular arrhythmias could be confirmed in the early phase of cardiac remodeling.

EXPERIMENTAL PROCEDURES

Materials and Methods

A detailed description of the materials and methods that were used is included in the supplementary 'Materials and Methods'.

Rat model of pressure over load

Animal care and handling was performed in accordance with the 'European Directive for the protection of Vertebrate animals used for Experimental and Scientific Purpose, European Community Directive 86/609/CEE'. All experiments were approved by the committee for experiments on Animals of the Utrecht University, The Netherlands. Male Wistar rats were housed at 21°C and 60% humidity with an artificial 12:12 h light dark cycle and were fed with standard chow and water (ad libitum).

Rats were followed in time and sacrificed at three different points; T4 (4 weeks post-TAC, n=17), T12 (n=4) and T16 (n=4). Sham operated rats (S) were used as experi-

mental controls for the electrophysiological analysis at S4 (n=13) and proteomics S12 (n=4).

Transverse Aortic Constriction

In brief, rats were anaesthetized with 2.5% isoflurane in 40% oxygen, ventilated at 75 breaths per minute with a peak pressure of 12 cm H_2O and placed in a supine position. The thorax was accessed by dissection of the pectoral muscles and the intercostal muscles left of the sternum. The aortic arch was cleared from connective tissue and fat, and ligated with a 22 Gauge (0.72 mm) needle between the truncus brachiocephalicus and the left common carotid artery.

Transthoracic echocardiography and Doppler measurements

Left ventricular internal diameter (LVID), thickness of the InterVentricular Septum (IVS), and posterior wall (LVPW), both in systole (s) and diastole (d) were measured using echocardiography. Fractional shortening (FS) was calculated as ([LVIDd-LVIDs]/LVIDd)*100.[12] Doppler echocardiography was used to estimate strictness of the constriction, using the Doppler estimated Bernoulli equation (4*(Vmax)2).[13,14]

Arrhythmia susceptibility testing

Hearts were extracorporated, Langendorff perfused and extracellular electrograms were recorded with a 247 or 208-point multi-terminal electrode grid. Recordings of LV and right ventricle (RV) were made during stimulation on the LV at a basic cycle length of 150 ms using burst pacing. Conduction velocity (CV) parallel (θL) and perpendicular (θT) to fiber direction was determined from the paced activation maps. Transmural CV was calculated from local activation times derived from electrograms recorded with three separate needle electrodes.

cAMP pull down for label free PKA-AKAP interaction analysis

The cAMP pull-down was performed with 2-AHA-cAMP coated agarose beads as previously described.[11]

Protein identification and quantification

Each sample was analyzed in duplicate on a Q-Exactive quadrupole orbitrap mass spectrometer (Thermo Scientific). For the label free analysis, raw files were processed using the MaxQuant software and MS/MS spectra were searched against the IPI rat database 3.36.

Quantitative reverse transcriptase-PCR

cDNA was generated using RT-PCR and QPCR was performed with iQTM SYBR Green supermix on the MYiQ2 Real Time PCR Detection System. Brain natriuretic peptides (BNP) levels were normalized against GAPDH.

Immunoblotting

LV samples were resolved by SDS-PAGE, electro-transferred to nitrocellulose membranes and immersed in TBST-buffer with 5% milk powder. Blots were incubated with respective antibodies (overnight) and developed on the Biorad ChemiDocXRS+. Protein levels were normalized against the digitized signals of Ponceau staining (total

transferred protein).

Immunohistology and Connexin43 (Cx43) heterogeneity, fibrosis quantification

Heterogeneity of Cx43 distribution was quantified using photomicrographs transformed in eight-bit black and white pictures, and a custom written script in MatLab was applied to assess for individual Cx43 pixels. For fibrosis the amount of pixels were measured using image-J software.

Statistical Analysis

Data were analyzed using R studio. Statistical significance of differences was evaluated by paired Student's t-test, ANOVA or Fisher's Exact test followed by post-hoc Bonferroni test as appropriate. Two-sided P-values <0.05 were considered statistically significant. Data are expressed as mean ± SEM.

To study the profile of PKA-AKAP interactions in progression to HF, the T4 group was compared to S12, the T12 group was compared to T4, and the T16 group was compared to T12.

*/±/+	P<0.05
**/±±/++	P<0.001
***/±±±/+++	P<0.0001

Hierarchical clustering was created in programming language R version 2.14.1, and the distance between the clusters was calculated by the "Pearson method".

RESULTS

Diagnosis of HF and characterization of phenotypes

Ongoing cardiac remodeling and progression to HF in the rats was analyzed using the following parameters: Brain Natriuretic Peptide mRNA expression (BNP, normalized to GAPDH), protein levels of Ca^{2+} calmodulin dependent protein kinase II (CaMKII-δ), presence of hypertrophy, echocardiographic parameters: LVPW, IVS, LVID, and FS. The CaMKII- δ protein levels were measured based on their ion intensities from the proteomics data set. CaMKII- δ comes down as a direct interactor of the 2-AHA-cAMP beads (Supplemental Figure 1A) and this has been used as an indirect measure of the levels of enzyme in each group.

Based on the summation of above-mentioned parameters, the three TAC groups could be clearly separated in: 1) compensated; 2) transition, and 3) (early stage) HF (Table 1).

Parameter	T4	T12	T16
BNP	=	=	(+)
CaMKII	+	++	(++)
HW/TL	+	+	+
Septal Wall Thickness	=	+	++
Left Ventricular Dilatation	No	No	No
Fractional Shortening	-	--	---

Table 1 *Comparison of all TAC groups based on HF parameters. The number of + or – signs denote the degree of increase, or decrease, of a particular parameter arbitrarily (= denotes no change). Non-significant comparisons are placed within brackets.*

BNP levels were not significantly increased (Figure 1A). However, CaMKII-δ levels were increased at T4 with a further elevation at T12-T16 (Figure 1B). Hypertrophy, based on heart weight tibia length ratios (HW/TL) was significantly increased as compared to Sham in all three TAC groups (Figure 1C). FS showed a progressive and significant decrease: Sham:48%, T4:38%, T12:32% and T16:22% (Figure 1D).

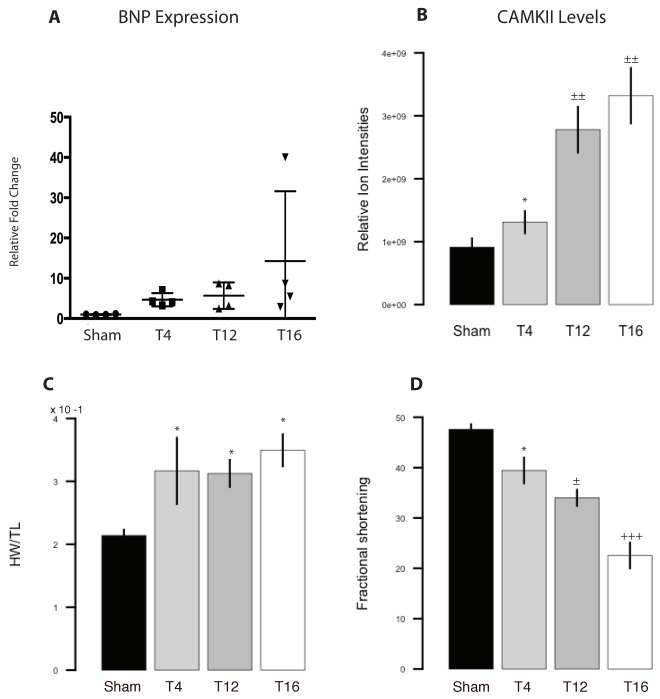

Figure 1 *Panel A: Progressive changes (from Sham to T16) in BNP mRNA expression level. Panel B: Ion intensities of CaMKII-δ levels on the cAMP beads as determined with mass spectrometry. Panel C: Absolute heart weight (HW, in grams) in relation to tibia length (TL, in cm). Panel D: Fractional-shortening (FS) measurements of all groups recorded from echocardiographic views.*

IVSd/s, LVPWd/s and LVIDs were not different at T4, while they were increased at T12. At T16, a further increase was denoted in IVSd/s and LVPWd/s with a decrease in LVIDd (Figure 2A-2F). Functional data in the Sham group (at 12 weeks) were stable during the time course of the experiment since they were highly comparable to data obtained in Sham animals at week 4 (Supplemental Figure 2).

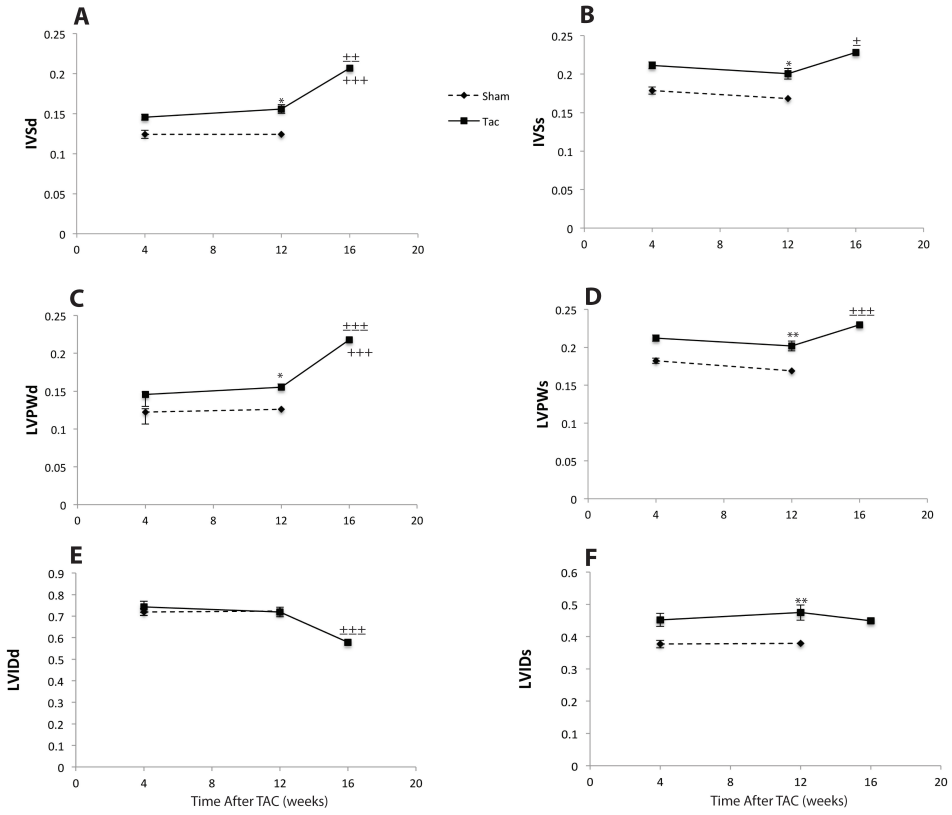

Figure 2 *Temporal changes in echocardiographic parameters (all in cm): Panels A-B: IVSd and IVSs. Panels C-D: LVPWd and LVPWs. Panel E-F: LVIDd and LVIDs. Statistical significance is represented as * vs. Sham, ± vs. T4, and + vs. T12.*

Though these data evidently show the development of a progressively increasing degree of hypertrophy in the TAC treated animals, absence of chamber dilatation in the proposed HF group T16 is indicative of the fact that these animals were not yet in end stage HF. An additional observation that supported this finding was the absence of pulmonary edema (based on lung weight measurements) in the T16 group (Supplemental Figure 1B).

Electrical Remodeling and arrhythmogenesis

In the early phase of remodeling (T4), pVTs were induced by programmed stimulation in 8/13 (62%) TAC animals compared to 0/13 in Sham rats (p=0.001) (Figure 3A). Epicardial electrical activation patterns during VT showed variable sites of earliest activation when analyzed in consecutive beats, and altering sites of functional conduction block (Figure 3B).

RV and LV epicardial CV longitudinal and transversal to fiber direction was not different between Sham and T4. However, transmural CV was slowed in T4 rats (37.6±2.9 vs. 58.5±3.9 cm·s-1; P<0.01) (Table 2).

	Sham	TAC
RV θ_L, cm·s^{-1}	68.6± 2.4	67.1± 3.4
RV θ_T, cm·s^{-1}	43.4± 2.3	39.0± 1.9
RV Anisotropic Ratio	1.64± 0.10	1.75± 0.09
RV ERP, ms	45.4± 2.7	54.6± 3.9
RV DoC, cm·s^{-1}	1.21± 0.088	1.32± 0.13
LV θ_L, cm·s^{-1}	62.8± 5.7	68.9± 3.3
LV θ_T, cm·s^{-1}	27.5± 2.5	27.9± 2.7
LV Anisotropic Ratio	2.29± 0.13	2.63± 0.20
LV ERP, ms	59.1± 4.1	67.5± 3.3
LV DoC, cm·s^{-1}	1.23± 0.075	**1.90 ± 0.087***
LV θ_{TM}, cm·s^{-1}	58.5± 3.9	**37.6± 2.9***

Table 2 *Data of electrical mapping study during Langendorff perfusion. RV/LV, right and left ventricle, respectively; θL/θT/θTM, conduction velocity longitudinal, transversal, or perpendicular to epicardial fiber direction, respectively, at a pacing cycle length of 150 ms; ERP, effective refractory period; DoC, dispersion of conduction. *, P<0.01 vs. Sham; †, P<0.01 vs. TAC-. Significant comparisons are highlighted in bold.*

Cx43 immunolabeling displayed a significantly more heterogeneous distribution pattern in T4 as compared to Sham. Some areas exhibited normal homogeneous Cx43 labeling, while in other regions Cx43 labeling was clearly reduced or even nearly absent (Figure 3C, 3E). The amount of fibrosis in T4 rats was significantly higher (Figure 3D, 3F), and in addition, dispersion of LV conduction velocity was also increased (1.23+0.08 to 1.9+0.09, p<0.01) (Table2).

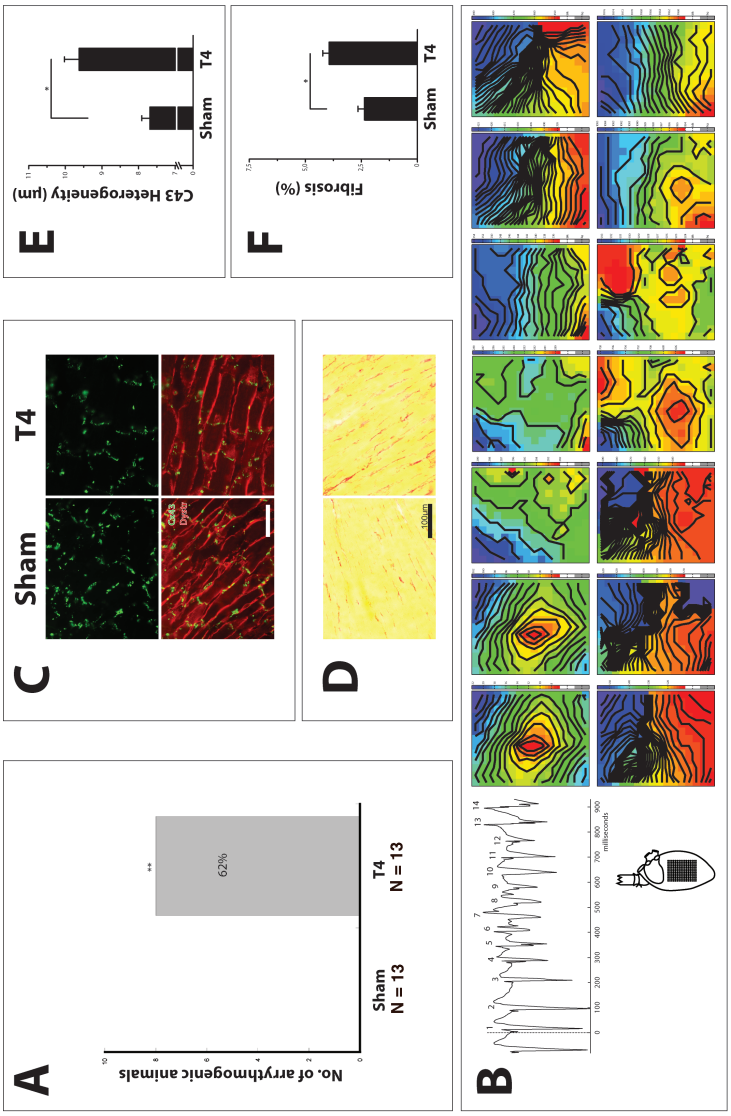

Figure 3 *Panel A: Relative incidence of arrhythmias (polymorphic ventricular tachycardia, pVT) in the Sham and T4 group. Panel B; Epicardial activation maps of a pVT induced in the left ventricle of a Langendorff perfused T4 heart. Simultaneously recorded activation maps of LV are displayed in chronological order to show evolution of the arrhythmia. The pVT was induced by 1 premature stimulus applied at the center of the recording electrode on LV. The first 2 activation maps are from the last basic and premature stimulus. Note the centrifugal spread of activation of these 2 maps of LV (red earliest activation, blue latest activation). Panel C-D: Anti-Cx43 labeling (green fluorescence) along with merge photographs of both anti-Cx43 and anti-dystrophin labeling (red fluorescence) from left ventricle, and representative examples of Sirius red staining on LV of Sham and T4 rats. Scale bar=100 µm. Panel E-F: Quantifications of Cx43 and collagen content (as assessed using Sirius Red staining).*

Phosphorylation of PKA substrates

PKA phosphorylation of various substrates was studied using an antibody that recognizes the phospho-motif (RRXS*/T*) of PKA substrates (Figure 4A, quantification 4B). The phosphorylation levels were normalized against Ponceau protein staining (Figure 4C) and appeared to be increased after 4 weeks of TAC, followed by a gradual and progressive decrease at T12 and T16.

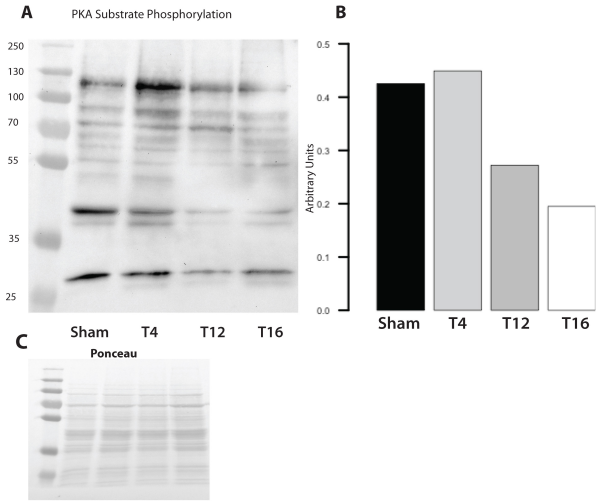

Figure 4 *PKA substrate phosphorylation levels in the different groups (n=4/group). Panel A: All bands represent proteins that are substrates for phosphorylation by PKA. Band intensities demonstrate the levels of phosphorylation of different substrates in the different groups. Panel B: Quantification of the western blot, showing different levels of PKA substrate phosphorylation in the four treatment groups. Panel C: Ponceau staining that was used to correct for quantificantion.*

cAMP and AKAPs with chemical proteomics

Levels of association of both PKA-R subunits, RI-α and RII-α, in the T4 group were similar to Sham animals whereas they were significantly increased in T12 where the maximal association level was seen. In T16 levels started to decline again (Figure 5A-B). In contrast, levels of PKA-RI and PKA-RII in the total lysate were not significantly different in the four groups (Supplemental Figure 3). In line with the levels of the PKA-R subunits, a bell shaped curve with the highest value reached at T12 was seen for PDE2A and PKG1-alpha (Figure 5C-D).

Significantly increased levels of association on the beads between PKA and AKAP1, AKAP18δ, SPHKAP and AKAP11 were seen in T4 (Figure 5E-H, respectively). Most AKAPs displayed a decrease at T12 and a return to baseline values at T16. SPHKAP, however, reached the maximum value at T12 followed by a reduction at T16.

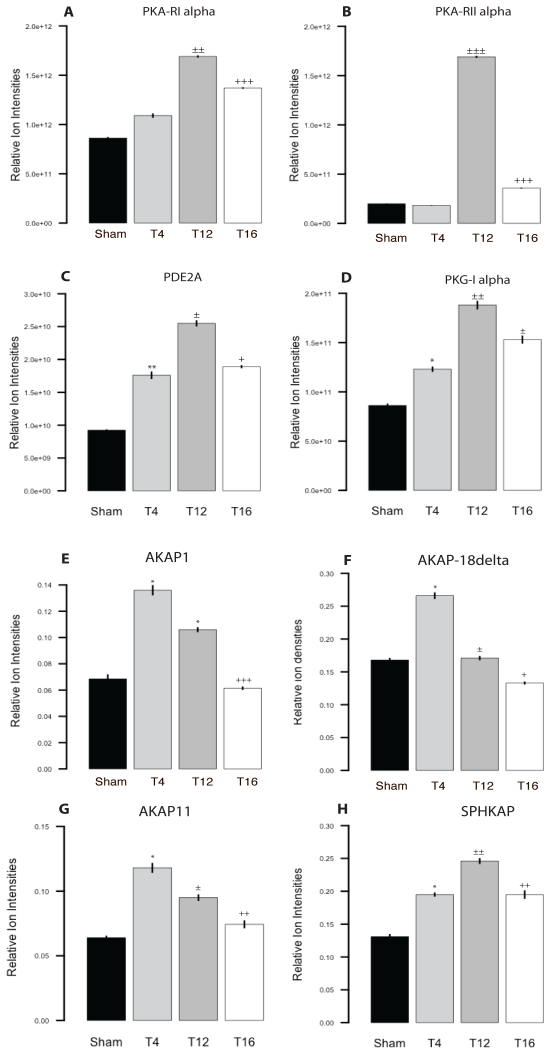

Figure 5 *Panels A-D: Alterations in primary interacting proteins of cAMP (n=4/group). Ratios of label free normalized intensity for primary interactors of cAMP of the four different treated groups. Horizontal bars represent mean normalized intensities and ratios were calculated based on the summed, normalized intensities. Panels E-H: Alterations in secondary interacting proteins of cAMP (n=4/group). Label free normalized intensities for all quantified AKAPs. Horizontal bars represent mean normalized intensities and ratios were calculated based on the summed intensities.*

Confirmation of different sub-groups

A clustering analysis revealed that all TAC groups were distinct from each other with the highest degree of similarity between T12 and T16 (Figure 6A). Finally, Figure 6B shows the survival curve of the total amount of TAC animals that were included (N=41). None of the 17 Sham animals died during the follow-up period (not shown).

For the TAC animals, no deaths were recorded until week 8, whereas a significant loss was observed between week 8 and 14.

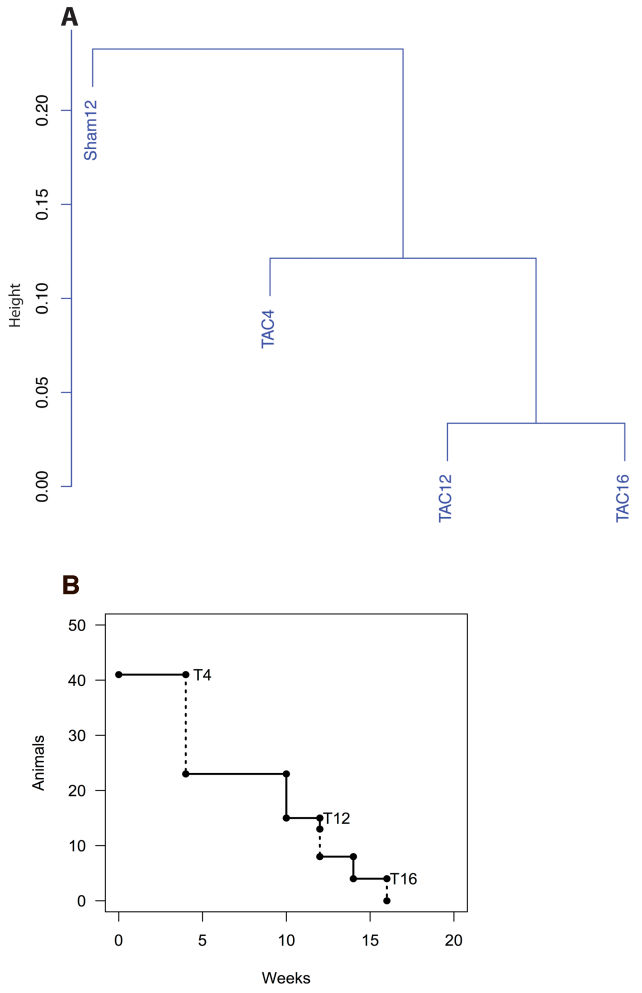

Figure 6 *Panel A: A hierarchical clustering of the complete cAMP interactome of the (all individual proteins and their intensities) four treatment groups, where the height represents the degree of similarity between the groups. Panel B: Survival curve of all animals (N=41) in the TAC group. Dashed lines represent animals that were sacrificed for experiments at the time points 4, 12 and 16 weeks.*

DISCUSSION

Development of HF has been described as a process where the heart goes through a series of phases.[1,2] Despite progress,[15] there are many questions that still remain unanswered when it comes to explicitly describing the nature of the remodeling processes, including in these different phases (re)organization of the cAMP/PKA/AKAP pathway. One of the main reasons for incompleteness of the information is

that in many studies only one stage of cardiac remodeling or single aspects within the gradual deterioration of cardiac performance has been studied. In our current approach we have followed the complete transition from a normal cardiac performance to early HF. The data set shows early electrical remodeling subsequently followed by contractile dysfunction. The applied proteomic approach allowed a simultaneous investigation of alterations in the adrenergic signaling pathway through analysis of the involved protein complexes. This also implies that we have been able to show in a quantitative manner, functional alterations since we studied real interactions of e.g. PKA with cAMP and as secondary interactors the AKAPs that guide/anchor the complex to its intracellular site of activity.

The New York Heart Association (NYHA) classification of HF divides progression of the disease into four classes. Of these four classes, the early ones are associated with high mortality rates owing to sudden cardiac death (SCD).[15,16] Many studies suggest an enhanced vulnerability to arrhythmias as the roots to SCD, though the evidence that confirms arrhythmogenicity to be a predominant reason for sudden cardiac death is often lacking. To demonstrate the time dependent changes, in the present study the rats were classified (table 1) in 3 different "phenotypes": 1) compensated hypertrophy, 2) transition phase and 3) early onset HF.

Alterations in the 3 groups

1) Compensated stage

In T4 rats, alterations were seen like an increased phosphorylation status of PKA substrates (Figure 4), a maximal attained increase in association of 3 AKAPs and an increase in PDE2A, PKG-1 alpha and SPHKAP interaction (Figure 5). In this phase, pVTs were easily induced with pacing in 62% of the animals, potentially explained by an increased dispersion of LV CV, a decreased transmural CV, an increased biventricular fibrosis and Cx43 heterogeneity (Figure 3).

2) Transition

In T12 rats, the phosphorylation status of PKA substrates was reduced below baseline (Figure 4). The PKA-RI and RII subunits, PDE2A, PKG-I alpha and SPHKAP (Figure 5) were maximally associated within the complex on the beads, while the other 3 AKAPs were starting to decrease.

3) Early onset HF

At T16, PKA phosphorylation status remained low (Figure 4), now combined with a reduced (but still increased when compared to Sham) association of PKA-RI, PDE2A and PKG-1 alpha, while PKA-RII was severely reduced and association of the 3 AKAPs returned back to baseline values. Association level of SPHKAP started to reduce but was still significantly higher when compared to Sham (Figure 5). These animals, however, could not be diagnosed for end stage HF comparable to what is seen in NYHA class IV patients, as we did not observe left ventricular chamber dilation or presence of any pulmonary edema. In that respect, the transitional changes as reported in this study can not be compared to a previously performed study with material obtained from human end stage HF .

Electrical Remodeling and arrhythmogenesis in Transition to HF

In the rat model, a period of asymptomatic "compensatory" hypertrophy (NYHA I/II in patients and T4 in the present study) in response to pressure overload has been clearly demonstrated before.[3,17,18] Vulnerability to arrhythmias may underlie SCD in those early stages after an insult. Here we confirm that arrhythmias occur early and may arise as a consequence of disturbed conduction due to increased levels of bi-ventricular fibrosis and Cx43 heterogeneity. Recently, Akar et al. even mentioned that arrhythmias could be induced as early as 2 weeks after TAC.[3]

The relationship between the occurrence of VT and dispersion in Cx43 expression has been shown in patients,[19,20] dogs,[3,21] rabbits,[22] and rats.[23,20] Heterogeneous electrical uncoupling affects conduction and repolarization across the ventricular wall. Importantly, there was a linear correlation between the amount of dispersion of LV-CV and heterogeneity of Cx43 expression in our study ($R2=0.769$; $P<0.001$). This inhomogeneous conduction is either due to heterogeneous downregulation of Cx43 and/or the increased levels of fibrosis.

Clinical circumspection has suggested that chronic pressure overload eventually leads to complete de-compensation.[24] Though the different stages of HF are known, the experimental evidence of a phase where the transition from compensation to early de-compensation occurs is not readily available. In this study, we used T12 as the phase of transition. It demonstrated increased levels of CaMKII-δ, whereas increased CaMKII-δ activity is known to have deleterious cardiac effects by inducing apoptosis, arrhythmias and altered gene reprograming through activation of HDAC4. A slight increase in CaMKII-δ levels was already seen in our compensated phenotype (T4), a finding consistent with our previous work in a large animal of chronic AV block. In that model, that results in compensated hypertrophy which does not deteriorate into HF, the slightly increased CaMKII-δ activity but did not induce activation of HDAC4, required for gene reprograming.[25] Ling et al., describes CaMKII-δ as a bridging molecule for the transition from pressure overload induced hypertrophy to heart failure.[18] On top of the progressive increase in levels of CaMKII (Figure 1B) other studies have shown that during pressure overload-induced hypertrophy this is also associated with increased activity of the kinase.[26,27]

PKA-AKAP alterations in progression to HF

The AKAP family forms an integral part of the β-receptor/cAMP/PKA pathway and is responsible for effective localization of PKA within the cardiomyocyte.[28] In HF, this pathway is affected in three main ways; (i) Desensitization and down regulation of β-adrenergic receptors, (ii) a decrease in R subunits of PKA, and (iii) a decreased phosphorylation of PKA substrates,[11,29] indicating an ineffective enzyme function due to ineffective localization of the catalytic subunits and a spatial and temporal reorganization of PKA-AKAP complexes. Most PKA-AKAP complexes are formed around a basic structure downstream of the cAMP-dependent β-adrenergic pathway and consist of the PKA holoenzyme, an AKAP (can be different for different PKA targets), a phosphodiesterase, adenylyl cyclases, protein phosphatases and the

respective PKA substrates. The latter ones can range from being receptors, structural proteins or ion channels.[30,31] Using cAMP as the bait we managed to pull down several of these PKA-AKAP complexes and evaluated their temporal organization in progression to HF.[11]

TAC results in an increased adrenergic drive and increased association levels of PDE2A and PKGI-alpha. Several PKA-AKAP complexes are known to include a phosphodiesterase (PDE) such as from the PDE3 or PDE4 family.[33,34] Though we are not aware of any evidence of a PDE2 family member being associated with an AKAP currently, we identified PDE2A abundantly in our pull-downs similarely as reported in our previous human study.[11] PDE2A is activated by binding of cGMP to its GAF domain and is known to degrade cAMP by hydrolysis.[35] PDE2A is elevated in experimental and human HF and at the same time overexpression of PDE2A 1) abolishes β-adrenergic responsiveness by inhibiting increases in L-type Ca^{2+} current via hydrolysis of cAMP and 2) protects against pathological hypertrophy.[36] These results are in line with the increase of PDE2A at T4, which might be a compensatory/protective mechanism against pathological hypertrophy by keeping cAMP levels in range. Increased hydrolysis of cAMP by PDE2A resulting in a negative inotropic effect is dependent on the cGMP/PKG/NO/PDE2A/β3-AR pathway.[35,36] Increased association of PKG-1 alpha is seen at T4 and may also underlie the compensating nature of this phase.

Figure 7 shows a schematic representation of alterations in PKA-AKAP complexes at different time points in progression to disease. Included are also the assumed unchanged levels of cAMP and PKA-C as based on experimental data from other studies 8. At T4 (Figure 7A), association of AKAPs goes up in order to assure appropriate PKA-R localization. The increased PKA substrate phosphorylation indicates an increase in the adrenergic drive. Both AKAP1 and SPHKAP are known mitochondrial AKAPs,[37-39] although the exact function of SPHKAP as cardiac mitochondrial AKAP is unknown. AKAP1 has been suggested to regulate the cardiac stress response and disappearance of AKAP1 is associated with mitochondrial dysfunction and increased cardiomyocyte death and in experimental models of pathological hypertrophy: a negative regulator of hypertrophy.[40,30] AKAP 18 arbitrates PKA dependent phosphorylation of the SERCA inhibitory protein phospholamban at serine 16.[41] The increased association of AKAP18δ with RII alpha is consistent with the expected increase in Ca^{2+} cycling in order to increase force of contraction.[42] AKAP11 shows a similar pattern of association but at the moment functional information on its role in the heart is lacking.

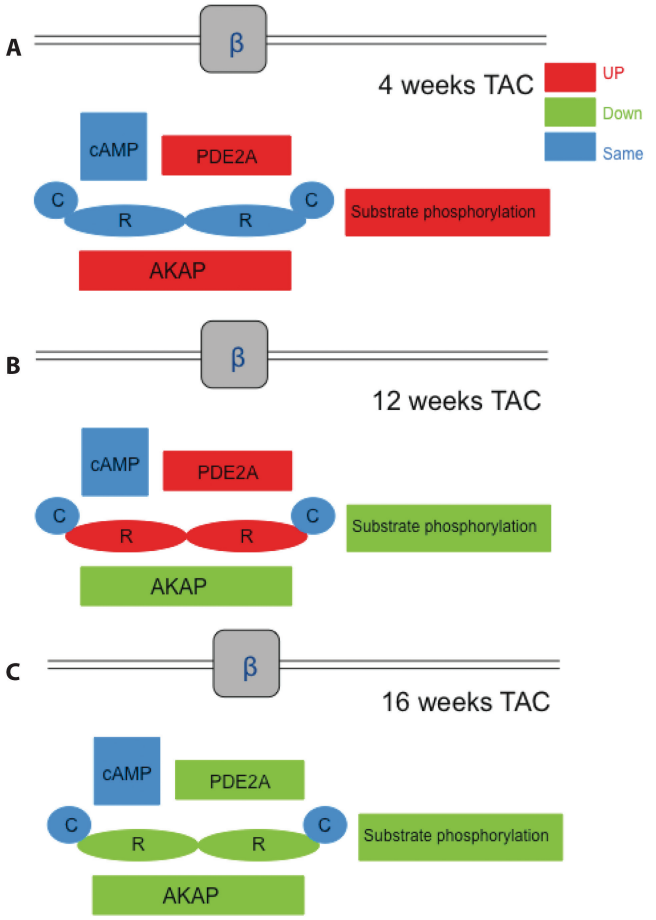

Figure 7 *Scheme summarizing the series of reorganization events that occur in PKA-complexes in progression to heart failure. Panel A: The T4 stage is associated with increased PKA substrate phosphorylation and increased association of AKAPs with the R subunits. Panel B: The T12 stage has increased levels of associated R subunits while the association with AKAPs decreases as does PKA substrate phosphorylation. Panel C: The T16 stage is accompanied by an exhaustion of the anchored cAMP machinery where the initially increased association of R subunits starts to go down as does PKA substrate phosphorylation.*

At T12 (Figure 7B), the transition phase, the system is imbalanced and sensitized leading to a reduction in the PKA substrate phosphorylation. The R subunit association to the beads increases which is suggestive for increased PKA activity. On the other hand however, AKAP association with the R subunits decreases. To speculate, this contradiction may be the result of a compensatory attempt of the myocytes to normalize the ineffective localization of PKA due to the decrease in PKA-AKAPs interaction. Progressing further, it seems at T16 that the system is

exhausted (Figure 7C). The decrease in the compensating R subunits along with a further decrease in AKAP association at this time, and cessation of anchored cAMP signaling results in a further decrease in PKA substrate phosphorylation.
Ineffective phosphorylation of PKA substrates directly affects cardiac function negatively. The substrates of PKA can range from receptors, ion channels to myofilament proteins. For example, reduced phosphorylation of myofilament proteins troponin-I and myosin-binding protein C in dilated cardiomyopathy and HF respectively has been observed.[29,43] Decreased phosphorylation of these proteins could be due to ineffective PKA localization due to a decreased association of the AKAPs with the PKA-R subunits. In order to translate the findings in our study current understanding regarding which specific AKAP guides the phosphorylation of the multiple proteins that are targets for PKA, is however far from complete.

Integration of arrhythmias with reorganized PKA-AKAP

Another class of PKA substrates, being the ion channels may be affected by the alterations found in the signaling pathway. The L-type Ca^{2+} channel, IKs channel and SERCA are important substrates of PKA and affect normal physiology.[44] In the event of disturbed PKA/AKAP signaling during heart failure, modification of their phosphorylation may lead to electrical remodeling and arrhythmogenesis. This study opens up the scope for new questions related to the mechanisms underlying PKA substrate phosphorylation and their functional and arrhythmic outcomes in disease.
Also the currently studied model, the initial beneficial adaptations that lead to (the necessary) compensated remodeling seem to cause an enhanced propensity for ventricular arrhythmias. The remodeling initiated by, among others, the β-adrenergic pathway shows negative consequences directly from the start. Whether these changes are reversible or treatable by specific medication is a future perspective, but for the prevention of sudden cardiac death in "a healthy" population in depth knowledge has to be improved.

Study limitations

Given the high mortality rate between week 8 and 14 after TAC, and the results published in the paper by Akar et al.,[3] we did not opt for further time dependent determination of arrhythmia induction beyond T4. Moreover, as expressed in our aims we were primarily interested to evaluate early arrhythmogenesis. In our electrophysiological evaluation, repolarization parameters have not been measured. In addition we have not performed cellular electrophysiological and contractile measurements thereby potentially underestimating the relevance of focal arrhythmogenic mechanisms for the initiation and perpetuation of polymorphic VTs. Regarding the proteomics that have been performed we were faced with a significant loss of animals in the second half of the follow-up time. With that in mind the obvious question is whether the ones that did survive were the ones with a less severe degree of HF as compared to the ones that were lost, and that this might have had an effect on the recorded data.

CONCLUSION

The early stage of compensated hypertrophy (T4) shows arrhythmias while phosphorylation status is up possibly by increased interaction with 3 AKAPs. The transition (T12) group had the maximal upregulation of associated PKA-R subunits and a 50% mortality, whereas T16 displayed a general decreased interaction, which we interpret as the first signs of exhaustion of the downstream components of cAMP driven signaling.

ACKNOWLEDGMENTS

This study was funded by grants from Utrecht University Focus & Massa (To Dr. T.A.B van Veen and Dr. A. Scholten) and Fondation Leducq Transatlantic Alliance for CaMKII-δ (To Prof. Dr. A.J. Heck and Prof Dr M. A. Vos). The mass spectrometry proteomics data have been deposited to the ProteomeXchange Consortium (http://proteomecentral.proteomexchange.org) via the PRIDE partner repository with the dataset identifier PXD000436.

REFERENCES

(1) Katz, A. M. *Cardiovasc. Drug. Therapy.* **2002**, *16*. 245-9.
(2) Oros, A.; Beekman, J. D.; Vos, M. A. *Pharmacol. Ther.* **2008**, *119*. 168-78.
(3) Akar, F. G.; Spragg, D. D.; Tunin, R. S.; Kass, D. A.; Tomaselli, G. F. *Circ. Res.* **2004**, *95*. 717-25.
(4) Freeman, K.; Colon-Rivera, C.; Olsson, M. C.; Moore, R. L.; Weinberger, H. D.; Grupp, I. L.; Vikstrom, K. L.; Iaccarino, G.; Koch, W. J.; Leinwand, L. A. *Am. J. Physiol. Heart Circ. Physio* **2001**, *280*. H151-9.
(5) Taylor, S. S.; Buechler, J. A.; Yonemoto, W. *Annual review of biochemistry* **1990**, *59*. 971-1005.
(6) Smith, F. D.; Langeberg, L. K.; Scott, J. D. *Trends Biochem Sci* **2006**, *31*. 316-23.
(7) Fink, M. A.; Zakhary, D. R.; Mackey, J. A.; Desnoyer, R. W.; Apperson-Hansen, C.; Damron, D. S.; Bond, M. *Circ. Res.* **2001**, *88*. 291-7.
(8) Zakhary, D. R.; Moravec, C. S.; Stewart, R. W.; Bond, M. *Circulation* **1999**, *99*. 505-10.
(9) Patel, H. H.; Hamuro, L. L.; Chun, B. J.; Kawaraguchi, Y.; Quick, A.; Rebolledo, B.; Pennypacker, J.; Thurston, J.; Rodriguez-Pinto, N.; Self, C.; Olson, G.; Insel, P. A.; Giles, W. R.; Taylor, S. S.; Roth, D. M. *J. Biol. Chem.* **2010**, *285*. 27632-40.
(10) Bristow, M. R.; Ginsburg, R.; Umans, V.; Fowler, M.; Minobe, W.; Rasmussen, R.; Zera, P.; Menlove, R.; Shah, P.; Jamieson, S.; et al. *Circulation research* **1986**, *59*. 297-309.
(11) Aye, T. T.; Soni, S.; van Veen, T. A.; van der Heyden, M. A.; Cappadona, S.; Varro, A.; de Weger, R. A.; de Jonge, N.; Vos, M. A.; Heck, A. J.; Scholten, A. *J Mol Cell Cardiol* **2012**, *52*. 511-8.
(12) Stypmann, J.; Engelen, M. A.; Epping, C.; van Rijen, H. V.; Milberg, P.; Bruch, C.; Breithardt, G.; Tiemann, K.; Eckardt, L. *Int J Cardiovasc Imaging* **2006**, *22*. 353-62.

(13) van Empel, V. P.; Bertrand, A. T.; van Oort, R. J.; van der Nagel, R.; Engelen, M.; van Rijen, H. V.; Doevendans, P. A.; Crijns, H. J.; Ackerman, S. L.; Sluiter, W.; De Windt, L. J. *J Am Coll Cardiol* **2006**, *48*. 824-32.
(14) Boulaksil, M.; Noorman, M.; Engelen, M. A.; van Veen, T. A.; Vos, M. A.; de Bakker, J. M.; van Rijen, H. V. *Neth Heart J.* **2010**, *18*. 509-15.
(15) Gradman, A.; Deedwania, P.; Cody, R.; Massie, B.; Packer, M.; Pitt, B.; Goldstein, S. *J Am Coll Cardiol* **1989**, *14*. 564-70; discussion 571-2.
(16) Chakko, C. S.; Gheorghiade, M. *Am. Heart J.* **1985**, *109*. 497-504.
(17) Litwin, S. E.; Katz, S. E.; Weinberg, E. O.; Lorell, B. H.; Aurigemma, G. P.; Douglas, P. S. *Circulation* **1995**, *91*. 2642-54.
(18) Ling, H.; Zhang, T.; Pereira, L.; Means, C. K.; Cheng, H.; Gu, Y.; Dalton, N. D.; Peterson, K. L.; Chen, J.; Bers, D.; Brown, J. H. *J. Clin. Invest.* **2009**, *119*. 1230-40.
(19) Kitamura, H.; Ohnishi, Y.; Yoshida, A.; Okajima, K.; Azumi, H.; Ishida, A.; Galeano, E. J.; Kubo, S.; Hayashi, Y.; Itoh, H.; Yokoyama, M. *J. Cardiovasc. Electrophysiol.* **2002**, *13*. 865-70.
(20) Boulaksil, M.; Winckels, S. K.; Engelen, M. A.; Stein, M.; van Veen, T. A.; Jansen, J. A.; Linnenbank, A. C.; Bierhuizen, M. F.; Groenewegen, W. A.; van Oosterhout, M. F.; Kirkels, J. H.; de Jonge, N.; Varro, A.; Vos, M. A.; de Bakker, J. M.; van Rijen, H. V. *Eur. J. Heart Fail.* **2010**, *12*. 913-21.
(21) Poelzing, S.; Akar, F. G.; Baron, E.; Rosenbaum, D. S. *Am. J. Physiol. Heart Circ. Physiol.* **2004**, *286*. H2001-9.
(22) Wiegerinck, R. F.; van Veen, T. A.; Belterman, C. N.; Schumacher, C. A.; Noorman, M.; de Bakker, J. M.; Coronel, R. *Heart Rhythm* **2008**, *5*. 1178-85.
(23) Gutstein, D. E.; Morley, G. E.; Vaidya, D.; Liu, F.; Chen, F. L.; Stuhlmann, H.; Fishman, G. I. *Circulation* **2001**, *104*. 1194-9.
(24) Aoyagi, T.; Fujii, A. M.; Flanagan, M. F.; Arnold, L. W.; Brathwaite, K. W.; Colan, S. D.; Mirsky, I. *Circulation* **1993**, *88*. 2415-25.
(25) Bourgonje, V. J.; Schoenmakers, M.; Beekman, J. D.; van der Nagel, R.; Houtman, M. J.; Miedema, L. F.; Antoons, G.; Sipido, K.; de Windt, L. J.; van Veen, T. A.; Vos, M. A. *Heart Rhythm* **2012**, *9*. 1875-83.
(26) Zhang, T.; Maier, L. S.; Dalton, N. D.; Miyamoto, S.; Ross, J., Jr.; Bers, D. M.; Brown, J. H. *Circ. Res.* **2003**, *92*. 912-9.
(27) Colomer, J. M.; Mao, L.; Rockman, H. A.; Means, A. R. *Mol. Endocrinol.* **2003**, *17*. 183-92.
(28) Wong, W.; Scott, J. D. *Nat. Rev. Mol. Cell Biol.* **2004**, *5*. 959-70.
(29) Zakhary, D. R.; Moravec, C. S.; Bond, M. *Circulation* **2000**, *101*. 1459-64.
(30) Abrenica, B.; AlShaaban, M.; Czubryt, M. P. *J Mol Cell Cardiol* **2009**, *46*. 674-81.
(31) Hulme, J. T.; Lin, T. W.; Westenbroek, R. E.; Scheuer, T.; Catterall, W. A. *Proc Natl Acad Sci U S A* **2003**, *100*. 13093-8; Kapiloff, M. S.; Jackson, N.; Airhart, N. *Journal of cell science* **2001**, *114*. 3167-76; Marx, S. O.; Kurokawa, J.; Reiken, S.; Motoike, H.; D'Armiento, J.; Marks, A. R.; Kass, R. S. *Science* **2002**, *295*. 496-9; Perez Lopez, I.; Cariolato, L.; Maric, D.; Gillet, L.; Abriel, H.; Diviani, D. *Mol Cell Biol* **2013**; Zhang, M.; Patriarchi, T.; Stein, I. S.; Qian, H.; Matt, L.; Nguyen, M.; Xiang, Y. K.; Hell, J. W.

J. Biol. Chem. **2013**.
(32) Mongillo, M.; McSorley, T.; Evellin, S.; Sood, A.; Lissandron, V.; Terrin, A.; Huston, E.; Hannawacker, A.; Lohse, M. J.; Pozzan, T.; Houslay, M. D.; Zaccolo, M. *Circ. Res.* **2004**, *95*. 67-75.
(33) Terrenoire, C.; Houslay, M. D.; Baillie, G. S.; Kass, R. S. *J. Biol. Chem.* **2009**, *284*. 9140-6.
(34) Mongillo, M.; Tocchetti, C. G.; Terrin, A.; Lissandron, V.; Cheung, Y. F.; Dostmann, W. R.; Pozzan, T.; Kass, D. A.; Paolocci, N.; Houslay, M. D.; Zaccolo, M. *Circ. Res.* **2006**, *98*. 226-34.
(35) Mehel, H.; Emons, J.; Vettel, C.; Wittkopper, K.; Seppelt, D.; Dewenter, M.; Lutz, S.; Sossalla, S.; Maier, L. S.; Lechene, P.; Leroy, J.; Lefebvre, F.; Varin, A.; Eschenhagen, T.; Nattel, S.; Dobrev, D.; Zimmermann, W. H.; Nikolaev, V. O.; Vandecasteele, G.; Fischmeister, R.; El-Armouche, A. *J Am Coll Cardiol* **2013**.
(36) Sardanelli, A. M.; Signorile, A.; Nuzzi, R.; Rasmo, D. D.; Technikova-Dobrova, Z.; Drahota, Z.; Occhiello, A.; Pica, A.; Papa, S. *FEBS letters* **2006**, *580*. 5690-6.
(37) Means, C. K.; Lygren, B.; Langeberg, L. K.; Jain, A.; Dixon, R. E.; Vega, A. L.; Gold, M. G.; Petrosyan, S.; Taylor, S. S.; Murphy, A. N.; Ha, T.; Santana, L. F.; Tasken, K.; Scott, J. D. *Proc Natl Acad Sci U S A* **2011**, *108*. E1227-35.
(38) Kovanich, D.; van der Heyden, M. A.; Aye, T. T.; van Veen, T. A.; Heck, A. J.; Scholten, A. *Chembiochem* **2010**, *11*. 963-71.
(39) Perrino, C.; Feliciello, A.; Schiattarella, G. G.; Esposito, G.; Guerriero, R.; Zaccaro, L.; Del Gatto, A.; Saviano, M.; Garbi, C.; Carangi, R.; Di Lorenzo, E.; Donato, G.; Indolfi, C.; Avvedimento, V. E.; Chiariello, M. *Cardiovasc. Res.* **2010**, *88*. 101-10.
(40) Lygren, B.; Carlson, C. R.; Santamaria, K.; Lissandron, V.; McSorley, T.; Litzenberg, J.; Lorenz, D.; Wiesner, B.; Rosenthal, W.; Zaccolo, M.; Tasken, K.; Klussmann, E. *EMBO reports* **2007**, *8*. 1061-7.
(41) Altamirano, J.; Bers, D. M. *Circ. Res.* **2007**, *101*. 590-7.
(42) El-Armouche, A.; Pohlmann, L.; Schlossarek, S.; Starbatty, J.; Yeh, Y. H.; Nattel, S.; Dobrev, D.; Eschenhagen, T.; Carrier, L. *J Mol Cell Cardiol* **2007**, *43*. 223-9.
(43) Scott, J. D.; Santana, L. F. *Circulation* **2010**, *121*. 1264-71.

SUPPLEMENTAL INFORMATION

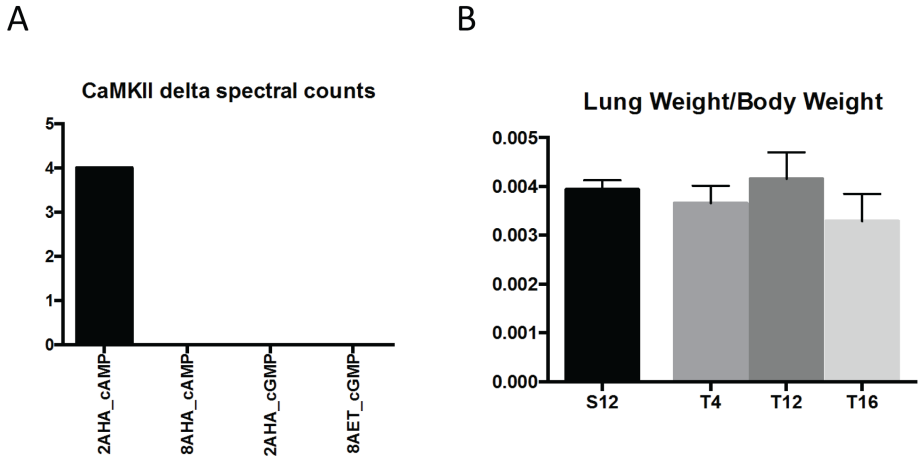

Supplemental Figure 1 *Panel A: Interaction of CamKII on the beads that were used in the experimental approach followed (coated with 2AHA-cAMP) in relation to the absence of interaction with beads that were coated with 3 different configurations of cAMP/cGMP. Panel B: Absolute lung weight (in grams) in relation to body weight (in grams) of the four groups (n=4 in all groups). Two-way Anova showed no significant differences between the four ratios, hence ruling out the presence of pulmonary edema; a condition witnessed in end stage heart failure.*

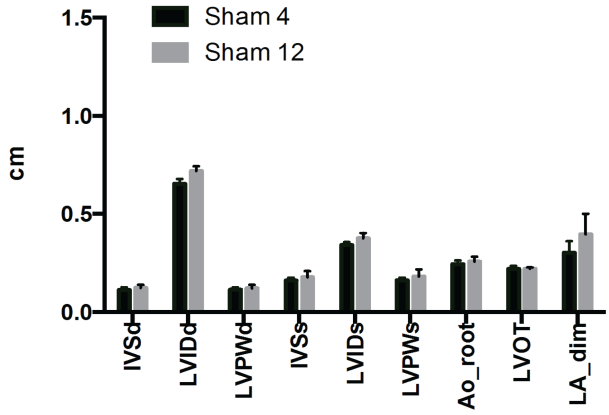

Supplemental Figure 2 *A comparison between all echocardiographic parameters of the Sham group at 4 and 12 weeks, all differences are statistically non significant (n=4 at both time points). This figure presents the lack of age-related effects of the Sham animals in the experimental model. Ao_root, LVOT and LA_dim are the dimensions of the aorta, LV outflow tract and the left atrium, respectively.*

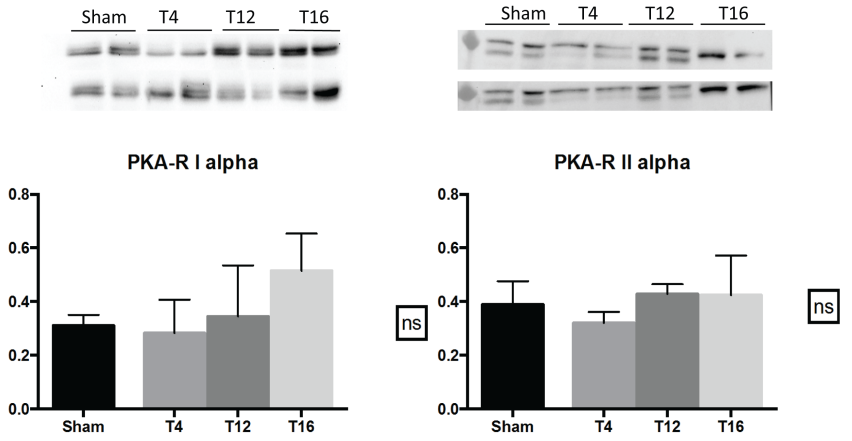

Supplemental Figure 3 *Western blots of total lysates isolated from the four groups (4 animals for each group). Blots were labeled for PKA-RI alpha (left) and PKA-RII alpha (right). Quantification revealed no significant differences in protein levels of both proteins between the four groups.*

SUPPLEMENTAL METHODS

Transverse aortic constriction

The TAC procedure was adapted from the murine protocol.[1-3] In short, rats were anaesthetized with 2.5% isoflurane in 40% oxygen ventilated (Bear Medical Systems) at 75 breaths per minute with a peak pressure of 12 cm H2O and placed in a supine position. The chest was shaved and a parasternal incision was made just below the jugulum to expose the pectoral muscles. These, and the intercostal muscles left of the sternum and just below the second rib, were bluntly dissected to access the thorax. The thymus lobes were then bluntly separated, the aortic arch cleared from connective tissue and fat, and subsequently ligated with a 22 Gauge (0.72 mm) needle and 5-0 silk (Perma-Hand, Ethicon) between the truncus brachiocephalicus and the left common carotid artery. After ligation, thymus and muscles were repositioned and the skin sutured intradermally (5-0 Vicryl, Ethicon).

Transthoracic echocardiography and Doppler measurements

To study contractile and structural remodeling, rats were subjected to echocardiography after 4, and if applicable 12, and 16 weeks using Philips SONOS 5500 with a linear probe (15-6L linear probe, Philips Medical Systems). Upon mild isoflurane anesthesia (1.5 % in 40% oxygen) rats were placed in supine position to obtain: left ventricular internal diameter (LVID), thickness of the InterVentricular Septum (IVS), and posterior wall (LVPW), both in systole (s) and diastole (d). From this, fractional shortening (FS) was calculated as ([LVIDd-LVIDs]/LVIDd)*100.[4] Doppler echocardiography was used to estimate the gradient over the constriction, using the Doppler estimated Bernoulli equation (4*(Vmax)2). Only animals with a calculated pressure gradient larger than 50 mmHg were included.[2,3]

Isolation of hearts and arrhythmia susceptibility testing

From an additional group of animals (n=26), 4 weeks after surgery, hearts were extracorporated and extracellular electrograms were recorded with a 247 or 208-point multi-terminal electrode. Because of the elaborate Langendorff procedure and, because of that, the inability to use these hearts for protein isolation, these animals were not included in the pull-down experiments designed for the proteomics part of this study.

Recordings of LV and right ventricle (RV) were made during stimulation from the center of the grid on the LV at a basic cycle-length of 150 ms using single extra stimuli or burst pacing. Simultaneous epicardial recordings were made from LV and RV in 4 of the 13 TAC, and 5 of the 13 Sham operated animals. In the remaining hearts, LV and RV were mapped sequentially with the 19x13 electrode.

Conduction velocity (CV) parallel (θL) and perpendicular (θT) to fiber direction was determined from the paced activation maps. Calculating the maximal difference at each recording site with neighboring activation times, so called phase differences, delivered dispersion of epicardial conduction.[5] Transmural CV (θTM, perpendicular to epicardium) was calculated from local activation times derived from electrograms recorded with three separate needle electrodes, each equipped with 3-6 electrodes.

Anesthetics and Euthanasia

Animals used for the langendorff perfusion studies and proteomics analysis were anaesthetized with 2.5% isoflurane in 40% oxygen. Heparin (1 ml, 5000 I.U, IP) was administered to avoid the formation of any clots. Hearts were extracorporated via an incision in the thoracic cavity. The ones used for the proteomics experiments were immediately frozen in liquid nitrogen.

cAMP pull down for XIC-based label free PKA-AKAP interaction analysis

An immobilized cAMP based chemical proteomics approach was used to enrich and quantify PKA/AKAP complexes and other associated proteins in the cAMP interactome.[6] Pull-down of the cAMP-protein interactome was performed with 2-AHA-cAMP agarose beads (100µl dry volume, BIOLOG, Bremen, Germany, ligand concentration: 6µmol/ml) in the presence of 10 mM ADP and GDP on lysates (10mg input per rat) prepared form rats of each group, as described previously.[7] After pull-down, bound proteins were eluted with 150 µl of 1X sample buffer (Invitrogen) and in-gel digestion was performed as described previously,[8] in order to prepare samples for mass spectrometric analysis. After in gel digestion the samples were cleaned up on an Oasis-HLB elution plate (Waters).

Since we used cAMP as the bait and the PKA-R subunits are its primary interactors, enrichment of AKAPs and other interactors (named secondary interactors) is based on their association with PKA and not on their absolute expression. To correct for this bias, we normalized the AKAP ion intensities to their respective PKA-R subunit ion intensities.

Liquid chromatography and mass spectrometry

Each sample was analyzed in duplicate. Peptides were separated on an in-house made 50 cm column, 75 µm inner diameter, packed with 1.8 µm C18 resin (Agilent Zorbax SB-C18) at a constant temperature of 40 °C. The column was connected to a Q Exactive quadrupole orbitrap mass spectrometer (Thermo Scientific) through a nanoelectrospray ion source.

Injected peptides were first trapped with a double fritted trapping column (Dr Maisch Reprosil C18, 3 µm, 2 cm x 100 µm) at a pressure of 800 bar with 100% solvent A (0.1 % formic acid (FA) in water) before being chromatographically separated by a linear gradient of buffer B (0.1% FA in acetonitrile) from 7% up to 30% in 150 min at a flow rate of 150 nl/min. Total measurement time for each sample took 180 minutes. The eluent was sprayed via a distal coated fused silica emitter (360 µm o.d., 20 µm i.d., 10 µm tip i.d.; constructed in-house) butt-connected to the analytical columns.

Mass spectra were acquired on the Q Exactive in a data dependent mode with an automatic switch between a full scan and up to 20 data-dependent MS/MS scans. Target value for the full scan MS spectra was 3,000,000 with a maximum injection time of 250 ms and a resolution of 35,000 at m/z 200. The twenty most intense ions with charge two or more from the survey scan were selected with an isolation window of 1.5 m/z and fragmented by HCD with normalized collision energies of 25. The ion target value for MS/MS was set to 50,000 with a maximum injection time of 120

ms and a resolution of 17,500 at m/z 200. Repeat sequencing of peptides was kept to a minimum by dynamic exclusion of the sequenced peptides for 40 s.

Data analysis

For the label free analysis, the raw files were processed using the MaxQuant version 1.3.0.5.[9] The MS/MS spectra were searched against the IPI rat database 3.36 (42,689 sequences; 22,370,705 residues) using the Andromeda search engine.

Database search was performed with the following parameters: an initial mass tolerance of ±20 ppm for precursor masses and a final mass tolerance of ±7 ppm, a mass tolerance of ±0.05 Da for HCD fragment ions, and up to two missed cleavages allowed. Cysteine carbamidomethylation was used as a fixed modification and methionine oxidation and protein N-terminal acetylation as variable modifications. For the identification, the false discovery rate was set to 0.01 for peptides and proteins. The minimum peptide length allowed was set to seven amino acids and a minimum peptide score of 0. The match between runs feature was set on.

Quantitative reverse transcriptase-PCR

RNA was isolated from tissue using Trizol Reagent (#15596-026, LifeTechologies). The isolated RNA was DNase treated with RQ1 RNase-Free DNase (#M6101, Promega). cDNA was created with SuperScript® II Reverse Transcriptase (#18064-071, LifeTechologies). For performing Q-PCR the cDNA was diluted 10X. Q-PCR was performed in a 25μL reaction with iQ™ SYBR® Green Supermix (#170-8880, BioRad) on the MyiQ2 Real Time PCR Detection System (BioRad)

Immunoblotting

LV samples were resolved prior to, and after cAMP affinity purification, by SDS-PAGE, electro-transferred to nitrocellulose membranes (Amersham bioscience) and immersed in TBST-buffer (20 mM Tris-HCL, pH 7.5, 0.5M NaCl, 0.1% Tween 20) with 5% (w/v) milk powder. Antibodies used; PKA-phosphosubstrate (Cell Signaling), PKA-RIalpha and PKA-RIIalpha (both Santa Cruz). The PKA-Phospho-substrate blot was performed with pooled samples, i.e. all samples within each group were pooled to make one master sample for that particular group.

Immunohistology

Expression and distribution of total Connexin43 (Cx43) (Becton & Dickson-610062) was determined by immunohistochemistry as described previously.[10] Heterogeneity of Cx43 distribution was quantified in 1280 x 1024 pixel size photomicrographs of the Cx43 labeling (each pixel corresponding to 0.34 μm). These photomicrographs were transformed in eight-bit black (Cx43) and white (background) pictures. A custom written script in MatLab (The MathWorks Inc., USA) was applied to assess for each Cx43 pixel in a virtual circle around it the shortest distance to its neighboring Cx43 pixel. Standard deviation of all shortest distances of all Cx43 pixels was used as a measure of spatial Cx43 heterogeneity.

The amount of fibrosis was quantified by picrosirius red staining. For fibrosis content, up to 40 digital photomicrographs from each stained section were taken,

depending on the size of the sections. Percentage of picroSirius red staining in each photomicrograph was determined and averaged.

Statistical Analysis

Data were analyzed using R studio. Statistical significance of differences was evaluated by paired Student's t-test or ANOVA followed by post-hoc Bonferroni test as appropriate. Arrhythmia incidence was compared with Fisher's Exact test. Statistical significance is represented as * for Sham vs. T4, ± for T4 vs. T12 and + for T12 vs. T16, unless and otherwise mentioned. Two-sided P-values <0.05 were considered statistically significant. Data are expressed as mean ± SEM.

*/±/+	P<0.05
**/±±/++	P<0.001
***/±±±/+++	P<0.0001

Hierarchical Clustering

Protein Ion Intensities of n=1075 proteins were analyzed using bioconductor (http://www.bioconductor.org/) package biostrings to compute the hierarchy of clusters among four treatment groups (Sham, T4, T12 and T16). The hierarchical clustering (HCL) was created in programming language R version 2.14.1 (http://www.r-project.org/). The distance between the clusters was calculated by the "Pearson" method.

REFERENCES

(1) Rockman, H. A.; Ross, R. S.; Harris, A. N.; Knowlton, K. U.; Steinhelper, M. E.; Field, L. J.; Ross, J., Jr.; Chien, K. R. *Proc Natl Acad Sci U S A* **1991**, *88*. 8277-81.
(2) van Empel, V. P.; Bertrand, A. T.; van Oort, R. J.; van der Nagel, R.; Engelen, M.; van Rijen, H. V.; Doevendans, P. A.; Crijns, H. J.; Ackerman, S. L.; Sluiter, W.; De Windt, L. J. *J Am Coll Cardiol* **2006**, *48*. 824-32.
(3) Boulaksil, M.; Noorman, M.; Engelen, M. A.; van Veen, T. A.; Vos, M. A.; de Bakker, J. M.; van Rijen, H. V. *Neth Heart J* **2010**, *18*. 509-15.
(4) Stypmann, J.; Engelen, M. A.; Epping, C.; van Rijen, H. V.; Milberg, P.; Bruch, C.; Breithardt, G.; Tiemann, K.; Eckardt, L. *Int J Cardiovasc Imaging* **2006**, *22*. 353-62.
(5) Lammers, W. J.; Schalij, M. J.; Kirchhof, C. J.; Allessie, M. A. *Am J Physiol* **1990**, *259*. H1254-63.
(6) Scholten, A.; Poh, M. K.; van Veen, T. A.; van Breukelen, B.; Vos, M. A.; Heck, A. J. *J. Proteome Res.* **2006**, *5*. 1435-47.
(7) Aye, T. T.; Soni, S.; van Veen, T. A.; van der Heyden, M. A.; Cappadona, S.; Varro, A.; de Weger, R. A.; de Jonge, N.; Vos, M. A.; Heck, A. J.; Scholten, A. *J Mol Cell Cardiol* **2012**, *52*. 511-8.
(8) Aye, T. T.; Mohammed, S.; van den Toorn, H. W.; van Veen, T. A.; van der Heyden, M. A.; Scholten, A.; Heck, A. J. *Mol. Cell. Proteomics* **2009**, *8*. 1016-28.
(9) Cox, J.; Mann, M. *Nature Biotechnol.* **2008**, *26*. 1367-72.
(10) van Veen, T. A.; van Rijen, H. V.; Wiegerinck, R. F.; Opthof, T.; Colbert, M. C.;

Clement, S.; de Bakker, J. M.; Jongsma, H. J. *J Mol Cell Cardiol* **2002**, *34*. 1411-23.

Chapter 5

Charting the interactome of PDE3A in human cells using an IBMX based chemical proteomics approach

Eleonora Corradini[1, 2,*], Gruson Klaasse[3,*], Ulrike Leurs[1,4], Albert J.R. Heck[1, 2], Nathaniel I. Martin[3], Arjen Scholten[1, 2, 5]

Manuscript under review

[1] Biomolecular Mass Spectrometry and Proteomics, Bijvoet Center for Biomolecular Research and Utrecht Institute for Pharmaceutical Sciences, Science Faculty, Utrecht University, Padualaan 8, 3584 CH Utrecht, the Netherlands.

[2] Netherlands Proteomics Centre, Padualaan 8, 3584 CH Utrecht, the Netherlands

[3] Department of Medicinal Chemistry and Chemical Biology, Utrecht Institute for Pharmaceutical Sciences, Utrecht University, Universiteitsweg 99, 3584 CG Utrecht, The Netherlands

[4] Current address: Department of Drug Design and Pharmacology, University of Copenhagen, Universitetsparken 2, 2100 Copenhagen, Denmark.

[5] Current address: Janssen, Infectious Diseases and Vaccines, Crucell Holland, Newtonweg 1, 2333 CP, Leiden, The Netherlands

[*] These authors contributed equally to this work

ABSTRACT

In the cell the second messenger cyclic nucleotides cAMP and cGMP mediate a wide variety of external signals. Both signaling molecules are degraded by the superfamily of phosphodiesterases (PDEs) consisting of more than 50 different isoforms. Several of these PDEs are implicated in disease processes inspiring the quest for and synthesis of selective PDE inhibitors, that unfortunately have led to very mixed successes in clinical trials. This may be partially caused by their pharmacological action. Accumulating data suggests that small differences between different PDE isoforms may already result in specific tissue distributions, cellular localization and different involvement in higher order signal protein complexes. The role of PDEs in these higher order signal protein complexes has only been marginally addressed, as no screening methodology is available to address this in a more comprehensive way. Affinity based chemical proteomics is a relatively new tool to identify specific protein-protein interactions. Here, to study the interactome of PDEs, we synthesized a broad spectrum PDE-capturing resin based on the non-selective PDE inhibitor 3-isobutyl-1-methylxanthine (IBMX). Chemical proteomics characterization of this resin in HeLa cell lysates led to the capture of several different PDEs. Combining the IBMX-resin with in-solution competition with the available more selective PDE inhibitors, cilostamide and papaverine, allowed us to selectively probe the interactome of PDE3A in HeLa cells. Besides known interactors such as the family of 14-3-3 proteins, PDE3A was found to associate with a PP2A complex composed of a regulatory, scaffold and catalytic subunit.

INTRODUCTION

Cellular communication is important for coordinating multitudinous activities between various cells and their extracellular environment. In mammalian cells, the cyclic nucleotides cAMP and cGMP are among the earliest identified signal transduction systems acting as mediators in transmitting a wide variety of external signals (Kim and Park, 2003 and Wang et al., 2010). Although synthesis of cAMP and cGMP is carried out by entirely different enzymes, they are both degraded by the large superfamily of phosphodiesterases (PDEs).[1,2] The human genome encodes 21 PDE genes and thus far over 50 PDE isoforms categorized in 11 different families have been experimentally identified.[3] Given the complexity of the PDE family tree, it is now accepted that most of the different PDE variants are involved in specific physiological functions.[4] Many PDEs are reported to be localized along with other signaling proteins in so-called microdomains, allowing them to be strategically anchored throughout the cell.[5–7] In this regard, precise cellular compartmentalization of these enzymes allows control of cyclic nucleotide gradients and permits cAMP and cGMP their specificity in space and time, but also the integration of cyclic nucleotide signaling with other pathways.[8] PDEs have been implied in several disease processes, initiating the search for molecules with PDE inhibiting potential.[9] Naturally occurring methylxanthines, such as caffeine and theophylline were the first PDE-inhibitors to be discovered. These non-selective

inhibitors, together with derivatives such as the 3-isobutyl-1-methylxanthine (IBMX (1), Figure 1A), have been widely used as therapeutics. In particular, IBMX has been used to potentiate the effects of hormones that act via cAMP.[10] Later, more selective PDE inhibitors were synthetized[11] and applied as therapeutics for several diseases. For instance the PDE5 inhibitor, sildenafil was initially developed to treat pulmonary hypertension, however it has been approved as a drug to treat erectile dysfunction, since it displayed erectogenesis as a side effect. On the other hand PDE3 and PDE4 inhibitors were developed to treat cardiotonic, bronchodilatatory, vasodilatatory and anti-inflammatory activities. Unfortunately, their clinical use was not approved mainly due to intolerable side effects.[12,13]

These studies have taught us that generating PDE-inhibitors targeting a single PDE family branch with high potency is typically not sufficient. The reason for the reported side effects could also lie in the nature of the intracellular organization of PDEs. For instance, inhibiting a particular PDE-isoform localized at the cell membrane may induce the therapeutic effect while a subtly different splice isoform of the same PDE family localized at the ER may induce a side effect. Therefore, more information regarding cellular localization and interactomes has to be taken into account during the design of new protein inhibitors. To date, only a handful of PDE signaling nodes have been characterized in some detail. For example the complex of SERCA2, phospholambam, AKAP18 and the regulatory subunit of protein kinase A has been reported to interact with PDE3A in heart.[14]

Several methods have been developed for the identification of protein-protein interactions such as yeast two hybrid screens,[15,16] size exclusion chromatography,[17] sucrose gradient ultracentrifugation,[18] immunoprecipitation, and affinity purification of genetically tagged proteins.[19] Alternatively, several studies have proposed the use of small molecules such as activity based chemical probes,[20] inhibitors,[21,22] small peptides[23] and cyclic nucleotides[24] covalently linked to a resin for the isolation of specific enzyme classes and their higher order complexes. The combination of this enrichment technique with mass spectrometry and subsequent statistical and bioinformatics analysis is often termed chemical proteomics.

To chart the interactome of PDEs, here we set out to develop a quantitative, PDE-centric chemical proteomics approach. Therefore, the non-selective PDE inhibitor IBMX was modified to act as a specific PDE-bait. This broad PDE-capturing tool is combined with in solution competition with different more selective PDE inhibitors. Differential mass spectrometry analysis of such competed samples shows that the PP2A complex, composed by the PPP2CB catalytic subunit, the PPP2R1A scaffold subunit and the PPP2R2A regulatory subunit, binds in HeLa cells specifically to PDE3A, together with several of the known PDE3A interactors, i.e. the 14-3-3 proteins. Hence we expect that the application of our chemical proteomics method in different biological samples, using different specific competitive PDE inhibitors, will be a valuable approach for the identification of PDE containing signaling nodes.

EXPERIMENTAL PROCEDURES

Materials

tert-Butyl (6-bromohexyl)carbamate was purchased from Sigma Aldrich. NHS-Activated agarose slurry was purchased from Pierce (Thermo Fisher Scientific). Anhydrous dimethylsulfoxid (DMSO), triethylamine (TEA), ethanolamine and cilostamide were purchased from Sigma Aldrich. Papaverine-HCl was purchased from Santa Cruz Biotechnology.

Synthetic Procedures and Analytical Data

1-(4-methoxybenzyl)-3-methylurea (2)

To a solution of p-methoxybenzylamine (4.63 g, 34 mmol) in 400 ml of dry toluene triphosgene (15 g, 50 mmol) was added. The resulting mixture was refluxed at 115°C for 3.5 h. The volatiles were removed in vacuo and the residue was dissolved in 120 ml dry THF. An 8M MeNH2 solution in EtOH (12.5 ml, 100 mmol) was added and the mixture heated at 65°C for 30 minutes. The reaction mixture was concentrated in vacuo and purified with column chromatography (silica gel, 230-400 mesh, Merck type 60) (95:5 DCM/MeOH) yielding a white solid (5.8 g, 87%). **Analytical data:** Rf 0.25 (95:5 DCM/MeOH); 1H NMR (300 MHz, CD3OD) δ 7.18 (d, 2H), 6.84 (d, 2H), 4.22 (s, 2H), 3.75 (s, 3H) 2.69 (s, 3H); 13C NMR (75 MHz, CDCl3) δ 159.5, 158.7, 131.5, 128.6, 113.9, 55.2, 43.7, 26.9. HRMS (ESI) calcd for C10H15N2O2 [M+H]+ 195.1132, found 195.1137

6-amino-1-(4-methoxybenzyl)-3-methylpyrimidine-2,4(1H,3H)-dione (3)

Compound 2 (3.0 g, 15.4 mmol) was dissolved in 80 ml Ac2O. Cyanoacetic acid (3.0 g, 35.2 mmol) was added and the reaction mixture stirred at 85°C for 2.5 h. A second (1 g, 11.7 mmol) and a third (0.5 g, 5.8 mmol) addition of cyanoacetic acid were each followed by another 30 minutes of stirring. The mixture was concentrated in vacuo and the residue treated with 20% NaOH solution. The aqueous layer was extracted with DCM (3x 100ml), the organic layers combined, dried, concentrated in vacuo and the product was purified with column chromatography (silica gel, 230-400 mesh, Merck type 60) (95:5 DCM/MeOH) yielding an off-white solid (3.2 g, 79%). **Analytical data:** Rf 0.25 (DCM:MeOH 95:5); 1H NMR (300 MHz, CDCl3) δ n/a; 13C NMR (75 MHz, CDCl3) δ n/a; HRMS (ESI) calcd for C13H16N3O3 [M+Na]+ 284.1006, found 284.1005

3-(4-methoxybenzyl)-1-methyl-1H-purine-2,6(3H,7H)-dione (5)

To a suspension of compound 3 (3.2 g, 12 mmol) in H2O (65 ml) and AcOH (3.5 ml) NaNO2 (1 g, 14.5 mmol) was added and the reaction mixture was stirred for 2 h at 50°C. Formation of a purple color indicated formation of the nitroso derivative. Additional NaNO2¬ (1 g, 14.5 mmol) was added and the mixture stirred at 65°C for another 2 h. Again additional NaNO2 (300 mg, 4.3 mmol) was added and the reaction mixture stirred at 75°C for 45 minutes. The reaction mixture was cooled to 0°C on ice, the solids collected on a Buchner funnel and washed with cold water, followed by drying under vacuum overnight, yielding a purple solid (2.5 g, 72%) which was used in the next step without purification. To a suspension of the crude nitroso

intermediate (2.5 g, 8.61 mmol) in 25% NH4OH (50 ml) Na2S2O4 (8.7 g, 50 mmol) was added and the reaction mixture stirred at 50°C for 2.5 h. When the purple color had gradually disappeared, the reaction mixture was cooled to 0°C and the solid that formed was collected on a Buchner funnel, washed with cold water, and dried under vacuum overnight yielding the diamino intermediate **4** as a light green solid (1.74 g 73%) that was used immediately in the next step without further purification. To a suspension of intermediate 4 (1.74 g, 6.3 mmol) in EtOH (30 ml) was added triethyl orthoformate (8.3 ml, 50 mmol) and the mixture refluxed for 6 h. After cooling, the mixture was concentrated in vacuo and the product directly isolated by column chromatography (95:5 DCM/MeOH) yielding compound 5 as an off-white solid (1.5 g, 83%). **Analytical data:** Rf 0.25 (95:5 DCM/MeOH); 1H NMR (300 MHz, DMSO-d6) δ 8.04 (s, 1H), 7.30 (d, 2H), 6.83 (d, 2H), 5.08 (s, 2H) 3.68 (s, 3H), 3.22 (s, 3H); 13C NMR (75 MHz, DMSO-d6) δ 159.0, 154.8, 151.4, 147.9, 141.0, 129.8, 129.3, 114.1, 106.9, 55.4, 49.0, 46.0, 28.2; HRMS (ESI) calcd for C14H15N4O3 [M+H]+ 287.1144, found 287.1120

7-benzyl-3-(4-methoxybenzyl)-1-methyl-1H-purine-2,6(3H,7H)-dione (6)

Compound 5 (1 g, 3.5 mmol) was dissolved in 10 ml dry DMF. K2CO3 (0.74 g, 5.3 mmol) and benzyl bromide (0.65 ml, 5.3 mmol) were added after which the reaction mixture stirred at 35°C for 16 h. Water (10 ml) was added and after cooling to R.T. the product precipitated out of solution. After cooling on ice, the solids were collected on a glass filter funnel, dried under vacuum and purified by column chromatography (silica gel, 230-400 mesh, Merck type 60) (1:1 to 3:1EtOAc/ hexanes) yielding the desired compound in pure form as off-white crystals (1.01 g, 76%). **Analytical data:** Rf 0.4 (3:1 EtOAc/hexanes); 1H NMR (300 MHz, CDCl3) δ 7.57 (s, 1H), 7.48 (d, 2H), 7.34 (s, 5H), 6.82 (d, 2H), 5.48 (s, 2H), 5.21 (s, 2H), 3.76 (s, 3H), 3.39 (s, 3H); 13C NMR (75 MHz, CDCl3) δ 154.8, 150.5, 146.1, 139.9, 134.0, 128.1, 127.8, 127.1, 105.9, 49.3, 26.4; HRMS (ESI) calcd for C21H21N4O3 [M+H]+ 377.1614, found 377.1584

7-benzyl-1-methyl-1H-purine-2,6(3H,7H)-dione (7)

Compound 6 (300 mg, 80 mmol) was dissolved in 10 ml TFA and stirred overnight in a sealed high-pressure tube at 105°C. The reaction mixture was cooled to R.T., concentrated in vacuo and the product isolated by column chromatography (silica gel, 230-400 mesh, Merck type 60) (95:5 DCM/MeOH) yielding compound 7 a white solid (191 mg, 90%). **Analytical data:** Rf 0.5 (95:5 DCM/MeOH); 1H NMR (300 MHz, CDCl3) δ 10.91 (s, 1H), 7.63 (s, 1H), 7.36 (s, 5H), 5.50 (s, 2H), 3.40 (s, 3H); 13C NMR (75 MHz, CDCl3) δ 154.8, 150.5, 146.1, 139.9, 134.0, 128.1, 127.8, 127.1, 105.9, 49.3, 26.4. HRMS (ESI) calcd for C13H13N4O2 [M+H]+ 257.1039, found 257.1029

tert-butyl (6-(7-benzyl-1-methyl-2,6-dioxo-1H-purin-3(2H,6H,7H)-yl)hexyl) carbamate (8)

To a solution of compound 7 (100mg, 0.39 mmol) in 10 ml dry DMF, K2CO3 (69mg, 0.5 mmol) and tert-butyl (6-bromohexyl)carbamate (140 mg, 0.5 mmol) were added. The reaction mixture was stirred at 60°C for 16 h, concentrated in vacuo, redissolved in DCM, washed with 20 ml H2O, and the organic layer dried with Na2SO4.

After solvent removal under vacuum the desired product was isolated by column chromatography (95:5 DCM/MeOH) yielding 8 as a colorless oil which crystallized upon standing (140 mg, 78%). **Analytical data:** Rf 0.3 (95:5 DCM/MeOH); 1H NMR (300 MHz, CDCl3) δ 7.55 (s, 1H), 7.35 (m, 5H), 5.48 (s, 2H), 4.07 (t, 2H) 3.38 (s, 3H), 3.07 (d, 2H), 1.74 (t, 2H), 1.41 (m, 15H); 13C NMR (75 MHz, CDCl3) δ 155.9, 155.3, 151.3, 148.6, 140.8, 135.3, 129.1, 128.6, 128.1, 107.0, 50.3, 43.4, 40.4, 29.8, 28.4, 28.0, 27.9, 26.3, 26.2. HRMS (ESI) calcd for C24H34N5O4 [M+H]+ 456.2611, found 456.2608

tert-butyl (6-(1-methyl-2,6-dioxo-1H-purin-3(2H,6H,7H)-yl)hexyl)carbamate (9)

Compound 8 (290 mg, 0.63mmol) was dissolved in 10 ml dry MeOH. PdO.H2O (100 mg) was added and the reaction mixture was shaken in a Parr apparatus at an initial pressure of 50 PSI of H2 for 72 h. Shorter reaction times resulted in incomplete conversion. The catalyst was removed by filtration over celite and the filtrate concentrated in vacuo, yielding white crystals (220 mg, 95%). **Analytical data:** Rf 0.1 (90:10 DCM/MeOH); 1H NMR (300 MHz, CD3OD) δ 7.81 (s, 1H), 4.07 (t, 2H), 3.36 (s, 3H), 3.01 (t, 2H), 1.75 (t, 2H), 1.42 (15H); 13C NMR (75 MHz, CDCl3) δ 157.1, 155.8, 151.7, 147.9, 141.5, 108.8, 78.3, 43.4, 39.8, 29.4, 27.6, 27.4, 27.0, 26.1, 25.9; HRMS (ESI) calcd for C17H27N5O4 [M+H]+ 366.2141, found 366.2147

3-(6-aminohexyl)-1-methyl-1H-purine-2,6(3H,7H)-dione (10, IBMX-L(inkable))

Compound 9 (220 mg, 0.6 mmol) was dissolved in 20 ml dry DCM and 20 ml TFA was added. The reaction mixture was stirred at R.T. for 1.5 h, after which thin layer chromatography indicated complete deprotection. The mixture was concentrated in vacuo and lyophilized to yield the product as a colorless glass/oil (204 mg, 90%). **Analytical data:** 1H NMR (300 MHz, D2O) δ 7.9 (s, 1H), 3.79 (t, 2H) 3.11 (s, 3H) 2.78 (t, 2H) 1.45 (m, 4H), 1.18 (m, 4H); 13C NMR (75 MHz, D2O) δ 155.6, 151.8, 145.9, 140.21, 118.0, 114.2, 107.1, 44.0, 39.2, 28.0, 26.9, 26.4, 25.1; HRMS (ESI) calcd for C12H20N5O2 [M+H]+ 266.1617 found 266.1602

Preparation of IBMX-resin

10 ml of NHS-activated agarose 50% slurry was equilibrated in 3x5 ml of anhydrous DMSO. The 5 ml of equilibrated beads were incubated with IBMX-L (**10**, 100 mM in anhydrous DMSO) to achieve a final coupled concentration of 6 μmol IBMX-L/ml of dry beads. The mixture was supplemented with 90 μl of 100% TEA, used as base for the formation of the amide bond and incubated at room temperature on an end-over-end shaker, for 6 hours in the dark. Coupling efficiency was determined by measuring 5 μl of the supernatant at different time points by UV-HPLC (Shimadzu LC-10ADvp equipped with a Zorbax Eclipse Plus C18, 2.1x50 mm, 1.8 μm, Agilent, λ= 289 nm). After IBMX-L coupling with a final density on the beads of 6 μmol/ml of beads, the non-reacted NHS-groups were blocked by incubation with 1.2 ml of 98% ethanolamine at room temperature on the end-over-end shaker overnight. In parallel, the active sites of 5 ml of dry NHS-activated agarose beads were blocked

with 1.2 ml of ethanolamine, following the same procedure, to subsequently use the beads as negative control, later referred to as empty beads. After blocking the NHS-groups, the beads were washed with 3x 10 ml of PBS and stored in PBS with 0.1% NaN3 at 4°C in a 25% slurry.

Cell culture

HeLa cells were grown to 80% confluence at 37° with 5% CO2 in Dulbecco's modified Eagle's medium containing 10% of fetal bovine serum (Lonza) and 0.1% Pen/Strep (Lonza). After harvesting with trypsin, cells were washed in PBS, snap frozen in liquid nitrogen and kept at -80°C until further use.

Sample preparation and pull down assay

$1x10^8$ HeLa cells were subjected to dounce homogenization on ice in 5 ml of PBS, 0.2% Tween-20 containing protease (Complete mini EDTA-free mixture, Roche Applied Science) and phosphatase inhibitors (PhosSTOP, Roche Applied Science). After centrifugation (20,000 x g for 10 min at 4°C), the protein concentration of the supernatant was measured using the Bradford assay. 12 mg of proteins were incubated for 2.5 h either with 240 µL of dry IBMX-resin or empty beads as a control. Samples were eluted with Laemmli sample buffer and proteins were separated on a 4-12% Bis-Tris gradient gel. Gel lanes were digested according to standard procedure[25] by cutting 13 bands from each entire gel lane. Peptides were extracted from the gel bands with acetonitrile and dried in vacuo before LC-MS/MS analysis on an Orbitrap Elite. For the experiments including in-solution competition, 12 mg of HeLa protein lysate, was either incubated with 350 nM cilostamide, 250 nM papaverine or DMSO (Control) at 4°C for 30 minutes on an end-over-end shaker. The samples were subsequently incubated with 240 µL of dried IBMX-resin for 2.5 hours. Samples were then subjected to washes with 3x 1 ml of PBS 0.1% Tween-20 for the control or with washing buffer supplemented with either cilostamide 350 nM or papaverine 250 nM. Bound proteins where then washed with 3x 1 ml of PBS before elution. Proteins were eluted at 95°C with 300 µL of a solution containing 2% SDS and 50 mM DTT. The volume was reduced to 30 µL using a 3 kDa cut off centrifugation filter (Millipore). 7 µl of Laemmli sample buffer 4X (Biorad) was added to the eluted proteins and incubated at 95°C for 5 minutes. Samples were then run into a 4–12% Bis-Tris gradient gel (Bio-Rad) for about 1 cm to concentrate the sample prior to in-gel tryptic digestion. In-gel trypsin digestion was performed according to standard procedures. After digestion the peptides were concentrated and desalted, using an OASIS solid phase extraction plate (Waters). Subsequently in solution dimethyl labeling was performed.[26,27] Peptides originating from the control sample were labeled as light (L), while the pull downs competed with cilostamide and papaverine were labeled as intermediate (M) and heavy (H) respectively. Samples were mixed in a 1:1:1 ratio prior LC-MS/MS analysis on an Orbitrap QExactive.

PDE3A co-immunoprecipitation

Cultured HeLa cells were lysed with a dounce homogenizer in lysis buffer (50 mM Tris–HCl (pH 8), 150 mM NaCl and 0.5% Triton) in the presence of phosphatase

inhibitors and protease inhibitors. 400 μg of proteins were diluted in 500 μl of lysis buffer and subsequently incubated for 3 h with 4 μg of PDE3A antibody (abcam, ab99236) at 4°C, in presence or absence of 350 nM cilostamide. 20 μl of proteinA magnetic beads slurry (Life Technologies) were added to the samples and incubated overnight at 4°C. Samples were then washed with 3x 400 μl washing buffer (50 mM Tris–HCl (pH 8), 150 mM NaCl and 0.05% Triton). A parallel immunoprecipitation using rabbit IgG was performed as negative control following the same procedure. Samples were eluted with Laemmli sample buffer and proteins were separated on a 4-12% Bis-Tris gradient gel. The gel lanes were divided in 5 parts and subjected to trypsin digestion as described above. Extracted peptides were analyzed on a TripleTOF 5600 AB Sciex, Concord, ON, Canada) mass spectrometer.

nanoLC-MS/MS

Pull downs performed with IBMX-resin and empty beads were analyzed on an Orbitrap Elite mass spectrometer (Thermo Scientific, San Jose, CA), IBMX pull downs performed in presence of cilostamide and papaverine were analyzed on a Q-Exactive both coupled to a Proxeon Easy-nLC 1000 (Thermo Scientific, Odense, Denmark), while the PDE3A IP were analyzed on a TripleTOF 5600 (AB Sciex, Concord, ON, Canada) coupled to an Agilent 1290 Infinity System (Agilent Technologies, Palo Alto, CA).

After reconstitution in 10% FA, 5% dimethyl sulfoxide, the peptides were separated on an in-house made 50 cm column with a 50 μm inner diameter packed with 2.7 μm C18 resin (Poroshell, Agilent Technologies Palo Alto, CA) operated at a constant temperature of 40°C. The column was connected to the mass spectrometer through a nanoelectrospray ion source. The injected peptides were first trapped with a double fritted trapping column (Dr Maisch Reprosil C18, 3 μm, 2 cm x 100 μm) at a pressure of 600 bar with 100% solvent A (0.1 % formic acid in water) before being chromatographically separated by a linear gradient of buffer B (0.1% formic acid in acetonitrile) from 7% up to 30% in 35 or 150 min (for the in-gel digested bands or for the whole pull downs respectively) at a flow rate of 100 nl/min.

Nanospray was achieved with an in-house pulled and gold-coated fused silica capillary (360 μm outer diameter, 20 μm inner diameter, 10 μm tip inner diameter) and an applied voltage of 1.7 kV. Full-scan MS spectra (from m/z 350 to 1500) were acquired in the Orbitrap with a resolution of 35,000 for the Q-Exactive and 30,000 for the Orbitrap Elite. Up to ten most intense ions above the threshold of 500 counts were selected for fragmentation. HCD fragmentation was performed when using the Q-Exactive with a data dependent mode, as previously described.[28] RapidCID was performed when using the Orbitrap Elite as described before.[29]

For the TripleTOF 5600 a voltage of 2.7 kV was applied to the needle. The survey scan was from 350 to 1250 m/z and the high resolution mode was utilized, reaching a resolution of up to 40,000. Tandem mass spectra were acquired in high sensitivity mode with a resolution of 20,000. The 10 most intense precursors were selected for subsequent fragmentation using an information dependent acquisition, with a

minimum acquisition time of 100 ms.

Data analysis

The raw files collected from the TripleTOF were first recalibrated based on two background ions with m/z values of 371.1012 and 445.1200. The calibrated raw files were converted to mgf by the AB Sciex MS Data Converter (version 1.1 beta) program.

Peak lists were generated using Proteome Discoverer (version 1.4, Thermo Scientific, Bremen, Germany) for the raw files obtained from the Orbitrap instruments and for the mgf files generated from the AB Sciex program using a standardized workflow. Peak lists, were searched against a Swiss-Prot database (taxonomy Human, 20,407 protein entries) supplemented with frequently observed contaminants, using Mascot (version 2.4 Matrix Science, London, UK). The database search was performed using the following parameters: a mass tolerance of 50 ppm for the precursor masses and ±0.6 Da for CID fragment ions and ±0.05 or ±0.15 Da for HCD fragments for the files acquired on the Orbitrap or on the TripleTOF, respectively. Enzyme specificity was set to Trypsin with 2 missed cleavages allowed. Carbarmidomethylation of cysteines was set as fixed modification, oxidation of methionine, dimethyl labeling (L, I, H) of lysine residues and N termini (when dimethyl labeling was performed) were used as variable modifications. Percolator was used to filter the PSMs for <1% false discovery-rate. When applicable, triplex dimethyl labeling was used as quantification method, with a mass precision of 2 ppm for consecutive precursor mass scans. A retention time tolerance of 0.5 min was used to account for the potential retention time shifts due to deuterium. To further filter for high quality data we used the following parameters: high confidence peptide spectrum matches, minimal Mascot score of 20, minimal peptide length of 6 and only unique rank 1 peptides. For the identification and quantitation of the proteins, only unique peptides were considered. Protein ratios were normalized based on the protein median. Proteins showing an on/off situation were manually quantified by giving them an arbitrary value of 100 or 0.01 for extreme up- or down-regulation, which corresponds to the maximum allowed fold change in the used Proteome Discoverer settings. The mass spectrometry proteomics data have been deposited to the ProteomeXchange Consortium[30] via the PRIDE partner repository with the dataset identifier PXD001781

RESULTS

Design and synthesis of the immobilized IBMX-resin

To specifically capture PDEs and elucidate their interactomes we decided to make use of chemical proteomics. Although some PDEs can be efficiently captured using immobilized cyclic nucleotides, such approaches enrich primarily also for the kinases PKA and PKG and their interactors[31] Therefore, we argued a more PDE-centric tool would be beneficial. Here we describe the design, synthesis and first application of such a chemical proteomics tool. The involvement of PDEs in several diseases made their catalytic site an attractive target for medicinal chemists. One of the first

pharmacological tools to study PDEs was the molecule IBMX, a competitive, non-selective synthetic derivative of the naturally occurring methylxanthines caffeine and theophylline. The exact inhibition mode of these compounds became more clear upon solving several crystal structures of isolated catalytic domains of human PDEs bound to IBMX.[32–35] All these structures show two common features: (I) the interaction of the planar xanthine ring forms a π-π electron-stacking interaction with a conserved phenylalanine in the catalytic sites and (II) the formation of a hydrogen bond with an invariant glutamine.[36] All the structures show that the isobutyl at the N3-position seems not to be essential for the binding of IBMX (Figure 1B). Making use of these similar binding modes we decided to synthesize a linkable form of IBMX (IBMX-L, **10**) by substituting the isobutyl group with a hexylamine group, permitting covalent attachment of the molecule to a solid support via amine coupling.

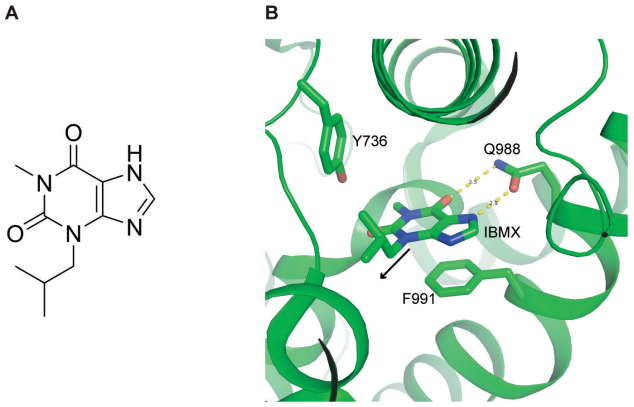

Figure 1 *A, Structure of IBMX (1). B, X-ray crystal structure of IBMX with PDE3B revealing the binding, but also the accessibility of the isobutyl group which points outwards along the black arrow.[32] Oxygen atoms are shown in red and nitrogen atoms are in blue.*

The synthesis of IBMX-L **10** is illustrated in Figure 2 and is based on previously described approaches for the preparation of substituted 1-methylxanthines.[37,38] To begin, p-methoxybenzylamine was treated with triphosgene to generate the corresponding isocyanate which was directly treated with methylamine to yield asymmetric urea **2**. The urea was next heated with cyanoacetic acid followed by treatment with aqueous sodium hydroxide to generate the 6-amino uracil species **3**. Nitrosation of **3** was then performed by treatment with sodium nitrite in acetic acid after which dithioninte reduction in aqueous ammonium hydroxide yielded the diamino intermediate **4**. Treatment of **4** with triethyl orthoformate at elevated temperature then led to formation of intermediate **5** containing the intact xanthine core. Benzylation of the 7-position with benzyl bromide in DMF generated compound **6** after which the p-methoxybenzyl group at position 3 was removed by treatment with TFA to yield intermediate **7**. Alkylation of 7 with tert-butyl (6-bromohexyl)carbamate under basic conditions led to formation of compound **8** after which hydrogenation

over palladium oxide cleanly removed the benzyl group to provide precursor **9**. Final Boc group removal with trifluoroacetic acid yielded the "linkable" IBMX-L species **10**. We could then form an amide bond between the IBMX-L and the N-hydroxy-succinimide (NHS) ester on NHS-activated agarose beads. We resuspended the IBMX-L in anhydrous DMSO at a concentration of 100 mM, and incubated it at room temperature in darkness for 6 hours. IBMX exhibits IC50s for mammalian PDEs that vary between 1 and 80 μM, except for PDE8 and PDE9 that do not bind substantially to IBMX (IC50> 100 μM) 39. Therefore, in order to have a final concentration of the IBMX bound to the beads high enough to enrich a broad range of PDE families using a small volume of beads, we decided to immobilize IBMX with a final concentration of 6 μmol/ml of dried beads.

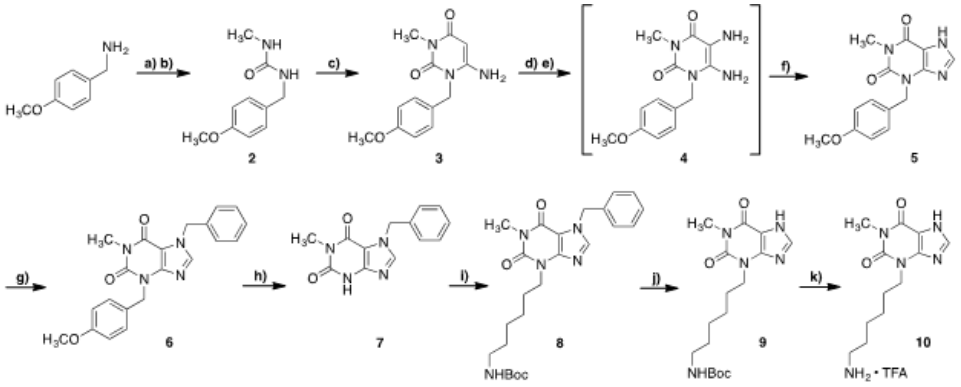

Figure 2 *Synthesis of linkable IBMX-L 10. Reagents and conditions: a) Triphosgene, Toluene, 115 °C; b) 8M $MeNH_2$ in EtOH, THF, 65 °C, 87% over 2 steps; c) 1. Cyanoacetic acid, Ac_2O, 85 °C, 2. NaOH, H_2O, 79%; d) $NaNO_2$, AcOH, 65 °C; e) $Na_2S_2O_4$, NH_4OH, 50 °C, 53% over 2 steps; f) $CH(OEt)_3$, EtOH, reflux, 83%; g) BnBr, K_2CO_3, DMF, 35 °C, 76%; h) TFA (neat), 105 °C, 90%; i) tert-butyl (6-bromohexyl)carbamate, K_2CO_3, DMF, 65 °C, 78%; j) PdO, H2, MeOH, 95%; k) TFA, CH_2Cl_2, 90%.*

IBMX-resin affinity enrichment in HeLa cell lysates

After generating sufficient amounts of the IBMX-resin, we aimed to achieve the enrichment of endogenously expressed PDEs from a HeLa cell lysate (Figure 3A). Whole cell extracts from HeLa cells were therefore incubated with the IBMX-resin. To confirm the specificity of the proteins that bound to the IBMX-resin we incubated the same amount of total protein lysate with NHS-activated beads blocked with ethanolamine. After incubation and washing, the proteins were eluted and separated on SDS-PAGE (Figure 3B). Through digesting both gel lanes in 13 identical bands and subsequent analysis by LC-MS/MS (Supplemental table 1), we identified 543

protein groups (see materials and methods for details on acceptance criteria) in the IBMX-resin lane and 516 proteins in the empty beads control. Using spectral count quantitation we found that PDE1A, PDE3A and PDE10A (Figure 3C and Supplemental table 1) were specifically and highly enriched in the IBMX-resin pull down when compared to the control. This provides the first proof that the IBMX-resin can be used to enrich and identify several low abundant PDE families in a single experiment directly from a complex cell lysate.

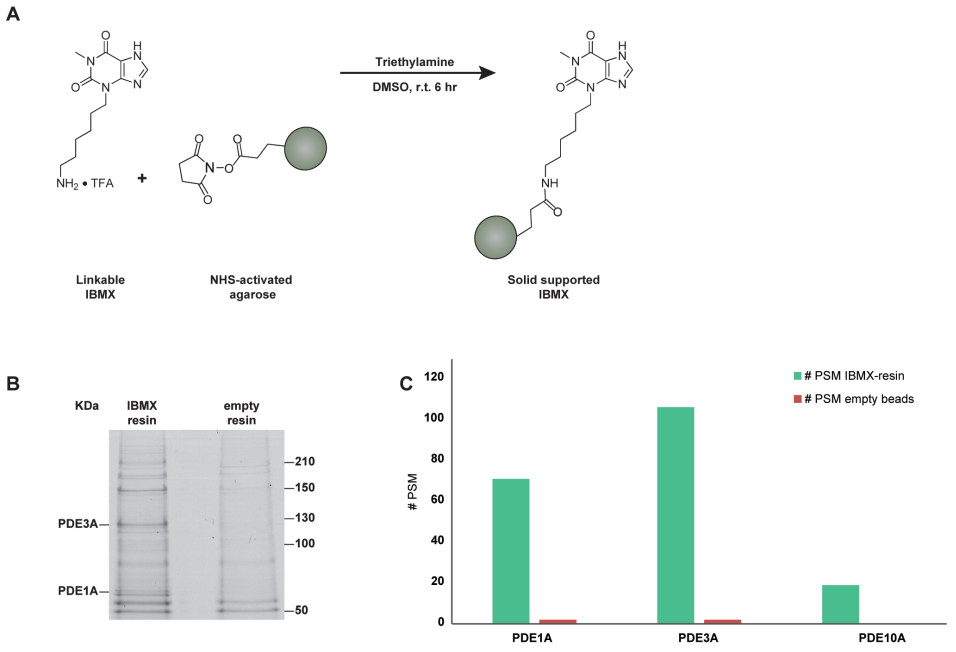

Figure 3 *Characterization of immobilized IBMX. A, Immobilization of IBMX-L* **(10)** *on NHS-activated agarose beads. B, Silver staining of the pull down performed in HeLa cells with IBMX-resin and NHS-agarose beads blocked with ethanolamine (control, empty beads). PDE3A and PDE1A were identified after in gel digestion and LC-MS/MS analysis (supplemental table 1). C, Bar graph depicting the number of peptide spectral matches observed for each captured PDE in the gel lane of the IBMX-pull down and the pull down with the empty resin. PDE1A, PDE3A and PDE10A were highly enriched by the IBMX beads.*

Competition with selective PDE inhibitors

Closer inspection of the data gathered from the in gel digestion already indicated the presence of a few known PDE3 interactors, members of the 14-3-3 family of proteins (Supplemental table 1). To titrate out the exact interactome of PDE3A in HeLa cells, we further fine-tuned our method using specific PDE inhibitors to selectively compete single PDEs and their interactors off the broadly specific IBMX-resin. Cilostamide

was described as the first potent selective inhibitor of PDE3 in platelets[40] with an IC50 of 70 nM. Papaverine is at present one of the most specific and selective inhibitors for PDE10A with an IC50 of 36 nM, however it also inhibits PDE3A in vitro with about a 40-fold poorer selectivity.[41] Therefore, by using these two inhibitors, we could follow the affinity trend of both PDE isoforms in a single experiment. Therefore, three identical amounts of a HeLa lysate were incubated either with DMSO at a final concentration of 0.5% v/v (control), cilostamide (350 nM) or papaverine (250 nM). After the affinity enrichment, the three samples were digested and labeled with in solution dimethyl labeling.[26,27] The DMSO treated control samples were labeled as light (L), the affinity enrichments supplemented with cilostamide were labeled as intermediate (M) and the affinity enrichments supplemented with papaverine were labeled as heavy (H). The three samples were mixed in a 1:1:1 ratio and the peptides were analyzed via LC-MS/MS. The dimethyl ratios were evaluated using Proteome Discoverer whereby two biological replicates were compared. As expected, in both duplicates we identified PDE3A, PDE10A and PDE1A again. When inspecting the cilostamide/control ratios (figure 4A), this M/L protein ratio showed that PDE3A binding to the IBMX-resin was completely abolished showing an averaged M/L ratio for the two biological replicates of ~0.01.In contrast, PDE10A and PDE1A did not show any response towards cilostamide with M/L ratios close to 1 (Supplemental table 2A), indicating that adding cilostamide prevented only PDE3A to bind to the resins.

A different result was obtained upon competition with papaverine. The two biological replicates revealed now that PDE10A binding to the IBMX beads was completely abolished, while binding of PDE3A was only partially abolished by addition of papaverine (with respective averaged ratios of 0.01 and 0.1) (Figure 4B).

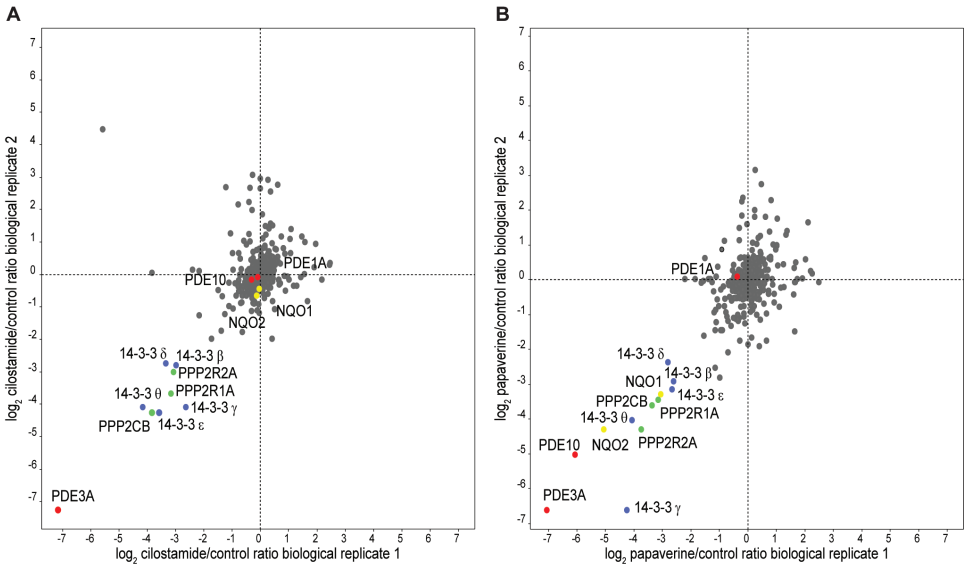

Figure 4. *Specifically enriched proteins following IBMX-based affinity enrichments in lysates supplemented with A. cilostamide and B. papaverine. A, shows the correlation of the cilostamide/control ratios in two biological replicates. Proteins showing at least 2-fold lower enrichment in both biological replicates and at least two unique peptides were considered as possible PDE3A interactors. Upon competition with cilostamide, PDE3A binding to the beads is completely disrupted, while PDE10A and PDE1A remain at a ratio close to 1. In B, are reported the papaverine/control ratios in the two biological replicates. After competition with papaverine, PDE3A and PDE10A binding to the beads is blocked, while the PDE1A ratio does not change. Phosphodiesterases are showed in red, serine/threonine protein phosphatases in green, 14-3-3 proteins in blue, and putative PDE10A binding proteins in yellow.*

On the other hand, PDE1A binding to IBMX is not affected by the presence of papaverine. In vitro measurements of papaverine's IC50 for PDE3A, show a higher value when compared to the concentration we used in our experiments; 1.3 μM vs. 250 nM. We believe this may be explained by the different biological context where the measurements were performed in. Here, the effects of inhibitors were tested in a more physiological context, instead of with recombinant truncated PDEs in vitro. Therefore chemical proteomics approaches are an interesting tool to understand the mechanisms that take place during the PDEs inhibition and help in the design of even more specific PDE inhibitors.

Novel PDE3A Interacting proteins

Competing with free cilostamide in solution did not only prevented PDE3A from binding to the beads, also some other proteins were less enriched and maybe therefore be regarded as putative interactors (Figure 4A, supplemental table 2A). The M/L and H/L ratios of these proteins were below 0.5 in both replicate experiments. We hypothesized that there are at least two different protein complexes that becomes less

enriched following competitive binding using cilostamide. One of these consists of several 14-3-3 isoforms, which were shown to interact with PDE3A previously. Several studies showed that these proteins bind to PDE3A in response to its phosphorylation, while their interaction is completely disrupted after dephosphorylation of PDE3A.[42–44] Next to the 14-3-3 proteins we identified another complex that showed consistent lower enrichment, with M/L and H/L ratios well below 0.5, in both biological replicates after competition of PDE3A with the inhibitors. This complex consisted of the β catalytic subunit of PP2A (PPP2CB), together with the α isoform of the scaffold subunit (PPP2R1A) and the α isoform of the regulatory subunit (PPP2R2A) (Figure 4A).

We hypothesized that the binding with PP2A takes place in presence of cilostamide, for further inhibition of PDE3A. To confirm this hypothesis we performed co-immunoprecipitation of PDE3A in presence or absence of cilostamide. In gel digestion and subsequent mass spectrometric analysis of the gel lanes showed that, while the 14-3-3 proteins are present in both the experiments, the regulatory subunit of PP2A is present only when the immunoprecipitation is performed in the presence of cilostamide (Figure 5A and Supplemental table 2B). From these data we conclude that PP2A binding to PDE3A takes place after the inhibition of PDE3A via both, specific and non-specific inhibitors. Upon competition with papaverine, not only PDE3A binding to the beads became less effective (Figure 4B), also PDE10A showed a consistent H/L ratio around 0.01 in the two biological replicates. Together with PDE10A we also identified two other proteins displaying a H/L ratio below 0.5, the ribosyldihydronicotinamide dehydrogenase (NQO2) and the NAD(P)H dehydrogenase (NQO1). We could hypothesize that these two proteins have also an affinity for PDE10A, since they do not appear to change when the pull-down is performed in the presence of cilostamide. There is currently no evidence in the literature about these interactions and future follow up experiments are needed to confirm these results.

DISCUSSION

In the last decade, through chemical proteomics based approaches a wide variety of small molecules, small peptides or activity based chemical probes have been used for the characterization of protein targets.[21,22,45] An extensive variety of PDE inhibitors have been synthetized in the past years due to the involvement of these proteins in several diseases, however only few of these inhibitors have been clinically approved, because of their side effects. Previous chemical proteomics studies based on the high affinity PDE5 inhibitor (PF-4540124) showed that together with PDE5, other proteins were targets of the inhibitor, giving the possibility to improve the binding of one of the other targets by derivatizing the small molecule.[46] In this work we used an opposite approach, where we derivatized the broad range inhibitor IBMX in order to link it to agarose beads and enrich for a variety of PDEs.

It has been suggested that also PDEs are assembled in an isoform-specific manner

into specialized macromolecular complexes within discrete functional compartments, thereby allowing for precise spatiotemporal control of cyclic nucleotide signaling.[47,48] Therefore, we decided to use a competition with high affinity more specific inhibitors to identify possible interactors of enriched PDEs. With our method we were able to enrich for 3 isoforms of PDEs in HeLa cell lysates, PDE1A, PDE3A and PDE10A. In the past, particular attention has been directed towards PDE3 isoforms. For instance, analysis of signalosomes in cardiomyocytes suggested that upon phosphorylation PDE3A is incorporated into macromolecular regulatory complexes containing PDE3A, SERCA2, AKAP18 and the catalytic subunit of PP2A 14. PDE3B, on the other hand has been extensively studied in adipocytes, where it has been found that its deactivation is dependent on dephosphorylation by PP2A, but not PP1,[49] however the direct interaction of PDE3A with the whole PP2A complex as observed in our study was not shown previously.

PP2A is a heterotrimeric, evolutionary conserved serine/threonine phosphatase with regulatory functions in a wide range of cellular processes, including transcription, apoptosis, cell growth and cellular transformation.[50,51] The human genome encodes two catalytic subunits (PPP2CA, PPP2CB), two scaffolding subunits (PPP2R1A, PPP2R1B) and at least 15 known regulatory B subunits that, by combinatorial assembly, can potentially form a multitude of different trimeric PP2A complexes. [51,52]

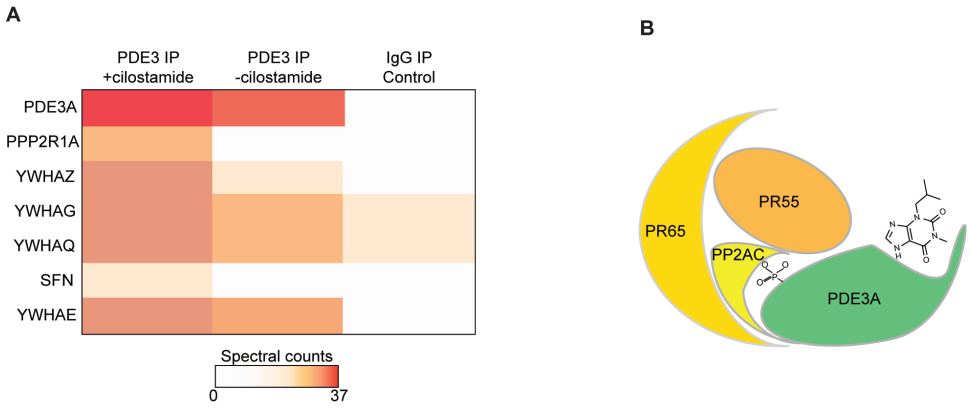

Figure 5 *A, Spectral count heat map illustrating the interactome of PDE3A. Co-immunoprecipitation of PDE3A performed in presence of the competitive binder cilostamide reveal that PP2A regulatory subunits are co-purified, while the family of 14-3-3 proteins binds to PDE3A in both experiments. B, Possible mechanism of interaction of PDE3A and PP2A after phosphodiesterase inhibition.*

The versatile nature of this combinatorial subunit arrangement provides substrate specificity as well as temporal and spatial control of phosphatase activity. Glatter et al. described an elegant affinity-purification method for the identification of protein-

protein interactions using the different subunits of PP2A as bait to study which PP2A complexes exist in human cells,[53] however in these studies PDE3A was not identified as a potential interactor. With our method we were able not only to identify known interactors of PDE3A, i.e. the 14-3-3 proteins, but also the PP2A complex composed by the same catalytic, regulatory and scaffold subunits in two biological replicates, confirming the validity of our methodology for the identification of PDE interactors. By comparing the immunoprecipitation of PDE3A in presence or absence of cilostamide we show that PDE3A is binding to PP2A when it is inhibited (Figure 5B). After competition with papaverine we were able to gather the same result for PDE3A as obtained when competing with cilostamide, moreover we were able to isolate PDE10A with two new possible interactors, NQO1 and NQO2. These two enzymes are ubiquitous cytosolic flavoenzymes that catalyze the reduction of quinones to hydroquinones.[54] Both mammalian NQO1 and NQO2 are known to be overexpressed during cellular oxidative stress and in several types of tumors, and to bioactivate a broad range of quinone anticancer drugs, characteristic that has made these two proteins attractive targets in cancer chemotherapy. It is interesting that despite their similarities their inhibitor specificities are extremely different,[21,55] and at the same time it is interesting how they both show to interact with PDE10 during competition with papaverine. However there is currently no evidence in the literature about these interactions and future follow up experiments are needed to confirm these results. As final result, we can confirm the validity of our chemical proteomics method and the possible future application in tissue samples for the identification of novel PDE interactors.

With the chemical proteomics method presented in this work we show that the use of a broad range PDE inhibitor such as IBMX, immobilized on agarose beads, in combination with in solution competition with specific PDE inhibitors is a powerful tool to screen for PDE interactors. This method can be applied in the future to any type of cell, but also directly to tissue lysates, to further screen for PDE complexes and identify new interactors at an endogenous level.

ACKNOWLEDGMENTS

We would like to acknowledge Dr. Weng Chuan Peng for his technical support on the use of PyMOL. This work was partly supported by the PRIME-XS project (grant agreement number 262067) funded by the European Union 7th Framework Programme. This work is also part of the project Proteins At Work, a program of the Netherlands Proteomics Centre financed by the Netherlands Organisation for Scientific Research (NWO) as part of the National Roadmap Large-scale Research Facilities of the Netherlands (project number 184.032.201).

REFERENCES

(1) Braumann, T.; Erneux, C.; Petridis, G.; Stohrer, W. D.; Jastorff, B. Biochim. *Biophys. Acta* **1986**, *871*, 199–206.

(2) Trong, H. L.; Beier, N.; Sonnenburg, W. K.; Stroop, S. D.; Walsh, K. A.; Beavo, J. A.; Charbonneau, H. *Biochemistry* **1990**, *29*, 10280–10288.
(3) Omori, K.; Kotera, *J. Circ. Res.* **2007**, *100*, 309–327.
(4) Bender, A. T.; Beavo, J. A. *Pharmacol. Rev.* **2006**, *58*, 488–520.
(5) Houslay, M. D.; Adams, D. R. *Biochem. J.* **2003**, *370*, 1–18.
(6) Scott, J. D. *Biochem. Soc. Trans.* **2006**, *34*, 465–467.
(7) Cooper, D. M. F. *Biochem. Soc. Trans.* **2005**, *33*, 1319–1322.
(8) Baillie, G. S. *FEBS J.* **2009**, *276*, 1790–1799.
(9) Francis, S. H.; Busch, J. L.; Corbin, J. D.; Sibley, D. *Pharmacol. Rev.* **2010**, *62*, 525–563.
(10) Schudt, C.; Hatzelmann, A.; Beume, R.; Tenor, H. *Handb. Exp. Pharmacol.* **2011**, 1–46.
(11) Russell, T. R.; Terasaki, W. L.; Appleman, M. M. *J. Biol. Chem.* **1973**, *248*, 1334–1340.
(12) Movsesian, M.; Wever-Pinzon, O.; Vandeput, F. *Curr. Opin. Pharmacol.* **2011**, *11*, 707–713.
(13) Tenor, H.; Hatzelmann, A.; Beume, R.; Lahu, G.; Zech, K.; Bethke, T. D. *Handb. Exp. Pharmacol.* **2011**, 85–119.
(14) Beca, S.; Ahmad, F.; Shen, W.; Liu, J.; Makary, S.; Polidovitch, N.; Sun, J.; Hockman, S.; Chung, Y. W.; Movsesian, M.; Murphy, E.; Manganiello, V.; Backx, P. H. *Circ. Res.* **2013**, *112*, 289–297.
(15) Fields, S.; Song, O. *Nature* **1989**, *340*, 245–246.
(16) Yarwood, S. J.; Steele, M. R.; Scotland, G.; Houslay, M. D.; Bolger, G. B. *J. Biol. Chem.* **1999**, *274*, 14909–14917.
(17) Kristensen, A. R.; Gsponer, J.; Foster, L. J. *Nat. Methods* **2012**, *9*, 907–909.
(18) Lange, M. S.; Müller, B.; Ueffing, M. *Methods Mol. Biol.* **2008**, *484*, 161–175.
(19) Lambert, J.-P.; Ivosev, G.; Couzens, A. L.; Larsen, B.; Taipale, M.; Lin, Z.-Y.; Zhong, Q.; Lindquist, S.; Vidal, M.; Aebersold, R.; Pawson, T.; Bonner, R.; Tate, S.; Gingras, A.-C. *Nat. Methods* **2013**, *10*, 1239–1245.
(20) Speers, A. E.; Cravatt, B. F. *Chembiochem* **2004**, *5*, 41–47.
(21) Bantscheff, M.; Eberhard, D.; Abraham, Y.; Bastuck, S.; Boesche, M.; Hobson, S.; Mathieson, T.; Perrin, J.; Raida, M.; Rau, C.; Reader, V.; Sweetman, G.; Bauer, A.; Bouwmeester, T.; Hopf, C.; Kruse, U.; Neubauer, G.; Ramsden, N.; Rick, J.; Kuster, B.; Drewes, G. *Nat. Biotechnol.* **2007**, *25*, 1035–1044.
(22) Wissing, J.; Jansch, L.; Nimtz, M.; Dieterich, G.; Hornberger, R.; Keri, G.; Wehland, J.; Daub, H. *Mol. Cell. Proteomics* **2007**, *6*, 537–547.
(23) Vermeulen, M.; Mulder, K. W.; Denissov, S.; Pijnappel, W. W. M. P.; van Schaik, F. M. A.; Varier, R. A.; Baltissen, M. P. A.; Stunnenberg, H. G.; Mann, M.; Timmers, H. T. M. *Cell* **2007**, *131*, 58–69.
(24) Scholten, A.; Poh, M. K.; van Veen, T. A.; van Breukelen, B.; Vos, M. A.; Heck, A. J. *J. Proteome Res.* **2006**, *5*, 1435–1447.
(25) Shevchenko, A.; Jensen, O. N.; Podtelejnikov, A. V; Sagliocco, F.; Wilm, M.; Vorm, O.; Mortensen, P.; Boucherie, H.; Mann, M. *Proc Natl Acad Sci U S A* **1996**, *93*, 14440–14445.

(26) Boersema, P. J.; Raijmakers, R.; Lemeer, S.; Mohammed, S.; Heck, A. J. *Nat. Protoc.* **2009**, *4*, 484–494.
(27) Kovanich, D.; Cappadona, S.; Raijmakers, R.; Mohammed, S.; Scholten, A.; Heck, A. J. *Anal. Bioanal. Chem.* **2012**, *404*, 991–1009.
(28) Frese, C. K.; Altelaar, A. F.; Hennrich, M. L.; Nolting, D.; Zeller, M.; Griep-Raming, J.; Heck, A. J.; Mohammed, S. *J. Proteome Res.* **2011**, *10*, 2377–2388.
(29) Corradini, E.; Vallur, R.; Raaijmakers, L. M.; Feil, S.; Feil, R.; Heck, A. J. R.; Scholten, A. *Mol. Cell. Proteomics* **2014**, *13*, 2004–2016.
(30) Vizcaino, J. A.; Cote, R. G.; Csordas, A.; Dianes, J. A.; Fabregat, A.; Foster, J. M.; Griss, J.; Alpi, E.; Birim, M.; Contell, J.; O'Kelly, G.; Schoenegger, A.; Ovelleiro, D.; Perez-Riverol, Y.; Reisinger, F.; Rios, D.; Wang, R.; Hermjakob, H. *Nucleic Acids Res.* **2013**, *41*, D1063–D1069.
(31) Aye, T. T.; Soni, S.; van Veen, T. A.; van der Heyden, M. A.; Cappadona, S.; Varro, A.; de Weger, R. A.; de Jonge, N.; Vos, M. A.; Heck, A. J.; Scholten, A. *J. Mol. Cell. Cardiol.* **2012**, *52*, 511–518.
(32) Scapin, G.; Patel, S. B.; Chung, C.; Varnerin, J. P.; Edmondson, S. D.; Mastracchio, A.; Parmee, E. R.; Singh, S. B.; Becker, J. W.; Van der Ploeg, L. H. T.; Tota, M. R. *Biochemistry* **2004**, *43*, 6091–6100.
(33) Wang, H.; Liu, Y.; Chen, Y.; Robinson, H.; Ke, H. *J. Biol. Chem.* **2005**, *280*, 30949–30955.
(34) Wang, H.; Liu, Y.; Huai, Q.; Cai, J.; Zoraghi, R.; Francis, S. H.; Corbin, J. D.; Robinson, H.; Xin, Z.; Lin, G.; Ke, H. *J. Biol. Chem.* **2006**, *281*, 21469–21479.
(35) Wang, H.; Ye, M.; Robinson, H.; Francis, S. H.; Ke, H. *Mol. Pharmacol.* **2008**, *73*, 104–110.
(36) Ke, H.; Wang, H. *Curr. Top. Med. Chem.* **2007**, *7*, 391–403.
(37) Merlos, M.; Gomez, L.; Vericat, M.; Bartroli, J.; Garcia-Rafanell, J.; Forn, J. *Eur. J. Med. Chem.* **1990**, *25*, 653–658.
(38) Hartz, R. A.; Nanda, K. K.; Ingalls, C. L.; Ahuja, V. T.; Molski, T. F.; Zhang, G.; Wong, H.; Peng, Y.; Kelley, M.; Lodge, N. J.; Zaczek, R.; Gilligan, P. J.; Trainor, G. L. *J. Med. Chem.* **2004**, *47*, 4741–4754.
(39) Rabe, G. D. K. F. *In Phosphodiesterase Inhibitors*; Elsevier, **1996**; pp. 41–64.
(40) Hidaka, H.; Hayashi, H.; Kohri, H.; Kimura, Y.; Hosokawa, T.; Igawa, T.; Saitoh, Y. *J. Pharmacol. Exp. Ther.* **1979**, *211*, 26–30.
(41) Siuciak, J. A.; Chapin, D. S.; Harms, J. F.; Lebel, L. A.; McCarthy, S. A.; Chambers, L.; Shrikhande, A.; Wong, S.; Menniti, F. S.; Schmidt, C. J. *Neuropharmacology* **2006**, *51*, 386–396.
(42) Pozuelo Rubio, M.; Campbell, D. G.; Morrice, N. A.; Mackintosh, C. *Biochem. J.* **2005**, *392*, 163–172.
(43) Rubio, M.; Geraghty, K.; Wong, B.; Wood, N.; Campbell, D. G.; Morrice, N. A.; Mackintosh, C. *Biochem J.* **2004**, *379*, 395–408.
(44) Meek, S. E. M.; Lane, W. S.; Piwnica-Worms, H. *J. Biol. Chem.* **2004**, *279*, 32046–32054.
(45) Salisbury, C. M.; Cravatt, B. F. *Proc. Natl. Acad. Sci. U. S. A.* **2007**, *104*, 1171–1176.

(46) Dadvar, P.; O'Flaherty, M.; Scholten, A.; Rumpel, K.; Heck, A. J. R. *Mol. Biosyst.* **2009**, *5*, 472–482.
(47) Steinberg, S. F.; Brunton, L. L. *Annu. Rev. Pharmacol. Toxicol.* **2001**, *41*, 751–773.
(48) Zaccolo, M.; Movsesian, M. A. *Circ. Res.* **2007**, *100*, 1569–1578.
(49) Resjö, S.; Oknianska, A.; Zolnierowicz, S.; Manganiello, V.; Degerman, E. *Biochem. J.* **1999**, *341*, 839–845.
(50) Virshup, D. M. *Curr. Opin. Cell Biol.* **2000**, *12*, 180–185.
(51) Lechward, K.; Awotunde, O. S.; Swiatek, W.; Muszyńska, G. *Acta Biochim. Pol.* **2001**, *48*, 921–933.
(52) Janssens, V.; Goris, J.; Van Hoof, C. *Curr. Opin. Genet. Dev.* **2005**, *15*, 34–41.
(53) Glatter, T.; Wepf, A.; Aebersold, R.; Gstaiger, M. *Mol. Syst. Biol.* **2009**, *5*, 237.
(54) Chen, S.; Wu, K.; Knox, R. *Free Radic. Biol. Med.* **2000**, *29*, 276–284.
(55) Vella, F.; Ferry, G.; Delagrange, P.; Boutin, J. A. *Biochem. Pharmacol.* **2005**, *71*, 1–12.

Chapter 6

Summary & Outlook
Samenvatting
Curriculum Vitae
List of Publications
Acknowledgements

SUMMARY AND OUTLOOK

Proteins generally function as part of large protein complexes that play vital roles in almost every cellular process. Even though immense progress has been made in mass spectrometry based proteomics for protein identification and quantification, it is still very challenging to chart and understand the role of protein-protein interactions. Part of this challenge stems from the fact that these interactions are dynamic and change in time, space and upon various perturbations induced by the environment or disease. This thesis describes the further development of chemical-proteomics technologies and the use of the most recent (phospho)proteomics approaches to increase our knowledge about protein-protein interactions, whereby I focus in particular on proteins operating in various cyclic nucleotide signaling pathways.

In **Chapter 1** I review the discovery and function of these important cyclic nucleotide signaling proteins and the technologies used in mass spectrometry based proteomics. In the first part I focus on the progress made in our understanding of the interplay in between protein phosphorylation and cyclic nucleotide signaling. In the second part, an overview of technologies and workflows suitable to perform a more targeted mass spectrometric analysis of these cyclic nucleotide signaling proteins is described.

In **Chapter 2** I introduce a new specific method to identify GKAPs (cGMP-dependent protein kinase anchoring proteins). In particular, I modified a broad spectrum cAMP-based chemical proteomics approach by employing competitive concentrations of free cyclic nucleotides in the lysate to isolate PKG and its secondary binding proteins (i.e. GKAPs). Using this approach I was able to identify Huntingtin associated protein 1 (HAP1) as a novel putative GKAP. Through sequence alignment with known GKAPs and secondary structure prediction analysis a small sequence domain mediating the interaction with PKG Iβ, but not PKG Iα, could be defined. In vitro binding studies and site directed mutagenesis further confirmed the specificity and affinity of HAP1 binding to the PKG Iβ N-terminus. Altogether these data define HAP1 as a genuine novel GKAP.

It is often thought that the function of a protein can be studied by using a system wherein this protein is genetically deleted. In **Chapter 3** I have used this approach by analyzing the proteome of a mouse cerebellum, wherein specifically PKGI had been deleted. I used therefore quantitative shotgun (phospho)proteomics on the cerebella of wild type and PKGI knock-out mice, to identify the affected molecular mechanisms. The identification of several interesting differentially regulated (phospho)proteins was followed up by Western blot and immunohistochemistry of specific proteins. The integration of the phosphoproteomics and the proteomics data using extensive network analysis showed that the differentially expressed proteins and proteins harboring differentially phosphorylated sites largely belong to a tight network in the Purkinje cells of the cerebellum. The involvement of important cGMP/cAMP and

Ca^{2+} signaling nodes could be identified. Our data revealed that the knock-out of PKGI could be linked to impaired cerebellar long-term depression at Purkinje cell synapses and revealed several novel players in PKGI-regulated synaptic plasticity.

In **Chapter 4** I showed how the application of chemical proteomics can be of relevance to monitor PKA signaling in a disease state. In particular I investigated the dynamics of signaling complexes in a model of disease-based perturbation. I used immobilized cAMP-based chemical proteomics combined with a label free mass spectrometry approach to follow the progressive alterations in the cAMP/PKA/AKAP complexes. More particular, I looked at the interaction of cAMP-signaling pathways at different time-points within a rat model of pressure overload, mimicking the progressive deterioration of the heart towards failure. Using this approach I showed that PKA signaling complexes deteriorate gradually in progression to heart failure and also that the pattern of disturbances in protein-protein interactions differed from phase to phase. These altered interactions are likely responsible for the characteristic decrease in phosphorylation of several crucial PKA substrates, which are vital for the normal physiological functioning of the heart.

Together with the cyclic nucleotide dependent kinases, other essential members in cyclic nucleotide dependent cell signaling are the cyclic nucleotide phosphodiesterases (PDEs). PDEs are presently important targets for the pharmaceutical industry. However, it is not well known in which protein complexes these PDEs are involved. Potentially, this hampers the synthesis of specific inhibitors due to possible unforeseen side effects. Therefore, in **Chapter 5** I sought to design a chemical proteomics method to isolate and study phosphodiesterases and their interactomes in detail by mass spectrometry. I describe the design and synthesis of a broad-spectrum PDE-capturing resin based on the non-selective PDE inhibitor 3-isobutyl-1-methylxanthine (IBMX). Characterization of this resin in HeLa cells showed that several PDEs could be enriched selectively by these affinity-beads. Combining the IBMX-resin with in-solution competition with two more selective PDE inhibitors, cilostamide and papaverine, allowed us to selectively probe the interactome of PDE3A in HeLa cells. Besides known interactors such as the family of 14-3-3 proteins, PDE3A was found to associate with a PP2A complex composed of a regulatory, scaffold and catalytic subunit after inhibition.

Proteins involved in various signaling mechanisms control all the biological pathways in cells and thus, ultimately, also in our body. Protein-protein interaction and proper protein localization are fundamental for cellular signaling. This is mostly mediated via the formation of multi protein complexes. Although many of these signaling nodes were already identified prior to the rise of mass spectrometry based proteomics, typically by meticulous, hypothesis-driven biochemistry experiments, proteomics has in the past decade revolutionized the way protein-protein interactions are being investigated, with a most prominent role for affinity-purification coupled to

mass spectrometry. In particular, recent advances in sample preparation,[1,2] peptide fractionation[3,4] and MS instrumentation[5,6] enabled researchers to interrogate cellular proteomes to a depth of up to 10,000 proteins in mammalian systems.[7–9] However, one of the key challenges still present in this field is a comprehensive understanding of the formation of protein-protein interactions. Kinases and phospho-binding proteins typically interact with phosphorylation sites in a transient manner, making these interactions challenging or even impossible to be captured by cellular or in vivo experiments alone. To solve this problem the combination of affinity purification and protein identification by MS is gaining momentum, mainly due to its high throughput and sensitivity and because these protein-protein interactions can now often be analyzed under near-physiological conditions.

Small molecule based chemical proteomics technologies are well suited for translational studies of drug action in patient tissues. For instance this technique is used to study drug resistance in patient cells caused by mutations within the drug target proteins with the final goal to develop more efficient and personalized patient therapies.[10] Moreover chemical proteomics is also well suited to enrich target proteins from complex biological samples with the intent to understand in which complexes these proteins are involved in.[11]

For instance, in drug development extensive effort needs to be put in the identification of the on- and off- protein targets. Secondary the so-called off-targets of these molecules can cause toxic side effects that sometimes may have severe therapeutic implications. It is therefore of critical importance to define all cellular target proteins of a (novel) therapeutic compound to understand its full mechanism of action in the cellular context. This can be partly achieved by chemical proteomics.[12,13] Chemical proteomics can also be used to study the temporal dynamics of protein-protein interactions in animal models. This technology can therefore be applied in tissues and cells of any origin giving the possibility to understand the interactions that take place within the relevant cellular, tissue or body context, as illustrated also in this thesis.

One of the major drawbacks of chemical proteomics approaches is the possible rapid dissociation of various components (especially weak and transient interactors) in the course of the sample preparation. This issue could possibly be overcome by combining chemical proteomics with in vivo or on beads chemical crosslinking. Recent applications of this approach have shown that it is possible to use it to investigate post-translational modification mediated protein-protein interactions.[14] Moreover, there is still a need to get accurate information about the biological roles of the enzymes in a given biological sample. Therefore, the use of activity based protein profiling to detect enzyme activity in vivo instead of abundance is of relevance as well.[13]

The understanding of protein-protein interactions is thus essential for the characterization and understanding of all biological processes, but also provides a framework for the design of more specific drug, targeting specifically the disruption of these protein-protein interactions. However, the vast number of interacting proteins and the complexity of protein interaction profiles require efficient means to display

and visualize them. To facilitate the handling of the vast amount of protein-protein interaction data, the biomedical community has developed several public databases (i.e. STRING,[15] BioGRID,[16] MINT[17]). Moreover, several tools are now available to analyze interaction-proteomics data and to generate and visualize protein interaction network (i.e. SAINT,[18] CRAPome,[19] Cytoscape[20]).

Overall, chemical proteomics approaches have proved to be attractive and powerful for the enrichment of protein complexes from samples under physiologically relevant conditions. The combination of these techniques with the continuous advances in sample preparation, sample analysis, and MS instrumentation will further assist in the comprehensive characterization of small molecule/protein-protein interactions and thereby contribute to our understanding of signaling dynamics. The integration of these techniques with complementary systems biology data, will then bring within reach a more comprehensive understanding of how cells communicate with and adapt to their environment.

REFERENCES

(1) Wiśniewski, J. R.; Ostasiewicz, P.; Mann, M. *J. Proteome Res.* **2011**, *10*, 3040–3049.

(2) Wiśniewski, J. R.; Zougman, A.; Nagaraj, N.; Mann, M. *Nat. Methods* **2009**, *6*, 359–362.

(3) Di Palma, S.; Hennrich, M. L.; Heck, A. J. R.; Mohammed, S. *J. Proteomics* **2012**, *75*, 3791–3813.

(4) Köcher, T.; Swart, R.; Mechtler, K. *Anal. Chem.* **2011**, *83*, 2699–2704.

(5) Michalski, A.; Damoc, E.; Lange, O.; Denisov, E.; Nolting, D.; Müller, M.; Viner, R.; Schwartz, J.; Remes, P.; Belford, M.; Dunyach, J. J.; Cox, J.; Horning, S.; Mann, M.; Makarov, A. *Mol Cell Proteomics* **2012**, *11*, O111.013698.

(6) Michalski, A.; Damoc, E.; Hauschild, J. P.; Lange, O.; Wieghaus, A.; Makarov, A.; Nagaraj, N.; Cox, J.; Mann, M.; Horning, S. *Mol. Cell. Proteomics* **2011**, *10*.

(7) Munoz, J.; Low, T. Y.; Kok, Y. J.; Chin, A.; Frese, C. K.; Ding, V.; Choo, A.; Heck, A. J. *Mol. Syst. Biol.* **2011**, *7*, 550.

(8) Geiger, T.; Velic, A.; Macek, B.; Lundberg, E.; Kampf, C.; Nagaraj, N.; Uhlen, M.; Cox, J.; Mann, M. *Mol. Cell. Proteomics* **2013**, *12*, 1709–1722.

(9) Geiger, T.; Wehner, A.; Schaab, C.; Cox, J.; Mann, M. *Mol. Cell. Proteomics* **2012**, *11*.

(10) Rix, U.; Hantschel, O.; Dürnberger, G.; Remsing Rix, L. L.; Planyavsky, M.; Fernbach, N. V; Kaupe, I.; Bennett, K. L.; Valent, P.; Colinge, J.; Köcher, T.; Superti-Furga, G. *Blood* **2007**, *110*, 4055–4063.

(11) Scholten, A.; Poh, M. K.; van Veen, T. A.; van Breukelen, B.; Vos, M. A.; Heck, A. J. *J. Proteome Res.* **2006**, *5*, 1435–1447.

(12) Bantscheff, M.; Eberhard, D.; Abraham, Y.; Bastuck, S.; Boesche, M.; Hobson, S.; Mathieson, T.; Perrin, J.; Raida, M.; Rau, C.; Reader, V.; Sweetman, G.; Bauer, A.; Bouwmeester, T.; Hopf, C.; Kruse, U.; Neubauer, G.; Ramsden, N.; Rick, J.; Kuster, B.; Drewes, G. *Nat. Biotechnol.* **2007**, *25*, 1035–1044.

(13) Speers, A. E.; Cravatt, B. F. *Chembiochem* **2004**, *5*, 41–47.

(14) Kaake, R. M.; Milenković, T.; Przulj, N.; Kaiser, P.; Huang, L. *J. Proteome Res.* **2010**, *9*, 2016–2029.
(15) Szklarczyk, D.; Franceschini, A.; Kuhn, M.; Simonovic, M.; Roth, A.; Minguez, P.; Doerks, T.; Stark, M.; Muller, J.; Bork, P.; Jensen, L. J.; von Mering, C. *Nucleic Acids Res.* **2011**, *39*, D561–D568.
(16) Stark, C.; Breitkreutz, B. J.; Reguly, T.; Boucher, L.; Breitkreutz, A.; Tyers, M. *Nucleic Acids Res.* **2006**, *34*, D535–D539.
(17) Cesareni, G.; Chatr-aryamontri, A.; Licata, L.; Ceol, A. *Curr. Protoc. Bioinformatics* **2008**, Chapter 8, Unit 8.5.
(18) Choi, H.; Larsen, B.; Lin, Z.-Y.; Breitkreutz, A.; Mellacheruvu, D.; Fermin, D.; Qin, Z. S.; Tyers, M.; Gingras, A.-C.; Nesvizhskii, A. I. *Nat. Methods* **2011**, *8*, 70–73.
(19) Mellacheruvu, D.; Wright, Z.; Couzens, A. L.; Lambert, J.-P.; St-Denis, N. A.; Li, T.; Miteva, Y. V; Hauri, S.; Sardiu, M. E.; Low, T. Y.; Halim, V. A.; Bagshaw, R. D.; Hubner, N. C.; Al-Hakim, A.; Bouchard, A.; Faubert, D.; Fermin, D.; Dunham, W. H.; Goudreault, M.; Lin, Z.-Y.; Badillo, B. G.; Pawson, T.; Durocher, D.; Coulombe, B.; Aebersold, R.; Superti-Furga, G.; Colinge, J.; Heck, A. J. R.; Choi, H.; Gstaiger, M.; Mohammed, S.; Cristea, I. M.; Bennett, K. L.; Washburn, M. P.; Raught, B.; Ewing, R. M.; Gingras, A.-C.; Nesvizhskii, A. I. *Nat. Methods* **2013**, *10*, 730–736.
(20) Cline, M. S.; Smoot, M.; Cerami, E.; Kuchinsky, A.; Landys, N.; Workman, C.; Christmas, R.; Avila-Campilo, I.; Creech, M.; Gross, B.; Hanspers, K.; Isserlin, R.; Kelley, R.; Killcoyne, S.; Lotia, S.; Maere, S.; Morris, J.; Ono, K.; Pavlovic, V.; Pico, A. R.; Vailaya, A.; Wang, P. L.; Adler, A.; Conklin, B. R.; Hood, L.; Kuiper, M.; Sander, C.; Schmulevich, I.; Schwikowski, B.; Warner, G. J.; Ideker, T.; Bader, G. D. *Nat. Protoc.* **2007**, *2*, 2366–2382.

SAMENVATTING

Eiwitten functioneren over het algemeen als onderdeel van grote eiwitcomplexen die elk een vitale rol spelen in bijna ieder cellulair process. Alhoewel er veel voortgang is geboekt met eiwit identificatie en kwantificatie door middel van proteomics via massa spectrometrie is het nog steeds een uitdaging om eiwit-eiwit interacties te karakteriseren en de rol ervan te begrijpen. Dit komt gedeeltelijk doordat deze interacties dynamisch zijn en veranderen in tijd, ruimte en wanneer er bepaalde perturbaties plaats vinden geinduceerd door het milieu of ziektes.

Dit proefschrift omvat de ontwikkeling van chemical-proteomics technologiën en het gebruik van de meest recente (phospho)proteomics benaderingen om onze kennis over eiwit-eiwit interacties uit te breiden. De hoofdstukken zijn voornamelijk gericht op eiwitten die opereren in verschillende cyclische nucleotide signalerings routes.

In **Hoofdstuk 1** herzie ik de ontdekking en functie van deze belangrijke cyclische nucleotide signalerings eiwitten en de technologiën die gebruikt worden in massa spectrometrie proteomics. In het eerste gedeelte focus ik op de voortgang over onze kennis ten opzichte van de interacties tussen eiwit fosforylatie en cyclische nucleotide signalering. In het tweede gedeelde is er een overzicht van de technologiën en workflows die passend zijn om een meer doelgerichte massa spectrometrische analyse van deze cyclische nucleotide signalerings eiwitten uit te voeren.

In **Hoofdstuk 2** introduceer ik een nieuwe, specifieke methode om GKAPs (cGMP-dependent protein kinase anchoring proteins) te identificeren. Om dit te kunnen uitvoeren heb ik een brede spectrum cAMP gebaseerde chemische proteomische aanpak gemodificeerd door middel van competitieve concentraties van vrije cyclische nucleotides het signalerings eiwit PKG (cGMP-dependent protein kinase) en zijn secundaire bindings eiwitten (bijv. GKAPs) in het lysaat te isoleren. Via deze aanpak was het mogelijk om Hungtingtin associated protein 1 (HAP1) te identificeren als een nieuw lid van de GKAP eiwit familie. Door middel van sequentie vergelijking met reeds geidentificeerde GKAPs en secundaire structuur analyse voorspellingen werd een klein domein gevonden dat de interactie tussen PKG Iβ, oftewel niet PKG Iα, bemiddel. In vitro binding studies en site directed mutagenesis studies hebben de specificiteit en affiniteit van HAP1 binding met de PKG Iβ N-terminus verder gedefinieerd. Samen gevat heeft deze data HAP1 uitgeroepen als een nieuwe GKAP.

Vaak wordt gedacht dat de functie van een eiwit bestudeerd kan worden door een systeem te gebruiken waarin het specifieke eiwit genetisch verwijdert is. In **Hoofdstuk 3** heb ik deze aanpak gebruikt door het proteoom van een muis cerebellum te analyseren die specifiek PKGI verwijdert heeft. Hiervoor heb ik kwantitatieve shotgun (phospho)proteomics gebruikt op de cerebellum van de wild type en PKGI knock-out

muizen om de aangegrepen moleculaire mechanismes te identificeren. De identificatie van enkele interessante gedifferentieerde gereguleerde (fosfo)eiwitten werd vervolgd met Western blots en immunohistochemie van specifieke eiwitten. De integratie van phosphoproteomics en de proteomics data via netwerk analyse toonde aan dat gedifferentieerde uitgedrukte eiwitten en eiwitten die gedifferentieerde gefosforyleerde aminozuren bevatten voornamelijk toebehoren aan een smal netwerk in de Purkinje cellen van het cerebellum. De betrokkenheid van belangrijke cGMP/cAMP en Ca^{2+} signalerings nodes werden hierdoor geidentificeerd. Onze data toonde aan dat de knockout van PKGI gelinkt kan worden aan verzwakt cerebellum lange termijn depressie bij de Purkinje cel synapses en openbaarde enkele nieuwe eiwitten die een rol hebben in PKGI gereguleerde synaptische plasticiteit.

In **Hoofdstuk 4** liet ik zien hoe de applicatie van de chemische proteomics relevant kan zijn om PKA signalering in een slechte gezondheidstoestand te monitoren. Hier heb ik de dynamiek van signalerings complexen in een gezondheids-perturbatie model bestudeerd. Geimmobiliseerde cAMP-gebaseerde chemische proteomics in combinatie met label vrije massa spectrometrie heb ik gebruikt om de progressieve veranderingen in de cAMP/PKA/AKAP complexes te volgen. Om preciezer te zijn heb ik gekeken naar de interactie tussen cAMP signalerings paden op verschillende tijdspunten in een rat model met te hoge druk, die de progressieve deteoratie van het hart totdat die bezwijkt goed weerspiegelt. Via deze aanpak toonde ik aan dat PKA signalerings complexen langzaam afbrokkelen totdat hartfalen toetreed en dat het patroon van verstoringen in eiwit-eiwit interacties verschilde tussen verschillende fases

Samen met de cyclische nucleotide afhankelijke kinases zijn andere essentiele leden in cyclische nucleotide afhankelijke cellulaire signalering de cyclische nucleotide phosphodiesterases (PDEs). PDEs zijn momenteel belangrijke doelwitten voor de farmaceutische industrie. Maar tot nu toe is het nog niet goed bekent tot welke eiwit complexen deze PDEs zijn betrokken. Dit kan ertoe leiden dat dit de synthese van specifieke remmers belemmert vanwege mogelijke onvoorziene neveneffecten. Daarom heb ik in **Hoofdstuk 5** geprobeert een chemische proteomics methode te ontwerpen om phosphodiesterases en hun interactomen te isoleren en bestuderen via massa spectrometrie. Ik beschrijf het ontwerp en de synthese van een brede spectrum PDE vangende resin gebaseerd op de non-selectieve PDE remmer 3-isobutyl-1methylxanthine (IBMX). Karakterisatie van deze resin in HeLa cellen toonde aan dat enkele PDEs selectief verrijkt kunnen worden op deze affiniteit beads. Door de IBMX-resin te combineren met in oplossing competitie via twee selectieve PDE remmers, cilostamide en papaverine, hebben we selectief de interactoom van PDE3A in HeLa cellen kunnen onderzoeken. Behalve bekende interactoren zoals de 14-3-3 eiwit familie werd ontdekt dat PDE3A zich ook verbind met een PP2A complex bestaande uit een regulatory scaffold en catalytische subunit na remming

CURRICULUM VITAE

Eleonora was born on the 8th of September 1984 in Rome. In 2006 Eleonora obtained her B.SC. degree in chemistry at the Sapienza University of Rome. In 2008 she graduated with a M.Sc. in analytical chemistry. During her studies she worked on the development of liquid chromatography and mass spectrometry methods. During her master she was introduced to the proteomics field and in 2010 she moved to the Netherlands to do an internship in the Prof. Dr. Albert Heck's group. In 2011 she started her PhD in the same lab under the direct supervision of dr. Arjen Scholten. Her PhD project mainly focused on the development of chemical proteomics methods with the aim to improve the knowledge about the interactions occurring between cyclic nucleotide signaling proteins. The results of her work are described in this thesis.

LIST OF PUBLICATIONS

Corradini, E.; Klaasse, G.; Leurs, U; Heck, A. J.; Martin, N. I.;Scholten A. Charting the interactome of PDE3A in human cells using an IBMX based chemical proteomics approach. *Submitted.*

Soni, S.; **Corradini, E.**; Boulaksil, M.; van der Nagel, R.; Kok, B. G.; Puchalska, P.; Bierhuizen, M. F.; de Bakker, J. M.; van Rijen, H. V.; Heck, A. J.; Scholten, A.; Vos, M. A.; van Veen T. A. Timed alterations in anchored cAMP signaling and arrhythmogenesis in a rat model with progression to heart failure. *Submitted.*

Corradini, E., Heck, A. J., Scholten, A. Separation of PKA and PKG signaling nodes by chemical proteomics. *Methods Mol. Biol.* **2015**, *1294*, 191-201.

Corradini, E.; Burgers, P. P.; Plank, M.; Heck, A. J.; Scholten, A. Huntingtin associated protein (HAP1) is a cGMP-dependent kinase anchoring protein (GKAP), specific for the cGMP-dependent protein kinase Iβ isoform. *J. Biol. Chem.* **2015**, *290*, 7887-96.

Corradini, E.; Vallur, R.; Raaijmakers, L. M.; Feil, S.; Feil, R.; Heck, A. J.; Scholten, A. Alterations in the cerebellar (Phospho)proteome of a cyclic guanosine monophosphate (cGMP)-dependent protein kinase knockout mouse. *Mol. Cell. Proteomics* **2014**, *8*, 2004-16.

Scholten, A.; Preisinger, C.; **Corradini, E.**; Bourgonje, V.; J., Hennrich, M. L.; van Veen, T. A.; Swaminathan, P. D.; Joiner, M. L.; Vos, M. A.; Anderson, M. E.; Heck, A. J. Phosphoproteomics study based on in vivo inhibition reveals sites of calmodulin-dependent protein kinase II regulation in the heart. *J. Am. Heart Assoc.* **2013**, *4*, e000318.

Zhou, H.; Ye, M.; Dong, J.; **Corradini, E.**; Cristobal, A.; Heck, A. J.; Zou, H.; Mohammed, S. Robust phosphoproteome enrichment using monodisperse microsphere-based immobilized titanium (IV) ion affinity chromatography. *Nat. Protoc.* **2013**, *3*, 461-80.

Preisinger, C.; Schwarz, J. P.; Bleijerveld, O. B.; **Corradini, E.**; Müller, P. J.; Anderson, K. I.; Kolch, W.; Scholten, A.; Heck, A. J. Imatinib-dependent tyrosine phosphorylation profiling of Bcr-Abl-positive chronic myeloid leukemia cells. *Leukemia* **2013**, *3*, 743-6.

ACKNOWLEDGEMENTS

I still think it is amazing how much I have learned in these years and this has been possible because of all the people I have met and worked with during this time. Without them this thesis might not have been written and therefore I want to thank all of them.

It seems yesterday that I left Italy to start my new life in the Netherlands. Of course this wouldn't be possible without Albert. Thank you for believing in me and giving me the possibility to work in your group, first as an exchange student and then as a PhD student.

A special thank goes to Arjen, my daily supervisor. At the very beginning I thought you had a very strange way to supervise me, by giving me some initial directions and letting me decide what to do. It took me some time to get used to it, but in the end this allowed me to put my hands on many different topics, giving me the possibility to learn many different techniques.

Shabaz and Christian, even though you were not my supervisors your guidance and trainings were essentials and I really appreciated what you did for me. Thank you.

I would like to thank all my collaborators. Without your contribution my thesis would be pretty empty. Therefore I would like to thank Prof. Marc Vos's group from the UMC. In particular Toon and Siddarth, thank you for the support and the help you gave me every time I asked for it. A special thank goes to Nathaniel Martin, Gruson and Ulrike: it was really great to collaborate with you on the IBMX project. Prof. Robert Feil and Raghavan, thank you for your expertise with mouse models and cGMP signaling.

Prof. Mark Anderson, I am really grateful to you for giving me the opportunity to visit your lab, allowing me to taste a complete different working atmosphere. I really enjoyed the time I spent in Iowa City and this wouldn't be possible without Mei-ling. Thank you for your hospitality and for all the fun I had while piloting the plane. I also made treasure of all the things you taught me in the lab.

These years wouldn't be the same without all the people I have met in the lab. I really want to thank all my officemates for the nice time I spent with you. Donna and Pepijn, thank you for the help you gave me every time I asked you something, even now that you are not in the lab anymore. Jamila, I'm sorry for making you spend a very warm winter in the office, and thanks a lot for letting me keep the heating on! Alba and Matina, it is always funny to hear you talking about the yoga classes. I wish you all the best with your PhD!

Piero and Sara thank you very much for all the fun, the laughs, the table football matches, and the support you gave me during this long journey. I really don't know how all these years could have been without you.

To work in the lab wouldn't be the same without all the other present but also former group members. I am really happy to have met you all, and I thank you for all the fun I had with you while sharing many Friday afternoon beers in the Inner Circle, lab days

out, the classes in the gym, but also many (and sometimes very long) days at work.

Of course many thanks go to Corine for being always available and helping me with all my questions, Dutch paperwork and PhD thesis planning.

Many thanks go also to the people outside the lab, in particular to the Hopakker 35 team for the all the talks, dinners, parties and the time we spent together.

Peng it was very nice to bike across the tulip fields but also visit New York with you! I wish you and Elisa all the best for your future in San Francisco.

Un rignraziamento particolare va a tutte le persone che mi hanno supportato (e sopportato) dall'Italia in tutti questi anni.

Giampiero, Stefania, Pina e Raffaele grazie per essere sempre stati presenti.

Andrea, grazie per aver sempre trovato un po' di tempo per poter prendere un caffè insieme e tenerci aggiornati facendomi fare quattro risate ogni volta che sono rimpatriata.

Ale e Andrea, i miei "fratellini", grazie per tutte le risate e tutte le storie che possiamo ranccontare dopo vari i fine settinama passati insieme qui in Olanda. A quando la prossima mezza fetta di pane?

Nonna, un giorno di questi ti farò salire su un aereo, così potrai vedere con i tuoi occhi quello che ti racconto ogni volta che ci vediamo.

Per ultimi, ma sicuramente non per importanza, vorrei ringraziare voi, mamma e papà per l'amore e per tutto il supporto che mi avete sempre dato, qualsiasi scelta abbia fatto nella mia vita. Sicuramente non sarei arrivata qui senza di voi.

Chapter 6